PROPANE AROMATIZATION OVER GALLIUM-CONTAINING ZEOLITES OF HIERARCHICAL PORE ARCHITECTURE: SYNTHESIS, CHARACTERIZATION AND KINETIC MODELING

BY

KEHINDE EMEKA OGUNRONBI

A Thesis Presented to the

DEANSHIP OF GRADUATE STUDIES

KING FAHD UNIVERSITY OF PETROLEUM & MINERALS

DHAHRAN, SAUDI ARABIA

In Partial Fulfillment of the
Requirements for the Degree of

MASTER OF SCIENCE

In

CHEMICAL ENGINEERING

MAY 2013

KING FAHD UNIVERSITY OF PETROLEUM & MINERALS

DHAHRAN- 31261, SAUDI ARABIA

DEANSHIP OF GRADUATE STUDIES

This thesis, written by **KEHINDE EMEKA OGUNRONBI (g201102690)** under the direction his thesis advisor and approved by his thesis committee, has been presented and accepted by the Dean of Graduate Studies, in partial fulfillment of the requirements for the degree of **MASTER OF SCIENCE IN CHEMICAL ENGINEERING.**

Dr. Sulaiman Al-Khattaf
(Advisor)

Dr. Usamah A. Al-Mubaiyedh
Department Chairman

Dr. Nabil Al-Yassir
(Co-Advisor)

Dr. Salam A. Zummo
Dean of Graduate Studies

Dr. Nadhir A.H. Al-Baghli
(Member)

28/5/13
Date

Dr. Abdullah Al-Shammari
(Member)

Dr. Mohammad Mozahar Hossain
(Member)

DEDICATION

This work is dedicated to the giver of inspiration and understanding to *homo sapiens*

ACKNOWLEDGMENTS

I would like to appreciate God for His help in the completion of my masters' degree program. My Profound appreciation also goes to my advisor and co-advisor in the persons of Dr. Sulaiman Al-Khattaf and Dr. Nabil Al-Yassir. Both of you have been of tremendous and immense help to me during my program. Words are not enough to articulate my gargantuan gratitude because my mental capability has really increased via my being submissive under your tutelage. Thank you for the academic, moral and financial support; I really appreciate you guys! My gratitude also extends to the members of my committee including Dr. Nadhir Al-Bagli, Dr. Mozahar Hossain and Dr. Abdullah Al-Shammari; thanks for your constructive contributions at all levels of my thesis.

This program would have been absolutely stressful without the moral and spiritual support of my parents – Philip and Kate Ogunronbi – who stood by me speaking words of power into my life. I really appreciate you from the depth of my heart. Thank you and thank you!

Lastly, I am expressing my gratitude to the staff of the Center of Refining and Petrochemicals for their various contributions in seeing to the materialization of the success of this work.

TABLE OF CONTENTS

LIST OF TABLES

LIST OF FIGURES

ABSTRACT

Full Name : **KEHINDE EMEKA OGUNRONBI**

Thesis Title : **PROPANE AROMATIZATION OVER GALLIUM-CONTAINING ZEOLITES OF HIERARCHICAL PORE ARCHITECTURE: SYNTHESIS, CHARACTERIZATION AND KINETIC MODELING.**

Major Field : **CHEMICAL ENGINEERING**

Date of Degree : **May, 2013**

Propane aromatization was carried out over conventional gallium-containing HZSM-5, gallium-containing HZSM-5 of random and ordered hierarchical pore arrangements, and over H-galloaluminosilicate of stable ordered hierarchical pore structure. The random and ordered hierarchical pore structures in gallium-containing HZSM-5 were introduced via post-treating the catalyst by desilication, CTAB-mediated hydrolysis and overgrowth of MCM-41 layer; while stable ordered microporous/mesoporous system in H-galloaluminosilicate was created via surfactant mediated base hydrolysis of steamed H-galloaluminosilicate. The textural and structural properties of these catalysts were determined using various characterization techniques. The performances of the mesoporous catalysts were compared with the microporous counterparts with respect to propane aromatization at different reaction conditions.

H-galloaluminosilicate with hierarchical arrangement showed enhanced aromatization performance and stability with respect to steamed H-galloaluminosilicate. Also, at

comparable conversion of 15%, all post-treated samples were more selective to the production of Benzene, Toluene and Xylene (BTX) than the microporous samples.

The enhancement of activity was further corroborated by kinetic studies carried out in a fixed bed reactor. The kinetic modeling results which show increase in cracking activation energy coupled with decrease in dehydrogenation activation energy; thus upon incorporation of gallium and subsequent mesoporosity introduction we reduced the cracking of propane and increased the ease of dehydrogenation thereby favoring the production of BTX.

ABSTRACT (ARABIC)

ملخص الرسالة

الاسم الكامل: كهندي يميكا وجرونبي

عنوان الرسالة: أرمتة البروبان على الزيوليت المحتوي على الجاليوم ذي التركيب المسامي الهرمي : التركيب ، الوصف، و التصميم الكيناتيكي

التخصص: الهندسة الكيميائية

تاريخ الدرجة العلمية: أيار **2013**

تم عمل تفاعل الأرمتة للبروبان على زيوليت محتوٍ على الجاليوم (Ga-HZSM-5) ، و على زيوليت محتوٍ على الجاليوم منتظم و عشوائي التركيب الهرمي المسامي ، و كذلك على الصيغة البروتونية المستقرة المنتظمة التركيب الهرمي المسامي للجاليو ألومينوسيليكات (H-galloaluminsilicate). تم عمل و إضافة الزيوليت المحتوي على الجاليوم (Ga-HZSM-5) ذي التركيب الهرمي المسامي المنتظم و العشوائي من خلال عملية استخلاص السيليكون ، التحليل الوسيط CTAB ، و كذلك النمو السريع لطبقة MCM-41 ، بينما تم تحضير النظام المتكون من المسامات (المايكرو/ الميزو) في الصيغة البروتونية المستقرة المنتظمة للجاليو ألومينوسيليكات (H-galloaluminsilicate) عن طريق التحليل السطحي القاعدي الوسيط للصيغة البروتونية للجاليو ألومينو سيليكات المعالجة بالبخار (H-galloaluminsilicate) . السمات السطحية و الخصائص التركيبية لهذه الحفازات تم تحديدها باستخدام تقنيات وصفية متعددة . أما أداء الحفازات ذات المسامات الصغيرة (ميزو) فقد قورن مع نظرائه من الحفازات ذات المسامات الصغيرة جدا (ميكرو) بالنسبة لأرمتة البروبان على ظروف تفاعل مختلفة . أظهرت الصيغة البروتونية للجاليو ألومينو سيليكات (H-galloaluminosilicate) ذات التركيب الهرمي أداء محَسَّنًا في تفاعل الأرمتة و الاستقرار بالنسبة للصيغة البروتونية للجاليو ألومينو سيليكات المعالجة بالبخار (H-galloaluminosilicate). إضافة لذلك فقد لوحظ أنه على نسبة تحول معينة 15 % فإن جميع العينات المعدلة كانت أكثر اختيارية لإنتاج البنزين و التولوين و الزايلين (BTX) من تلك العينات ذات المسامات الصغيرة جدا (الميكرو) . تم تأكيد و تأييد تحسن الإداء في النشاط التفاعلي من خلال دراسة كيناتيكية أجريت في مفاعل ذي كتلةٍ حفّازيّة ثابتة (fixed bed reactor) . أظهرت نتائج التصميم الكيناتيجي ارتفاعا في طاقة التنشيط لتفاعل التكسير مصحوبة بانخفاض في طاقة التنشيط لتفاعل نزع الهيدروجين و بالتالي فإن إضافة الجاليوم و من ثم إدخال المسامات ذات التركيب الصغير (الميزو) أدى إلى خفض و تقليل تكسير البروبان و زيادة سهولة حدوث تفاعل نزع الهيدروجين المسؤول عن إنتاج البنزين و التولوين و الزايلين (BTX) .

CHAPTER 1

INTRODUCTION

1.1 BACKGROUND INFORMATION ON PROPANE AROMATIZATION

Propane aromatization is the transformation of propane into more valuable aromatics which are essential materials used in both the chemical and petrochemical industry. The aromatics mainly useful are the benzene, toluene and xylene, otherwise known as BTX. Aromatics are essential raw chemicals for the petrochemical industry. They stand for a large percentage of the known organic compounds in the world.

The use of liquefied petroleum gas (LPG) as the starting raw material for the production of aromatics came as a result of the need to economize production cost in producing aromatics thereby eliminating naphtha feedstock which initially gulped about 80% of the production cost of aromatics [1]. Aromatics usually formed are benzene, toluene, xylene, para-xylene, ortho-xylene, meta-xylene, Ethylbenzene, 1-methyl-3-ethylbenzene, 1-methyl-4-ethylbenzene, 1,2,4-trimethylbenzene, Indan, naphthalene and 1-methylnaphthalene. Of all these products, the most often found in significant quantities are benzene (and Ethylbenzene), toluene, and xylene (comprising of its three isomers which are p-xylene, m-xylene, and o-xylene).

As mentioned earlier, the main aromatic compounds of commercial interest are benzene, toluene, ortho-xylene and para-xylene. The annual production rate of these compounds is approximately 35 million tonnes [2].

Xylene has a wide range of applications. It is used as the principal precursor to terephthalic acid and dimethyl terephthalate, both of which are used in the manufacture of plastic bottles made from polyethylene terephthalate (PET) and also polyester clothing [3]. Xylene is also used as solvent in the leather, printing and rubber industries. It also has various agricultural applications. Mixed Xylenes have a annual demand of approximately 43.4 million tonnes per year. This demand is known to be on the increase over the past decade. The percentage of demand allotted to each constituent of the mixed Xylenes is shown on a pie chart in Figure 1.1.

Toluene, an aromatic compound, is widely used as a solvent in chemical industries. It is also used, via side chain methylation, in the production of styrene. Its use is also found as an octane-enhancer in gasoline fuels used in internal combustion engines [4]. Toluene could also be dealkylated to benzene or even made to undergo oxidation to yield benzoic acid and benzaldehyde, the two of which are vital transients in the field of chemistry.

The global demand for toluene is approximately 28.9 million tonnes per year. This demand is also not unrelated to its numerous industrial applications.

Benzene is the simplest aromatic hydrocarbon. It is the smallest unit of all aromatics. Its demand is about 40.7 million tons/year (including its derivatives). Some of the aromatics which are derived from using benzene as a precursor are:

Alkylbenzene, Chlorobenzene, Cumene, Cyclohexane, Nitrobenzene and maleic anhydride. Of all these,

Ethylbenzene is the mostly demanded as shown in Figure 1.2. Its global demand is ca.52% per annum. Its demand is not unrelated to its inevitable use as an anti-knock agent in gasoline and octane number enhancer. It has also found its application in the oil industry where it is used in enhanced gas recovery [5]. Moreover, it found its principal application as a precursor in the production of polystyrene where it undergoes catalytic dehydrogenation to form styrene followed by a chain of reactions to yield the polymer.

Alongside Ethylbenzene, among the derivatives of benzene, is Cumene otherwise known as isopropylbenzene. This aromatic hydrocarbon is a very important intermediate in the Cumene process – commercial process for the production of phenol and acetone from the starting raw materials of benzene and propylene.

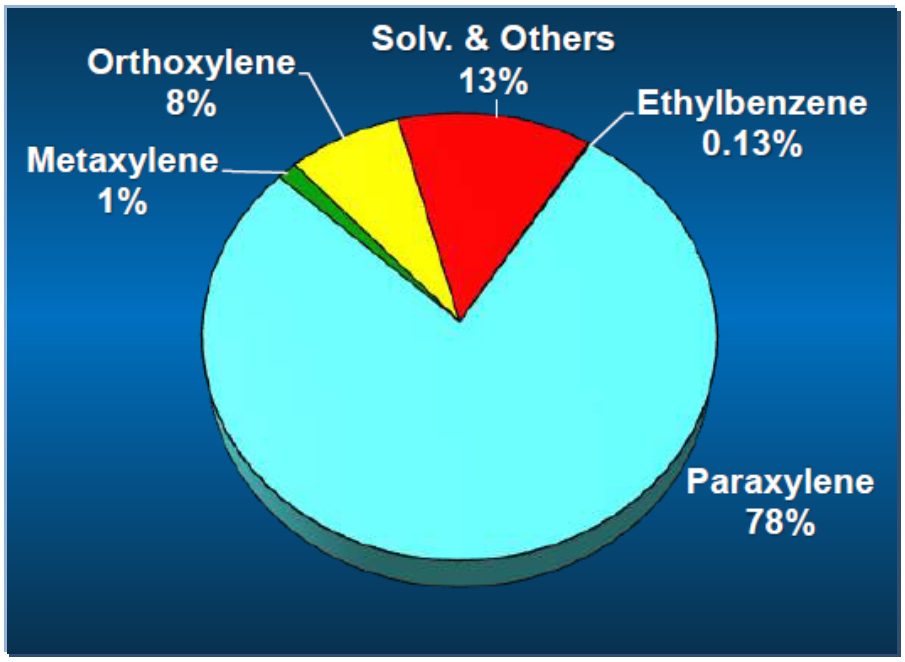

Fig. 1.1: Pie Chart showing the demand for constituents of mixed xylenes.

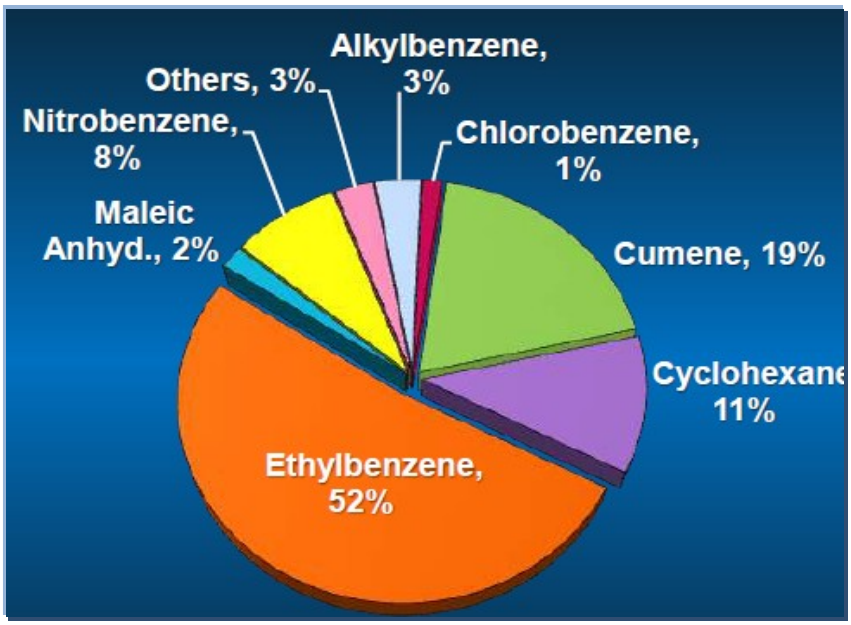

Fig 1.2: Pie chart showing the demand of benzene derivatives

1.2 Main Industrial Processes for Conversion of LPG into Aromatics

The three main processes are:

- M-2 Forming
- Cyclar
- Aroforming (IFP- Salutec)

1.2.1 M-2 Forming

This process was proposed by Mobil in 1986 as an alternative, to replace the capital-intensive catalytic reforming of naphtha, which offered new route to the production of aromatics. It also came as a succor to the lingering challenge of catalytic reforming processes in transforming light hydrocarbons with carbon numbers of five or less to aromatics [6]. The feeds used for this process are usually rich in unsaturated hydrocarbons viz. unsaturated gases from catalytic cracking processes, cracked gasoline and pyrolysis. This process operates at temperatures depending on the reactivity of the feedstock. For example, a paraffinic feedstock would aromatize at a higher reaction temperature than an olefinic feedstock.

1.2.2 Cyclar

This is a new dehydrocyclodimerization process that is designed in a way to accomplish the transformation of LPG into aromatics. It was announced by a joint venture of UOP and BP in 1984 [7] and was then commercialized. A schematic representation of this process is shown in Figure 1.3. This process was basically

designed to be partitioned into three segments viz. reactor segment, regenerator segment and product recovery segment. The operating temperature of the process is optimized such that it is high enough to eliminate non-aromatic scum and low enough to suppress thermal cracking reactions. The same is also done for space velocity and the reaction pressure. In order to maintain the endothermic nature of the reaction, fired-heaters are connected to the stacked reactor – in which catalysts flow under the law of gravity. The catalyst formulated by BP for this process was a gallium-modified zeolite catalyst. At present, there are two versions of the process design. The first is the low-pressure design which is certified for use only where optimum yield of aromatics is of paramount importance.

1.2.3 Aroforming

This process was designed by a joint venture between SALUTEC of Australia and IFP of France. It takes the exclusive advantage of transforming light naphtha, excess butanes and raffinate into aromatics. This process makes use of a fixed tubular reactor operated under an isothermal condition with zeolite catalysts which are cylindrical in shape.

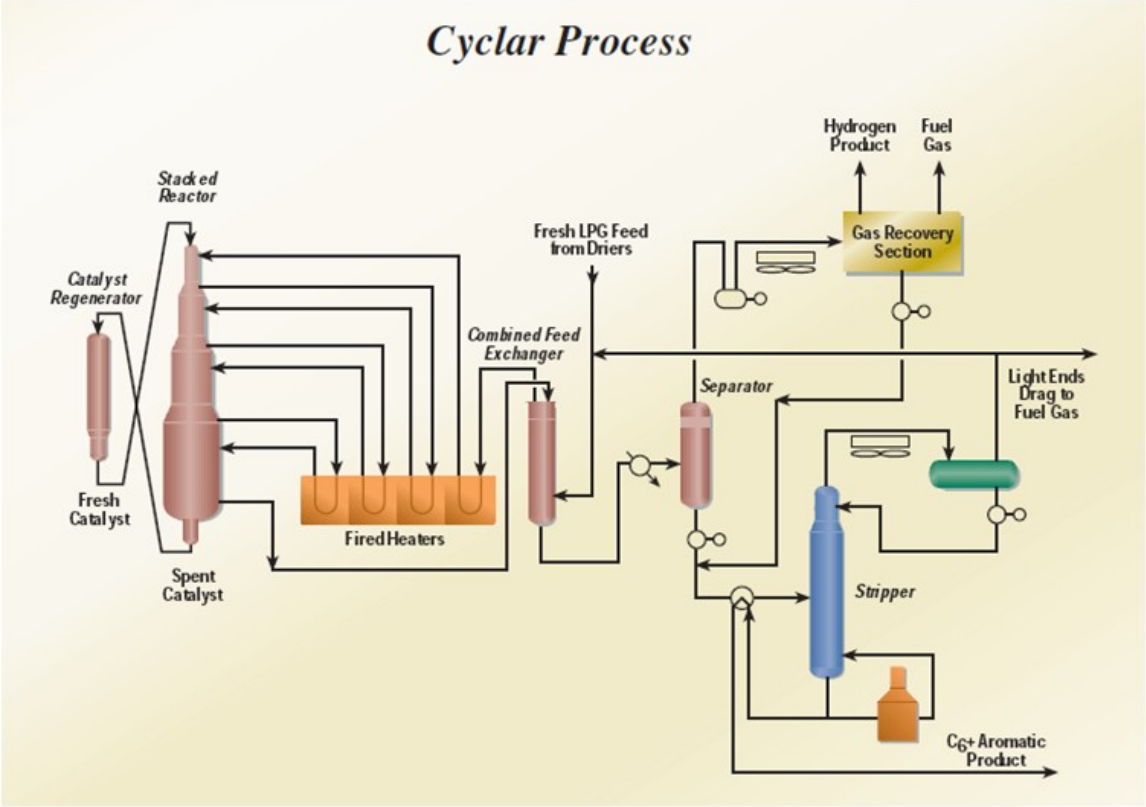

Fig.1.3: Schematic Diagram of the Cyclar Process [8]

1.3 Objective of this Thesis

The Objectives of this work are:

- To establish the improvement in catalytic activity of the commercial catalyst used in LPG aromatization that is gallium-containing HZSM-5 upon introduction of hierarchical pore topology.

- To compare the effect of different methods of introducing mesoporosity viz. desilication, surfactant mediated base hydrolysis and overgrowth of MCM-41 layer.
- To kinetically study the aromatization of propane using the above catalysts.

Elaborate specific objectives are given as follows:

1.3.1 Synthesis of Mesoporous Catalyst for Propane transformation into Aromatics

(i). Synthesis of mesoporous gallium-containing HZSM-5 catalysts via three different Methods which are desilication, surfactant mediated hydrolysis and overgrowth of MCM-41 layer.

(ii). Study the effect of these catalysts on the aromatization of propane.

(iii). Determination of the physicochemical properties of these catalysts by the use of BET, NH_3-TPD, XRD, FTIR of pure samples, FTIR of pyridine-absorbed samples, TPR and SEM of selected samples.

1.3.2 Catalyst Testing

The synthesized catalysts will be tested in a fixed bed reactor under an isothermal condition with temperature for optimum conversion at 540^{o}C. The time on stream for the screening test will be 5 hours under the flow of constant propane at 8mL/min.

1.3.3 Kinetic Modeling

A simplified model derived from a proposed mechanism for the propane aromatization over two catalysts –Ga/HZSM-5 and Ga/HZSM-5-SMH0.30 - will be developed. From

this model, kinetic parameters shall be determined and a comparison among the values of parameters from the three catalysts will be made

1.4 Thesis Overview

- **Chapter 2** dwells on the literature review on propane aromatization encompassing the varieties of catalysts used so far, drawbacks from the use of some of the catalysts, proposals on overcoming the drawbacks, advent of the use of mesoporous catalysts for aromatization, and an overview of various mechanisms proposed by different research groups.
- **Chapter 3** presents the experimental aspect of this work. The reactor and some of the equipment used are described. In addition, the synthesis and characterization of the catalyst used are explained in this section.
- **Chapter 4** deals with the results gotten from the use of the microporous and mesoporous gallium-containing HZSM-5 catalyst. Effect of varying the concentration of NaOH was also discussed.
- **Chapter 5** focuses on the development of the kinetic modeling for this reaction. MATLAB, via fourth order Runge-Kutta, was used in solving the system of differential equations and subsequently kinetic parameters (Activation energies and rate constants) were determined.
- **Chapter 6** presents the conclusions and recommendations for future work.

CHAPTER 2

LITERATURE REVIEW

2.1 Introduction

The aromatization of propane is an important reaction due to the ever-increasing demand for aromatics in the petrochemical industry. Increase in demand for aromatics has stirred up great interest in its production in the industry. This has also led to unending research, in the academia, on increasing selectivity towards benzene, toluene and xylene (BTX). Over the years, different catalysts for the conversion of paraffins to aromatics have been developed and it has been unanimously established that zeolite containing catalysts are the best for this conversion. The first exemplification of the use of ZSM-5 for the aromatization reaction is probably those of Chen [9] and of Cattanach [10] which describe the conversion of aliphatic liquids into aromatics. The M2-forming process, which uses HZSM-5, also gave encouraging result in the aromatization process but it has a low selectivity towards BTX [11].

T. Mole and J.R. Anderson [12] showed the better reactivity of Zinc-modified ZSM-5 over pure ZSM-5 when used for the transformation of propane to aromatics at temperatures within the bounds 730-820 K. Viswanadham N. et al [13] explained this by the stating that the zinc in the catalyst aids dehydrogenation of paraffins to form olefins which are the actual intermediates of the aromatization reaction.

Other metals which display the required dehydrogenating properties required for improved BTX selectivity and aromatic yield in the aromatization of alkanes are platinum, gallium, copper, iridium, germanium and rhenium. Thus, in order to enhance selectivity, metal-containing zeolites - Zn/ZSM-5, Pt/ZSM-5, Ga/ZSM-5- have been used for this aromatization reaction.

The use of Platinum for propane aromatization has been studied extensively and reported in the literature [23-27]. Platinum increases the transformation of propane into aromatics, most especially when it is properly dispersed [25, 26]. The doping of Platinum with HZSM-5 results in a different product distribution compared to when HZSM-5 is used. With this amalgamation, dehydrogenation to propene becomes the primary product because cracking, via acidic sites on HZSM-5, has been suppressed thereby leading to small amount of ethylene being formed. However, secondary reactions, which consequently reduce the selectivity of aromatics, are highly pronounced on platinum sites as shown below (not limited to this):

Hydrogenation of Olefins:

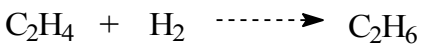

Hydrogenolysis of Methyl aromatics:

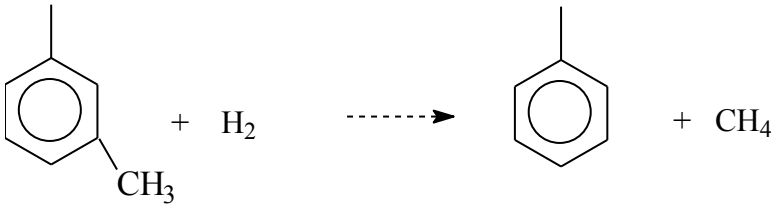

That is, a greater formation of methane and ethane is produced over Pt/HZSM-5 due to the intense hydrogenation of olefins and excessive hydrogenolysis of alkyl aromatics and alkanes on the metallic sites – this makes the reaction mechanism over Pt/HZSM-5 different from that of Ga/HZSM-5.

In order to reduce or eliminate this disadvantage of platinum staring researchers in the face, different metals were suggested to be added to it in such a way that platinum would serve as a promoting agent. Several authors have reported the addition of metals such as iridium, rhenium, lead, tin and lanthanum. The improvement in activity of the combination has been attributed to modification of the electron density of platinum with the exception of tin and lead because this caused a decrease in catalytic activity when tin [28-30] or lead [31,32] was used.

K. Arishtirova et al [33] reported the use of Cu/ZSM-5 for ethene aromatization. The presence of copper immensely improved the transformation as reflected and suggested in the changes observed in the dispersion and chemical state of copper via the use of electron paramagnetic resonance (EPR) and electron microscopy. With this catalyst, there was an increase in conversion of ethene and also increase in the yield of aromatics. They suggested copper takes part in the final stage of the transformation process which is the conversion of cycloalkanes into aromatics.

J. Guo et al [34] used rhenium-modified HZSM-5 catalyst for the aromatization of propane. There was a reduction of the strong acid sites upon introduction of rhenium into HZSM-5. The activity of this catalyst was compared with gallium-modified HZSM-5. The latter exhibited better selectivity to aromatics and yield of the same; although the

overall conversion of rhenium was higher than that of gallium. However, over this rhenium-modified HZSM-5 catalyst, the main reaction products at low conversion were ethylene and propylene.

Claudio et al [35] reported the transformation of propane over germanium-modified HZSM-5. Upon incorporation of germanium into HZSM-5, the activity for propane conversion increases; however decrease in aromatic selectivity was observed. NH_3-TPD revealed the decrease in strong acid site – which has been shown to be a major contributor to the cyclization of olefins to aromatics - upon addition of germanium. However, promoting this catalyst with platinum improved the selectivity to aromatics by decreasing the hydrogenolysis of propane.

Nevertheless, due to the reducing nature of the aromatization reaction, which comes from the generation of hydrogen in the first step of the reaction, a setback is created for the use of Zn/ZSM-5 because zinc is eluted from the catalyst during the reaction. On the other hand, the use of platinum as a promoter in the catalyst has been discouraged due to the high rate of coking which consequently blocks the pores of the zeolite.

The use of gallium-containing zeolite for propane aromatization has been well reported in the literature to be of great industrial application. It is well known that enhanced yield in aromatics over the catalyst is mainly attributed to the contribution of the gallium in the paraffin and naphthene dehydrogenation steps [36-38]. The literature on gallium-containing ZSM-5 indicates that the formation of aromatics is promoted over metal sites via the dehydrogenation of naphthenes which are formed from the complex reaction mechanism which involves the oligomerization of active olefins [39-43].

It has been established that this aromatization occurs over this catalyst via a bifunctional mechanism. In the light of this, the reaction mechanism for this aromatization reaction has been elaborated by different researchers and various conclusions have been drawn concerning the unique role of gallium cations in the reaction mechanism.

2.2 REACTION MECHANISM

Various researchers have proposed different reaction mechanisms for the aromatization of light alkanes. The most important step for this reaction is the activation of alkane which embodies the creation of initial carbenium ions [13]. Three paths have been outlined to be the different sources of these carbenium ions:

1. vestige of olefins that exist as scum or created through thermal decomposition;
2. amalgamation of paraffins with electron acceptor sites (EA) and subsequent decomposition [14-15]:

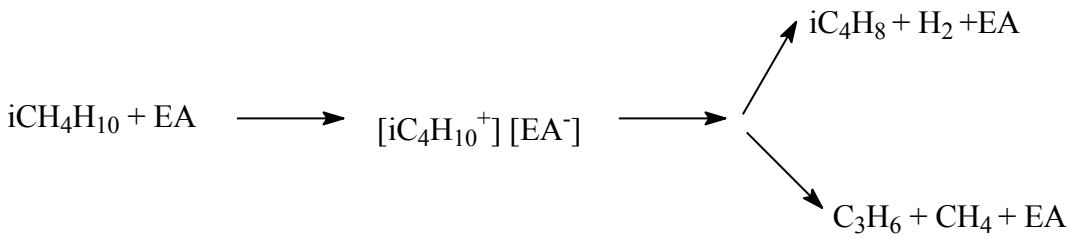

Scheme 1

3. amalgamation of alkanes with protons forming penta-coordinated carbonium ions and subsequent decomposition [16-18]:

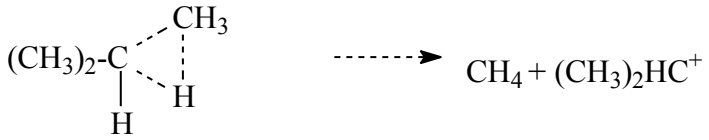

Scheme 2

This third path has been shown to be responsible for the primary products of methane and ethane from the transformation of propane over HZSM-5 at low conversion levels [19]. However, Kitagawa et al [20] showed the transient nature of the path as conversion of propane proceeds because of the sudden steady yield of methane as propane conversion proceeds. They suggested that the fashion of activation of propane changes after some time due to the withdrawal of hydride ions by carbenium ions (R^+).

$$C_3H_8 + R^+ \rightarrow RH + CH_3C^+HCH_3$$

M. Guisnet [21] has also shown that propylene, methane and ethylene are formed from the scission of the carbenium ion formed by the attack of the proton, from the acid site of the zeolite catalyst, on the propane species. This is also shown below:

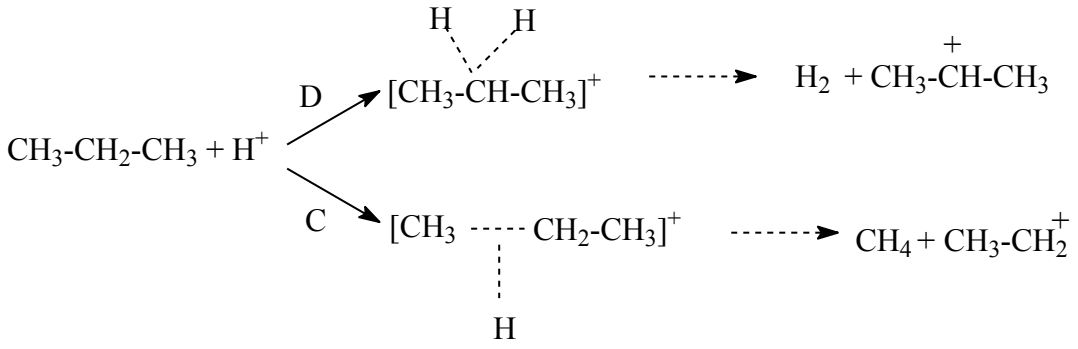

These carbenium ions formed usually react with alkenes to become larger carbenium ions or they may break down to give alkenes. Dessau and Haag [22] also proposed a similar mechanism for the cracking and dehydrogenation of propane as follows:

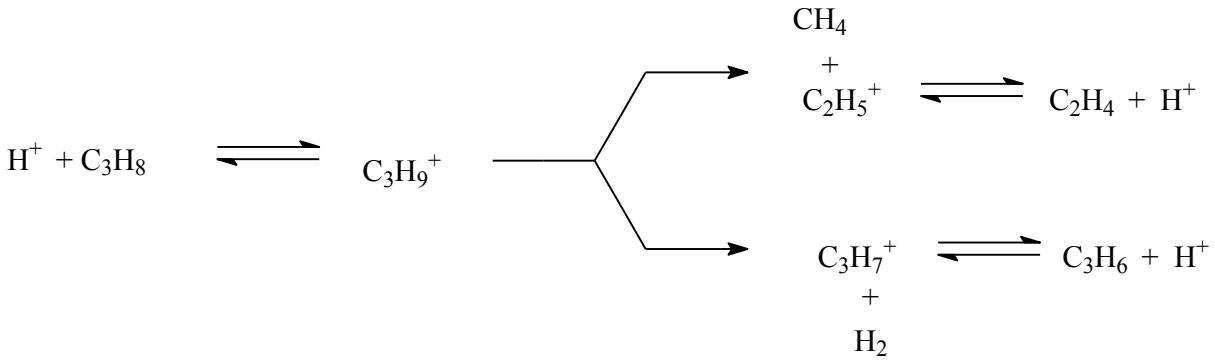

The next step is the attack, by proton from the acid site, of butylenes formed from the combination of two ethylene molecules:

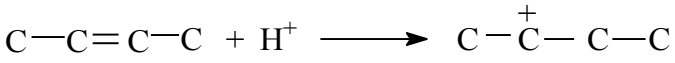

The butyl carbenium ion formed reacts with propane molecule as follows:

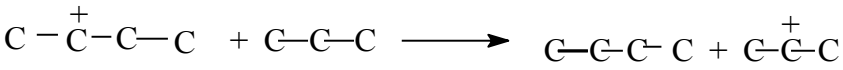

It also reacts with propene as follows:

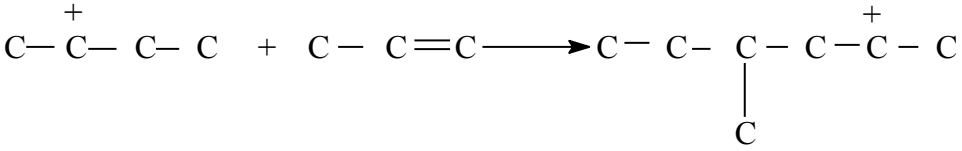

This carbenium ion has two options of splitting to give large olefinic hydrocarbons (hydrocarbons with carbon number greater than six):

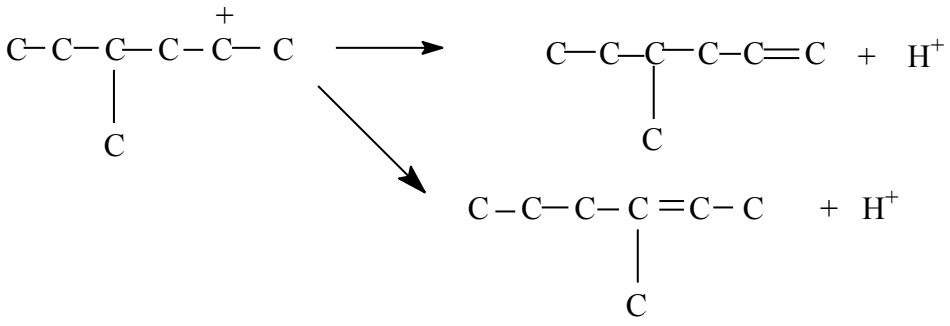

The next stage is the cyclization which also involved different steps because it is a complex reaction. The large olefins react with carbenium ion, via hydride transfer, formed from protonic attack on propane to form an olefinic carbenium ion:

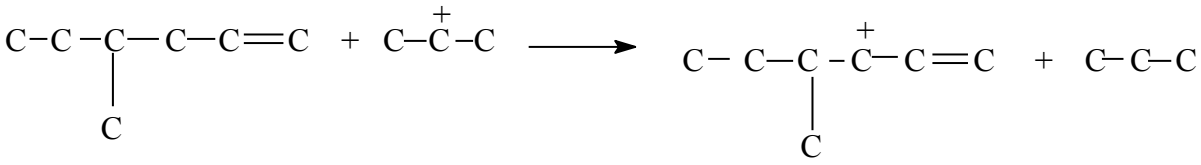

This olefinic carbenium ion then undergoes cyclization:

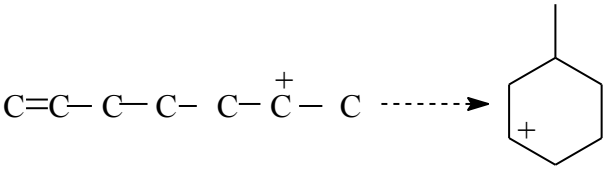

The last step is a series of hydrogen transfer reactions which involves the conversion of the cyclohexyl-carbenium ion into an aromatic compound:

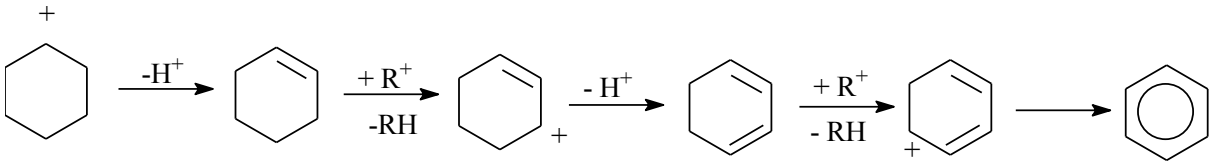

Consequently, according to the observation of the production distribution by Kitagawa et al, they proposed an overall mechanism given below:

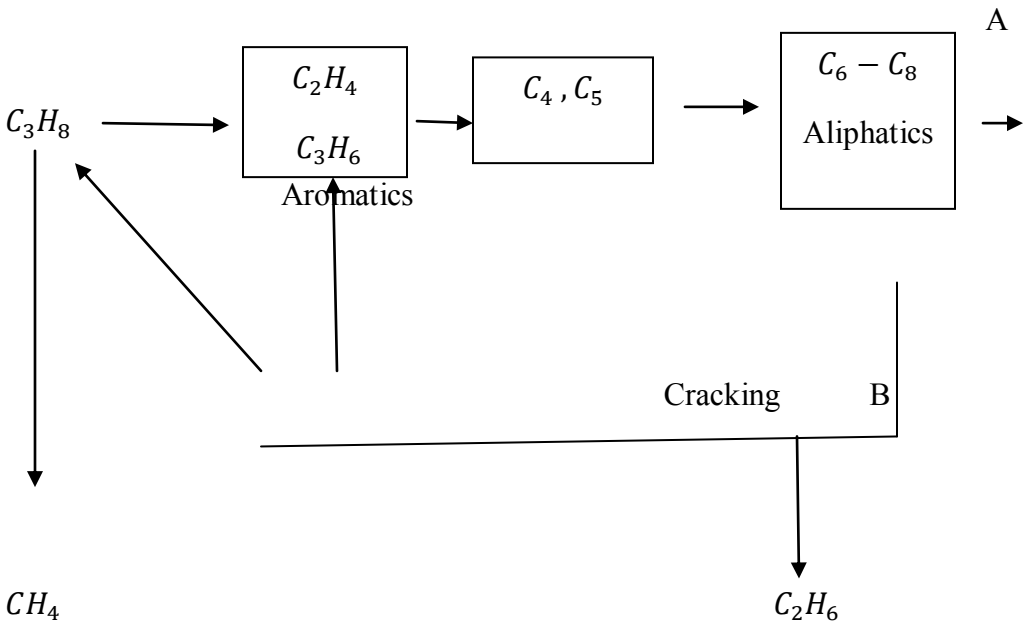

Overall Mechanism by Kitagawa et al[20]

The above mechanism suggests that aromatics and ethane come from the same source of large olefins where the aliphatics undergo cyclization to form aromatics or crack to form ethane. Also, propane yields ethylene and propylene which oligomerize in the hollows of the zeolite catalyst and subsequently undergo cracking to alkanes. Thus, under the reaction studied by Kitagawa, the dominant products of the reaction are alkanes and aromatics.

Guisnet M et al [7] also proposed an overall mechanism for the aromatization of propane as shown below:

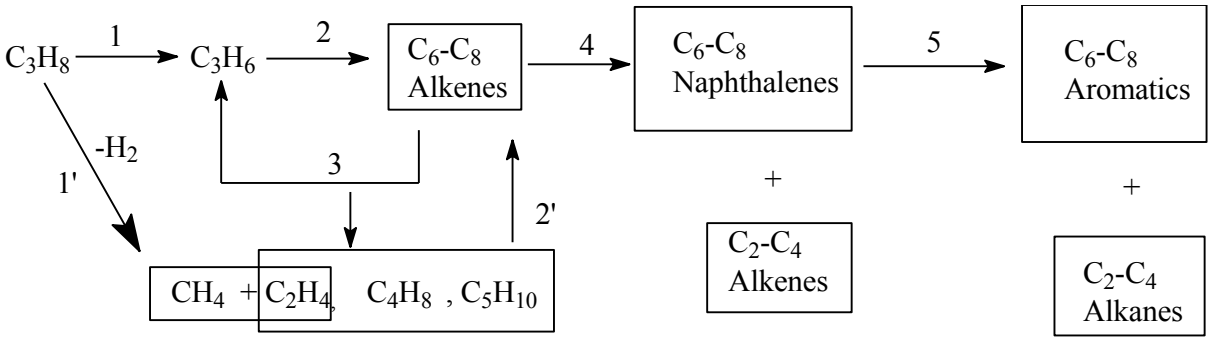

Overall Mechanism by Guisnet et al[7]

The above scheme was based on the product distribution seen when propane was transformed over HZSM-5. There was an ever increasing yield of methane which clearly suggests that it does not undergo secondary transformation. Also, they observed that propene and ethene underwent a maximum showing secondary transformation. Other secondary products include ethane, butanes, butenes and C_6-C_8 aromatics.

2.3 CONTEMPORARY APPROACH TO SOLVING AROMATIZATION PROBLEM

A lingering challenge that has been staring researchers, both in the academia and industry, in the face is the distribution and dispersion of gallium species in the catalyst structure. In proffering a solution to this challenge, different methods have been proposed. Izabela Nowak et al. [44] reported that pre-treatment of Ga/HZSM-5, obtained via ion exchange, under reducing-oxidizing cycles at 550^{o}C enhances the migration of gallium species into the zeolite structure. Moreover, V.R. Choudhary et al. [45] and N. Al-Yassir et al. [46] employed the in situ method, also called hydrothermal, for the proper dispersion of gallium species in the structure. This gave an encouraging result in

that there was proper interaction of the gallium species with protonic sites. However, extreme deactivation of the catalyst as a result of coking created a major set-back to its use.

Recently, researchers have introduced a method, which is the creation of mesopores in the zeolite crystals, for improving the dispersion and distribution of gallium species in the catalyst structure. This method creates a hierarchical pore arrangement in the structure in addition to the enlargement of the pores thereby preventing diffusional limitations on reactions that can cause high back pressure on flow systems [47]. Janssen et al. [48] reported mesopores formation in zeolite Y upon hydrothermal treatment (dealumination in acidic medium), which resulted into hollows in the crystals that connect the external surface to the interior of the crystal. Masaru Ogura et al. [49] also reported the formation of uniform mesopores in ZSM-5 Zeolite through treatment in alkaline solution.

Of great interest, both in the academia and industry, is the application of these zeolites with hierarchical pore arrangement to the conversion of lower alkanes to aromatics. M.N Akhtar et al. [50] investigated the role of intracrystalline mesoporosity of GaZSM-11 on the aromatization of lower alkanes and reported the development of intracrystalline mesoporosity with the structure upon treatment with alkaline solutions. They further observed improvement in the aromatization activity of this catalyst upon desilication. They supported their results by reporting that the higher conversion and improved selectivity can be credited to the enhanced accessibility to the active extra-framework Ga species owing to the generation of mesopores inside the zeolite particles which led to shortened contact time [50].

We have explored into the application of zeolites with hierarchical pore arrangement in propane aromatization and have reported the superior aromatization performance of mesoporous H-galloaluminosilicate obtained by CTAB-mediated base hydrolysis of steamed H-galloaluminosilicate. The catalyst displayed significant catalytic performance in propane aromatization with conversion of 56.3% as compared to 42.5% for steamed H-galloaluminosilicate. In addition, at comparable conversion level of ca.25%, the selectivity to aromatics of the ordered mesoporous H-galloaluminosilicate was 58.3% as compared to 42.5% for the conventional sample [51].

Thus, our first work [51] has shown for the first time that alkane aromatization over gallium-containing zeolites can be significantly improved upon the introduction of secondary network of mesopores connected to the native micropores of hydrothermally prepared Ga-containing zeolites. The proven advantages of hierarchical Ga-containing zeolite in alkane aromatization and the availability of wide range of approaches of distinctive effects to infuse mesoporosity into zeolite crystals have stimulated us to further continue the research work on developing Ga-containing HZSM-5 catalyst of hierarchal pore topology.

CHAPTER 3

EXPERIMENTAL SECTION

This section is divided into two parts:

PART A

3.1 Materials

No modification was carried out on all materials utilized in this experiment, that is, they were used the same way they were bought. Na_2SiO_3 solution, hydrated aluminum(III) tetraoxosulphate(VI)sulphate, hydrated gallium(III) trioxonitrate(VI), $(CH_3CH_2CH_2)_4$, $CH_3(CH_2)_{15}N(Br)(CH_3)_3$, tetraoxosulphate(VI) acid, Sodium Chloride, Ammonium Nitrate and β-Ga_2O_3 were bought from Sigma-Aldrich Company Ltd.

3.2 Zeolite synthesis and treatments

3.2.1 Hydrothermal (in situ) synthesis of conventional H-Galloaluminosilicate

The Catal. International company Ltd. (UK) was the supplier of the conventional HZSM-5, of Si/Al of 13.5, which was used. The H form of the gallium-containing aluminosilicate was prepared by hydrothermal crystallization from a mixture, of pH of 10, made up of H_2SO_4,$Al_2(SO_4)_3$,$Ga(NO_3)_3$,NH_4Br,$CH_3(CH_2)_{15}N(Br)(CH_3)_3$,and deionized H_2O. These were in an autoclave made of stainless steel at a temperature of 180^oC for 3 days. Classically, the preparation of galloaluminosilicate involves the mixing of two distinct solutions. The first was obtained by diluting a specific quantity of Na_2SiO_3 solution in deionized. The second solution was prepared by mixing a specific quantity of $Al_2(SO_4)_3$, $Ga(NO_3)_3$, $CH_3(CH_2)_{15}N(Br)(CH_3)_3$, tetraoxosulphate (VI) acid of 98% purity

and Sodium Chloride in deionized H_2O. These two were added together and vigorously agitated at room temperature for duration of one hour. Thereafter the mixture was placed in a 100ml Teflon container inside an autoclave made from stainless steel. This autoclave was then transferred into a rotating oven, rotating at 13 revolutions per minutes, at 180^oC and left for 3 days. At the end of 3 days, the content of the autoclave was filtered and washed several times with deionized H_2O, dried at room temperature for 8 hours, transferred into oven at 120^oC for further drying, then calcined in stagnant air at 550^oC for 5 hours with a heating ramp of 1^oC/min. In order to get the H form of the gallium-containing aluminosilicates, the resulting product was made to undergo a two-time ion-exchange with an ammonium nitrate solution of 2.2M concentration for three hours. Thereafter, the product was calcined. The steamed form of this catalyst was gotten by treating it with an air current, inside a reactor with volume of 200cm^3, of flow rate 50ml/min, which contains 60% steam at temperature of 550^oC and held for 3 hours.

3.2.2 Synthesis of ordered mesoporous H-Galloaluminosilicate and HZSM-5

Treatment of H-Galloaluminosilicate that had undergone steaming with CTAB hydrolysis under similar conditions to those reported by Wang et al. [58] leads to the hierarchical H-galloaluminosilicate. Usually, 2.45g of CTAB was dissolved in 55ml of NaOH solution of varying concentration between 0.10 and 0.65M. This was agitated at room temperature for two hours, after which 2.0g of either conventional HZSM-5 or steamed H-galloaluminosilicate was added and left to continue stirring for another two hours at room temperature. The solution was thereafter put in an autoclave of capacity 100ml made of stainless steel, placed in an oven at a temperature of 100^oC and left for 24

hours. After 24 hours, it was removed and cooled down and pH was adjusted to 9.0 using dilute tetraoxosulphate (VI) acid and then placed back into the oven and aged for another 24 hours in the same stationary form. The resulting product was then taken out, filtered, dried and calcined in order to be transformed into the H-form. The procedure for this is the same as that for the conventional H-galloaluminosilicate. We have assigned OH-/T to signify molar ratio of range 0.16 to 1.10, where T is the summation of the moles of Silicon, Aluminium and Gallium and OH- is the concentration of NaOH spanning 0.10 through 0.65M.

Samples prepared via this procedure are marked as ordered mesoporous H-Galloaluminosilicate (O.M.-Ga,AlZSM-5).

3.3 Characterization of catalysts

AAS (Atomic Absorption Spectroscopy) was used in the determination of the chemical composition of the prepared samples using Perkin-Elmer equipment.

Determination of the X-ray diffraction patterns at both low and high angles was achieved through the use of a Rigaku Miniflex II XRD system that uses CuKα radiation. These patterns were recorded between 2θ angles 1.2^{o} and 60^{o} at angular speed of 2^{o}/min and step size of 0.02^{o}. From this, the relative crystallinity of the two samples was calculated using the conventional relative crystallinity equation [59].

Surface areas of the catalyst samples were determined using Brunauer-Emmett-Teller (BET) technique. These textural properties were characterized using Quantachrome Autosorb 1-C analyzer engaging N_2 adsorption-desorption measurements. In a typical measurement, the samples were degassed at 220^{o}C under vacuum for 2h prior to N_2 physisorption. In order to determine the S_{BET} surface area, relative pressure in the

range from 0.02 to 0.3 on the desorption data was taken into consideration while at the same time Nitrogen molecule with cross-sectional surface area of 0.164nm^2 was assumed in the calculation. *t*-plot was used to discriminate between the influence from mesoporosity and microporosity in accordance to Lippens and de Boer [55]. Model proposed in the work of Kruk, Jaromiec and Sayari [60] was used to calculate mesopores size distribution.

To determine the morphology of few catalysts we have chosen, Electron Diffraction SEM (EDSEM) mappings and Scanning Electron Microscopy (SEM) images were carried out on them.

Microscopic equipment (JEOL JEM-2000 FX), which operates at 80 kV, was used to gather information on high resolution transmission electron microscopy images of selected samples. Ethanol was used to dissolve the samples ultrasonically in ethanol. Thereafter, they were placed on copper support with diameter of 3.0 mm.

Malvem Mastersizer, which is a particle size analyzer, was used in the measurement of the particle size of few chosen catalysts. This equipment covers sizes of particles which range between 0.02 and 2000μm.

^{27}Al and ^{71}Ga Magic Angle Spinning Nuclear Magnetic Resonance (MAS NMR) measurements were performed using Bruker Avance 400 MHz wide-bore spectrometer. ^{27}Al MAS NMR spectra were obtained by a single pulse length of π/4, and relaxation delay of 0.5 s. ^{71}Ga MAS NMR spectra were obtained using a Hahn-echo sequence with the following parameters: echo time to1/vr (*i.e.* ~ 70.6 us), repetition time to 2s, and spectral width to 1MHz. Rotors, of dimension 4mm, made of Zirconium oxide were used

to spin all samples at 12 kHz. References of Ammonium aluminum sulphate and gallium nitrate were used for the aluminum and gallium chemical shifts. In order to have accurate results, broadening of line and quadrupolar effects were avoided. This was achieved by placing specific samples, for a duration of 2 days, inside a desiccator which contains Ammonium Chloride of concentration 2.0M; thereby equilibrating them with water vapour. Quantachrome Autosorb 1-C analyzer was used for the experiment of temperature-programmed reduction in order to determine the degree of dispersion of gallium active species in the catalyst structure. In a typical determination, pretreatment (carried out under the flow of Helium) of about 0.25g of the desired catalyst was carried out for two hours at a temperature of 300^{o}C. Thereafter, the temperature was brought down to 50^{o}C under constant Helium flow. A mixture of Helium and Argon, with concentration of 66%, was used for the reduction at a temperature ramping of 10^{o}C/min with target temperature set at 1000^{o}C.

Bronsted and Lewis acid sites were determined via FTIR (Fourier Transform Infrared Ray) of selected samples upon which pyridine has been chemisorbed. This equipment is a Nicolet type of Magna 500 model. In a typical measurement, samples were made in wafer forms with weight of about 50 mg and diameter in alliance with that of the IR cell (i.e about 20 mm) made from Potassium Bromide. After placing the wafer in the IR cell, it was heated under vacuum at 450^{o}C for two hours. Thereafter, pyridine vapour was absorbed on the wafer for approx. 5 minutes followed by desorption of the same for two hours at a temperature of 150^{o}C. After two hours, the cell was cooled down and taken out of the set-up in order to measure the FTIR spectra. Removal of pyridine was also done at temperatures between 300^{o}C and 500^{o}C. Now, the following absorption

coeffients amd bands were used in characterizing the acid sites: pyridine (PyH^+) band at 1545 cm^{-1}, ε = 0.078 cm μmol^{-1}; pyridine (PyL) bands at 1454 cm^{-1}, ε = 0.165 cmμmol^{-1} [61,62].

Total acid sites (weak and strong) of the samples were determined by NH_3 adsorption-desorption technique. Samples were degassed at 300°C for 1 hr under a flow of He (50ml min^{-1}), after which temperature was brought down to 100°C. Thereafter, NH_3 was adsorbed for 15 min at 100°C. Samples were then degassed at 120°C for 1 hr, in order to remove physisorbed ammonia, after which further degassing was carried out at 700°C with heating rate of 15°C/min.

3.4 Catalytic experiments

The reactions of propane over microporous HZSM-5 and mesoporous gallium-containing HZSM-5 (ordered mesoporous H-galloaluminosilicate) were carried out in a fixed bed continuous flow micro-reactor with dimension$0.312\ I.D.\times$ $0.562\ O.D.\times 15.0\ cm\ length$. Reaction temperature was made constant at 540°C with flow rate of feed high enough to overcome any diffusional limitation. Catalysts were sieved to a particle size of 500-1000μm. Constant weight of the samples was used and fed into the reactor with constant volumetric flow rate of feed diluted with constant flow rate of N_2 (the ratio used was 2:1). The time on stream used for catalyst screening was 5 hours while that used for deactivation analysis was 10 hours. Analysis of reaction products was done on line using Varian GC with FID (Varian 450-GC), equipped with an HP-INNOWax capillary column (polyethylene glycol) (60m length × 0.32mm I.D. × 0.50μm film thickness). The total pressure in all experiments was 1atm.

PART B

Experimental

3.5. Materials and Reagents

The commercial ZSM-5 zeolites used in this study were supplied by Zeolyst; CBV2314, Nominal Si/Al_2 = 23, NH_4-form, and CBV8014, Nominal Si/Al_2 = 80, NH_4-form. Prior to post-synthesis treatments, the as-received NH_4-form zeolites were air-calcined at 550 °C for 5 h (3 °Cmin^{-1}), in order to get the H-form. Reagents used for post-synthesis treatments included gallium nitrate octahydrate, Tetraethylorthosilicate (TEOS, 98.99%, Aldrich), and Cetyl-trimethylammonium bromide (CTAB, Merck). All other reagents (e.g. NaOH, H_2SO_4, NH_4OH) were used without further purification.

3.6. Preparation of Ga-containing HZSM-5

Ga-containing HZSM-5 was prepared via aqueous incipient wetness impregnation method. In a typical preparation, appropriate amount of gallium nitrate octahydrate corresponding to Ga/(Al+Ga) of 0.1, 0.35 and 0.60 loadings was dissolved in deionized water. Subsequently, HZSM-5 powder (Si/Al = 11 or 40) was slowly added. The slurry was mixed at ambient temperature for 2 h, and then water was evaporated by placing the slurry inside an oven set at 50 °C. Finally, the resulting solid was dried at 100 °C and then calcined in standing air at 550 °C (holding time 5 h, ramping 3°Cmin^{-1}).

Samples obtained by impregnation are labeled as Ga(x)/HZ(y) where x and y indicate Ga/(Al+Ga), and Si/Al, respectively. For example, Ga0.1/HZ11 corresponds to Ga-containing HZSM-5 with Ga/(Al+Ga) of 0.1 and Si/Al of 11.

3.7. Synthesis of Mesoporous Ga-containing HZSM-5

Ga-containing HZSM-5 samples of hierarchical pore topology were prepared via variety of post-synthesis treatments in order to create random or ordered intracrystalline mesopores. In particular, four Ga-containing zeolites were modified: i) Ga/HZSM-5 of Si/Al = 11 and Ga/(Al+Ga) loading of 0.10 and 0.60; and ii) Ga/HZSM-5 of Si/Al = 40 and Ga/(Al+Ga) loading of 0.35 and 0.60. The procedures, which are presented in Scheme 1, are outlined below.

3.7.1. Alkaline treatments (Desilication)

Ga-containing HZSM-5 was modified by one cycle of desilication with 0.02, 0.05, 0.10 and 0.20 M NaOH solutions at 60 °C for 2 h, under atmospheric pressure. Typically, 240 ml of the desired NaOH solution was heated up to 60 °C in a flask connected to a reflux, then 4 g of Ga0.1/HZ11 (for example) was added and the mixture was vigorously stirred for 2 h. The zeolite suspension was then cooled down immediately using an ice bath, and subsequently was isolated by suction filtration. The product was washed thoroughly with deionized water until the pH is neutral. It was then dried at ambient temperature, followed by drying at 100 °C overnight. Then, the dried alkaline-treated samples were transformed into ammonium form by twofold ion-exchange with 2.2 M of ammonium chloride at 90 °C for 3 h (1.0 g solid per 50 ml solution) without calcination between ion-exchange procedures. The samples were subjected to typical drying treatments followed by calcination to get the H-form in standing air at 550 °C (holding time 5 h, 3°Cmin^{-1}). The samples are hereafter designated as Ga(x)/HZ(y)-DS(z), where x, y, z, and DS correspond to Ga/(Al+Ga), Si/Al, [NaOH], and desilication treatment, respectively. For example, Ga0.1/HZ11-DS0.10 corresponds to alkaline

treatment of Ga-containing HZSM-5 (Ga/(Al+Ga) = 0.1, Si/Al = 11) using 0.10 M of NaOH solution.

3.7.2. Surfactant-mediated assembly of Ga-containing HZSM-5 zeolite seed into mesoporous MCM-41 structure

Ga-containing HZSM-5 of hierarchal pore topology containing ordered mesopores was prepared via surfactant-mediated hydrolysis (that is, hydrothermal treatment with NaOH in the presence of cationic (CTAB) surfactant) of parent Ga-containing HZSM-5. The procedures were similar to those reported by Al-Yassir *et al.* [51 and reference therein]. In a typical synthesis, 2.45 g of CTAB was dissolved in a solution containing 55 ml of x M NaOH (x = 0.10, 0.20, 0.30, 0.40, and 0.50 M). The solution was stirred at ambient temperature for 1 h. Then, 2.0 g of Ga0.1/HZ11 (for example) was dispersed in the hydrolysis solution for 1 h at ambient temperature. The resulting mixture was transferred into 100 ml Teflon-lined stainless steel autoclave, which was hydrothermally aged at 100 °C for 24 h under static conditions. The pH of the mixture after cooling to ambient temperature was adjusted to *ca.* 9.0 by addition of dilute H_2SO_4 with stirring. The gel mixture was then hydrothermally aged again at 100 °C for another 24 h under static conditions. The resulting solid was separated and treated (drying, calcination and transformation into the H-form) following similar procedures as those of alkaline treated samples. Samples obtained by this method are designated as Ga(x)/HZ(y)-SMH(z), where x, y, z, and SMH correspond to Ga/(Al+Ga), Si/Al, [NaOH] in Molarity, and surfactant mediated hydrolysis, respectively (e.g. Ga0.1/HZ11-SMH0.40 corresponds to CTAB mediated hydrolysis of Ga/HZSM-5 (Ga/(Al+Ga) = 0.1, Si/Al = 11) using 0.40 M of NaOH solution).

3.7.3. Surfactant-mediated coating of Ga-containing HZSM-5 zeolite with mesoporous MCM-41 structure (overgrowth of MCM-41 layer)

The synthesis of MCM-41 on pre-added Ga-containing HZSM-5 was carried out according to a protocol described elsewhere [54] with few deviations. Typically, 2.45 g of cationic CTAB was dissolved in 50 ml aqueous HCl solution (0.30 M), and then 2.0 g of Ga0.1/HZ11 (for example) was added to the solution after 1 h. After stirring for 2 h, 3.50 g of TEOS was added dropwise under stirring to the mixture. The mixture was stirred for additional 2 h followed by pH adjustment to ca. 9.0 by adding concentrated NH_4OH (14.8 M). Then, the gel mixture was transferred into 100 ml Teflon-lined stainless steel autoclave and hydrothermally aged at 100 °C for 24 h under static conditions. The resulting solid was separated, washed thoroughly with deionized water, and then treated following similar drying and calcination procedures as those of alkaline treated samples. Overgrowth-type MCM-41 on pre-added Ga-containing HZSM-5 composite samples are designated as MCM-41//Ga(x)/HZ(y), where x and y correspond to Ga/(Al+Ga) and Si/Al ratios, respectively.

3.8. Synthesis of Mesoporous HZSM-5

Parent HZSM-5 containing mesostructure was prepared via the three post-synthesis methods described above; desilication, surfactant-mediated hydrolysis, and surfactant-mediated coating. The procedures were similar to those of Ga-containing HZSM-5 samples, with one exception that the starting material is the parent HZSM-5

(Si/Al = 11 or 40). Mesoporous HZSM-5 samples obtained by desilication, surfactant-mediated hydrolysis, and surfactant-mediated coating are hereafter noted as HZ(x)-DS(y) (x: Si/Al, DS: desilication, and y: [NaOH] in Molarity), HZ(x)-SMH(y) (x: Si/Al, SMH: surfactant-mediated hydrolysis, and y: [NaOH] in Molarity), and MCM-41//HZ(x) (x: Si/Al), respectively.

3.9. Synthesis of Ga-containing mesoporous HZSM-5

Ga-containing mesoporous HZSM-5 (regardless of the type of mesoporous HZSM-5) was prepared via aqueous incipient impregnation, following similar procedures as those of Ga-containing HZSM-5. The samples are hereafter designated as Ga(x)/DS(y)-HZ(z) (x, y, z, and DS correspond to Ga/(Al+Ga), [NaOH] in Molarity, Si/Al, and desilication treatment); Ga(x)/SMH(y)-HZ(z) (x, y, z, and SMH correspond to Ga/(Al+Ga), [NaOH] in Molarity, Si/Al, and surfactant mediated hydrolysis treatment); and Ga(x)/MCM-41//HZ(y) (surfactant-mediated coating treatment, x and y correspond to Ga/(Al+Ga), and, Si/Al)).

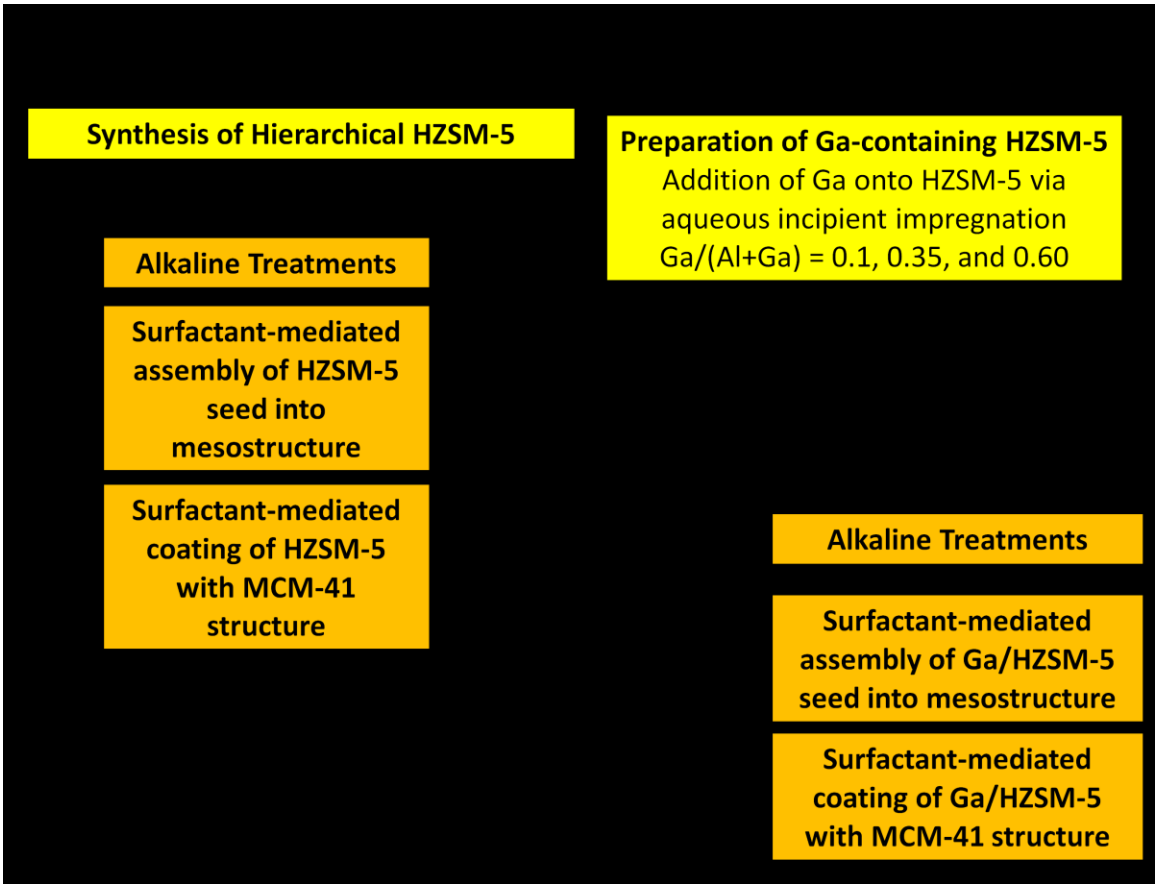

Scheme 1: Summary of experimental routes for the synthesis of selective Ga-containing HZSM-5 for lower alkane aromatization.

3.10. Characterization.

The amounts of Si, Al, and Ga in the solids and filtrates were determined by inductively coupled plasma spectrometer (ULTIMA 2, ICP-OES) from HORBIA scientific.

Textural properties were characterized by N_2 adsorption-desorption measurements at 77 K, using Quantachrome Autosorb 1-C adsorption analyzer. Samples were outgassed at 220 °C under vacuum (10^{-5} Torr) for 3 h before N_2 physisorption. The Brunauer-Emmett-Teller (BET) specific surface areas were determined from the dsorption data in the relative pressure (P/P_0) range from 0.06-0.3, assuming 0.164 nm^2 for the cross-section of the N_2 molecule. Contribution of micropore and mesopores was derived from the *t*-plot method according to Lippens and de Boer [55]. Whereas, the mesopore size distribution was calculated using the Barret-Joyner-Halenda (BJH) pore size model applied to the adsorption branch of the isotherm [56].

Hg porosimetry measurements were carried out in a Micromeritics Auto Pore IV system. This technique provides information about mesoporosity (thus further confirms the N_2 adsorption-desorption measurements), and accessibility and interconnectivity of the pores [57].

Low- and high- angle X-ray diffraction patterns were recorded on a Rigaku Miniflex II XRD powder diffraction system using CuKα radiation ($\lambda_{K\alpha 1}$ = 1.54051Å, 30 Kv and 15 mA). The XRD patterns were recorded in the static scanning mode from 1.2 - 60° (2θ) at a detector angular speed of 2 °/min and step size of 0.02°.

Transmission FTIR spectra of lattice vibration were recorded in the 400 - 1200 cm^{-1} range, at 4 cm^{-1} resolution, using Nicolet FTIR spectrometer (Magna 500 model).

Scanning Electron Microscopy (SEM) was performed on selected samples to determine the particle size, morphology, and surface elemental compositions. The SEM images, electron diffraction SEM (EDSEM) mappings, and energy-dispersive X-ray spectroscopy were recorded using FESEM/FIB (Tescan Lyra-3). The field Emission Dual Beam (Electron/ Focused Ion Beam) system combines high-end field-emission scanning electron microscope (FESEM) and high-performance focused ion beam (FIB) system in one chamber.

^{27}Al and ^{29}Si Magic Angle Spinning (^{27}Al and ^{29}Si MAS NMR) measurements were performed using Bruker Avance 400 MHz wide-bore spectrometer. ^{27}Al MAS NMR spectra were obtained by a single pulse length of $\pi/4$, and relaxation delay of 0.5 s. The ^{29}Si MAS NMR spectra were obtained by 20 pulse (B1~55HZ) followed by 13 ms acquisition with ^{1}H decoupling (tppm, B1~55 HZ). All studied samples were spun at ca.12 KHz in Air using 4 mm ZrO_2 rotors. The Al and Si chemical shifts were referenced to $(NH_4)Al(SO_4)_2$ and 4,4-dimethyl-4-silapentane-1-sulfonic acid, respectively.

Temperature-programmed reduction (TPR) measurements were carried out using Micromeritics chemisorb 2750. Typically, about 100 mg of sample was pretreated at 300 °C for 2 h (ramping rate of 10 ºCmin^{-1}) under argon flow. After cooling the sample to 50 ºC in argon flow, the reduction was performed in a mixture of 66% H_2/Ar flowing at flow of 20 mlmin^{-1} and heating rate of 10 °Cmin^{-1}, up to 1000 °C. Hydrogen consumed during TPR run was monitored by a thermal conductivity detector.

NH_3-Temperature-Programmed Desorption (NH_3-TPD) was carried out using Micromeritics chemisorb 2750 equipped with a mass spectrometry detector (Cirrus 2, mks, spectra products). Samples (ca. 50 mg) were pretreated at 300 °C in a flow of helium

(25 $mlmin^{-1}$) for 2 h. This was followed by the adsorption of 10% NH_3/He at 100 ºC for 30 min. Samples were then purged in a helium stream for 2 h at 100 ºC in order to remove loosely bound ammonia (i.e. physisorbed and H-bonded ammonia). Then, the samples were heated again from 100 to 700 ºC at a heating rate of 10 $ºCmin^{-1}$ in a flow of helium (25 $mlmin^{-1}$) while monitoring the evolved ammonia using TCD.

Infrared spectroscopy of adsorbed pyridine was used to determine the types of available acid sites (i.e. Brɒnsted and/or Lewis acid sites). The measurements were carried out using a Fourier transform infrared using Nicolet FTIR spectrometer (Magna 500 model). The samples in the form of a self-supporting wafer (*ca.* 40 mg in weight and 20 mm in diameter) were obtained by compressing a uniform layer of powder. The wafer was then placed in an infrared vacuum cell equipped with KBr windows (Makuhari Rikagaku Garasu Inc., JAPAN), and pretreated under vacuum (P = *ca.* 2 x 10^{-5} Torr) at 300 °C for 2 h. The pretreated wafer was then contacted with pyridine vapor at ambient temperature for 5 min, followed by evacuation at 150 °C for 1 h. The IR cell was then cooled down to ambient temperature and placed in an IR beam compartment while under vacuum and transmission spectra were recorded. Desorption of pyridine was also carried out at 350 and 450 °C in order to evaluate the strength of Brɒnsted and Lewis sites. For a quantitative characterization of acid sites, the extinction coefficient ratio ($R_\varepsilon = \varepsilon_{1450}/ \varepsilon_{1550}$) (1450 and 1550 cm^{-1} bands correspond to Lewis and Brɒnsted sites) was calculated experimentally.

3.11. Catalytic Experiments.

The aromatization of propane over conventional and mesoporous Ga-containing HZSM-5 as well as parent HZSM-5 was carried out in a fixed bed tubular reactor

(stainless steel tube (0.312 I.D. x 0.562 O.D. x 15.0 cm length)). In a typical experiment, the reactor was charged with 1.0 ml of catalyst previously sieved to a particle size of 0.5 - 1.00 mm diameter. The feed was propane in nitrogen (the ratio of N_2 to feed was 2:1). All reactions were carried out at reaction temperature of 540 ºC, GHSV (gas hourly space velocity) of 1600 h^{-1}, 5 hours TOS (time-on-stream), and atmospheric pressure. Space velocity was varied within the range of 2200 - 30,000 h^{-1} in order to evaluate the products selectivity at comparable propane conversion level. The quantitative analysis of the reaction products were carried out on line using Varian GC with FID (Varian 450-GC), equipped with an HP-INNOWax capillary column (Polyethylene glycol (PEG)) (60 m length x 0.32 mm I.D. x 0.50 μm film thickness).

CHAPTER 4

4A. RESULTS AND DISCUSSIONS

4.1. Chemical composition and structural-textural-morphological properties

It is clear the Si/Al and Si/(Al+Ga) ratios of typical HZSM-5 and H-Galloaluminosilicate respectively did not change significantly upon treatment with surfactant-mediated base hydrolysis as depicted in table 4.1. Furthermore, the concentration of sodium hydroxide used in the treatment had no considerable effect on the ratios irrespective of the precursors used in the zeolite. The experimental Si/(Al+Ga) ratio for ordered mesoporous H-Galloaluminosilicate was in the range of 8.90 – 9.10 for the OH^-/T molar ratio of 0.16 – 1.10, compared to 9.80 for steamed conventional H-Galloaluminosilicate. The range for the silicon to aluminum ratio for hierarchical HZSM-5 was between 11.6 and 11.1 as compared to 13.0 for conventional HZSM-5 (Table 4.1).

Table 4.1. Textural properties of conventional and ordered mesoporous H-Galloaluminosilicate and HZSM-5 catalysts

Catalyst	Si/M [a]	Textural Properties				Structural Parameters				RC (%) [h]
		S_{BET} (m^2g^{-1})	V_{tot} (cm^3/g) [b]	V_{micro} (cm^3/g) [c]	S_{meso} (m^2g^{-1}) [d]	d_{meso} (nm) [e]	d_{100} (nm)	a_0 (nm) [f]	t (nm) [g]	
con-HZSM-5	13.0	299	0.18	0.17	17.1	-	-	-	-	100
CTAB- mediated hydrolysis in NaOH ($x = OH^-/T$)										
x = 0.16	11.6	302	0.18	0.17	19.1	-	-	-	-	79
x = 0.41	11.5	343	0.29	0.16	31.0	-	-	-	-	63
x = 0.57	11.2	471	0.38	0.14	128	3.26	3.51	4.05	0.79	55
x = 0.65	11.2	473	0.39	0.13	130	3.26	3.53	4.08	0.82	48
x = 0.75	11.3	626	0.52	0.11	142	3.27	3.51	4.05	0.78	46
x = 1.10	11.1	645	0.59	0.08	306	3.26	3.48	4.02	0.76	33
con-Ga,AlZSM-5	9.74	324	0.20	0.17	38.4	-	-	-	-	77
s-Ga,AlZSM-5	9.80	277	0.19	0.16	31.5	-	-	-	-	74
CTAB- mediated hydrolysis in NaOH ($x = OH^-/T$)										
x = 0.16	8.90	341	0.24	0.16	40.1	-	-	-	-	67
x = 0.41	9.25	393	0.30	0.14	59.2	-	-	-	-	54
x = 0.57	9.31	421	0.32	0.12	107	2.90	3.48	4.01	1.11	51
x = 0.65	9.30	428	0.32	0.12	114	2.89	3.48	4.01	1.12	47
x = 0.75	9.27	434	0.35	0.11	120	2.88	3.48	4.02	1.14	41
x = 1.10	9.10	573	0.49	0.07	288	3.10	3.52	4.06	0.96	30

[a]: M = Al (HZSM-5) or Ga + Al (Ga,AlZSM-5); [b]: total pore volume calculated from the adsorption isotherm at $P/P_0 = 0.98$; [c]: micropore volume calculated using the *t*-plot [55]; [d]: S_{meso} includes the mesoporous and external surface area; [e]: mesopore average pore diameter was calculated using from the adsorption branch using the Kruk, Jaroniec, Sayari (KJS) method [60]; [f]: unit cell of the mesoporous phase (lattice parameter from the XRD data using the formula $a_0 = 2d_{100}/\sqrt{3}$), [g]: pore wall thickness ($t = a_0 - d_{meso}$), and [h]: Relative crystallinity (RC) based on XRD measurements.

The XRD patterns of conventional and ordered mesoporous H-Galloaluminosilicate and HZSM-5 at low- and wide-angle are shown in Fig. 4.1. Table 4.1 also shows the structural parameters of the catalysts. The XRD patterns of conventional H-Galloaluminosilicate and HZSM-5 (Fig.4.1A-B (a)) revealed the presence of highly crystalline MFI samples, as inferred from the sharpness of reflection lines in the 22.5 - 25.0 º 2θ range. No XRD reflections belonging to segregated bulk β-Ga_2O_3 particles can be resolved from the XRD patterns, which imply that Ga species exist as highly dispersed extracrystalline (nanosized) oxide at the external zeolite surface and/or dispersed framework or extra framework species. Figure 4.1Aa` depicts that there was no apparent difference in the crystallinity of conventional H-galloaluminosilicate after steaming was carried out. The XRD patterns of ordered mesoporous H-Galloaluminosilicate and HZSM-5 display well-resolved patterns with reflection lines in the low- and high- 2θ regions. In the low 2θ region, that is 1.2 - 4°, the patterns display three distinct diffraction peaks indexed as (100), (110) and (200). These peaks are characteristic of 2D-hexagonal mesostructure MCM-41 with a space group of *p6mm* symmetry [63]. In the high 2θ region, that is, 5.0 - 45°, all of the major peaks that are characteristics of HZSM-5 can be identified. The XRD patterns also showed that the formation of ordered mesostructure and presence of high crystallinity zeolites are dependent on the [NaOH] (OH^-/T). No sign of ordered mesostructure can be seen for samples obtained with low [NaOH] (OH^-/T ratio up to 0.41), whereas high OH^-/T ratio (1.10) resulted in poorly crystalline zeolites (Table 4.1). It can be also seen that the unit cell of MCM-41 phase for ordered mesoporous H-Galloaluminosilicate and HZSM-5 was slightly affected by the OH^-/T ratio.

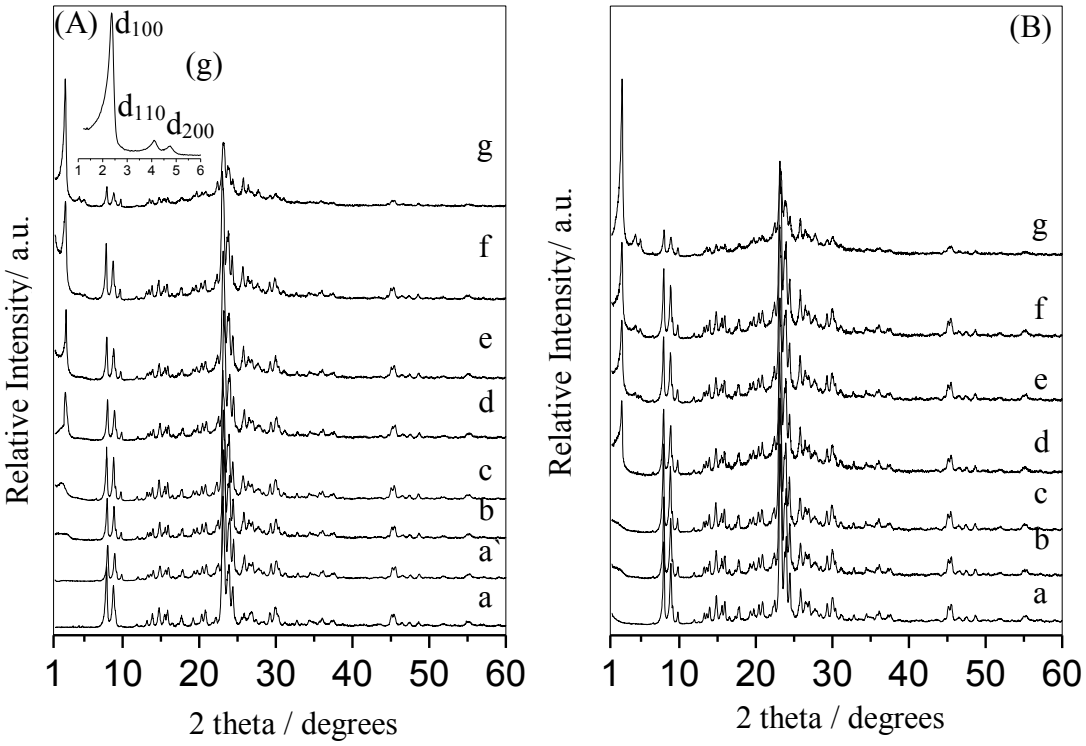

Figure 4.1. Low- and wide- angle X-ray powder diffraction patterns of calcined conventional and ordered mesoporous H-Galloaluminosilicates (A) and HZSM-5 (B) formed by CTAB-mediated hydrolysis using different [NaOH] (expressed in terms of (OH^-/T)); a) con-HZSM-5 or con-Ga,AlZSM-5, a`) s-Ga,AlZSM-5, b) 0.16, c) 0.41, d) 0.57, e) 0.65, f) 0.75 and g) 1.10.

Figure 4.2 shows the FTIR spectra of the typical HZSM-5 and structured mesoporous H-galloaluminosilicate. These spectra are clearly seen in the lattice vibration region (400 - 1400 cm^{-1}). Features of peaks designation [64,65] are also depicted in the figure. This figure clearly revealed the strong band around 550 cm^{-1} for the steamed conventional H-Galloaluminosilicate. Moreover, we see gradual reduction of the 550 cm^{-1} band relating to the ordered mesoporous samples upon a rise in the OH^-/T ratio irrespective of the zeolite precursor. So we see a consistency of the FTIR result with the XRD result in that the crystallinity of zeolite is gradually lost. The FTIR further revealed the movement of the band around 1100 cm^{-1} to lower wave number as a result of increase in the concentration of NaOH, that is, for the hierarchical zeolite there was a decrease from 1089 to 1073 cm^{-1}; while for the typical zeolite there was a drop from 1098 to 1080 cm^{-1}.

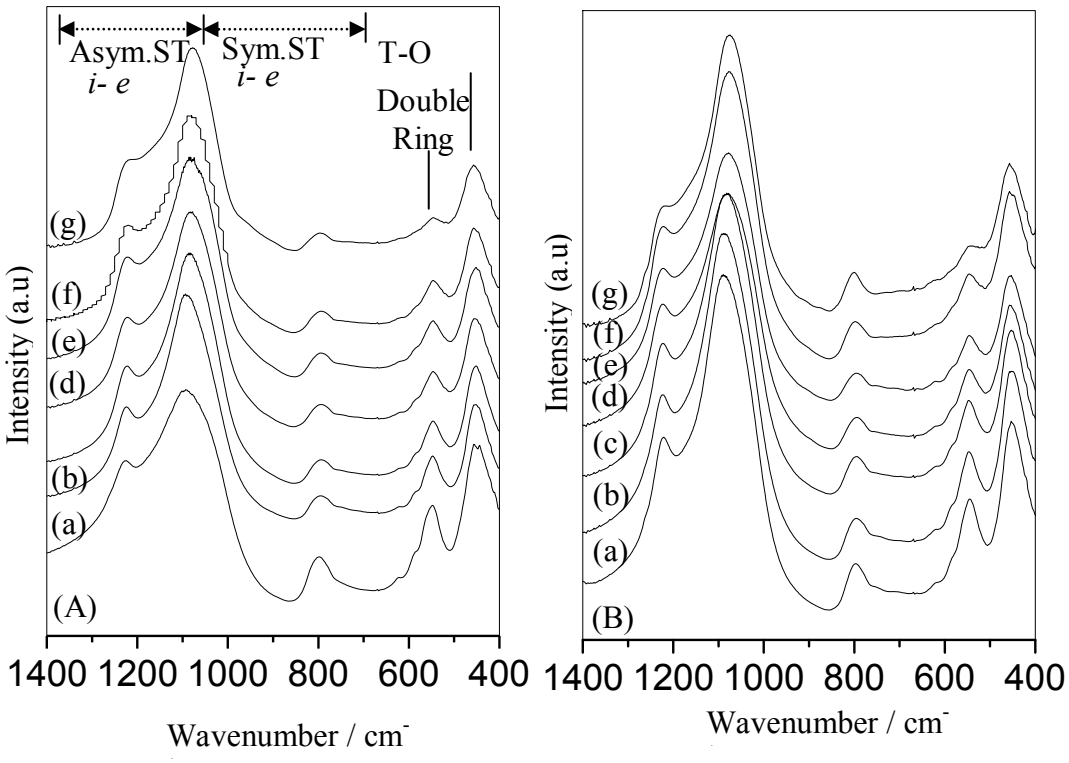

Figure 4.2. FT-IR spectra of conventional and mesoporous HZSM-5 (A) and H-Galloaluminosilicate (B) formed by surfactant mediated hydrolysis in NaOH of variable concentration (OH^-/T); a) 0.0 (con-HZSM-5 or con-GaAlZSM-5), b) 0.16, c) 0.41, d) 0.57, e) 0.65, f) 0.75, and g) 1.10. (T = framework cation (Si, Al or Ga); Asym.ST and Sym.ST correspond to asymmetric and symmetric stretch, respectively; and i-e: Internal (intra-tetrahedral)-External (inter-tetrahedral) vibrations).

The Nitrogen sorption isotherms for conventional and ordered hierarchical HZSM-5 and that of H-Galloaluminosilicate with optimum hydrolysis concentration ($OH^-/T = 0.57$) are shown in Figure 4.3A. Also, Table 4.1 shows the textural properties of all samples used in this study. The microporous nature of both the steamed conventional H-Galloaluminosilicate and conventional HZSM-5 is exhibited via the isotherm shape (type I) of the nitrogen adsorption-desorption (Figure 4.3). After treating these catalysts by the surfactant mediated hydrolysis route, we observed a Nitrogen sorption isotherm characteristic of mesoporous materials. These isotherms are of the fourth type [63,66] irrespective of the NaOH concentration (OH^-/T higher than 0.41) and zeolite precursors. These isotherms display sharp inclination at very low relative pressures (between 0.2 and 0.4). The sharp inclination is simply as a result of the filling of the secondary networks (mesopores) with nitrogen. At higher relative pressures, there is an enhanced adsorption of nitrogen in the pores of the catalyst structure due to loss of part of the hexagonal mesopores therefore leading to haphazardly-structured particles. A side-by-side analysis of the isotherms of conventional ordered mesoporous HZSM-5 and the one for hierarchical H-galloaluminosilicate showed that the latter displays more inclined step at low relative pressures (P/P_o). That was not the case for ordered mesoporous HZSM-5 which displayed a lesser inclination at low pressures and a little movement to higher relative pressures.

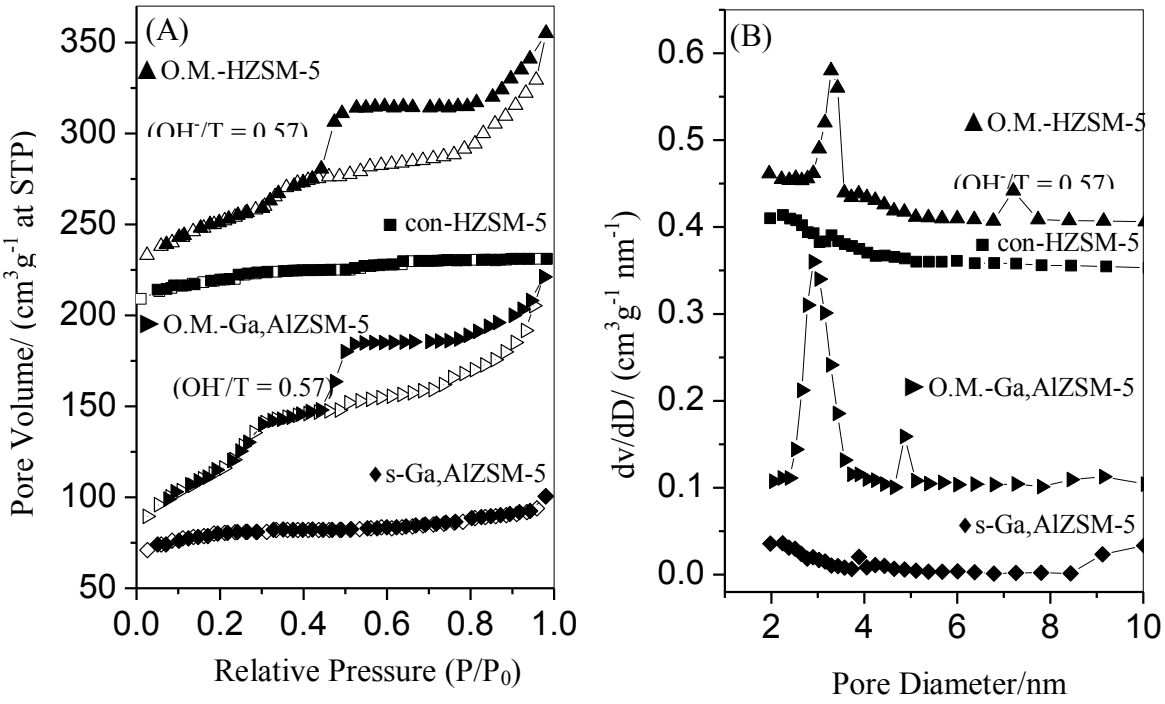

Figure 4.3. N_2 adsorption-desorption isotherms (A) and derived BJH mesopore size distribution (adsorption branch) (B) of conventional and ordered mesoporous H-Galloaluminosilicate formed by surfactant-mediated hydrolysis in NaOH of OH^-/T = 0.57.

In support of these, Figure 4.3B shows the Pore Size Distribution of these samples depicting the freshly created mesopores having pore diameter of approximately 3.00 nm. Ordered mesoporous H-Galloaluminosilicate, having a hydrolysis concentration-metallic (Si+Al+Ga) molar ratio of 0.57, displayed a surface area attributed to mesopores and having a numerical value that equals 107 m^2/g. This value is 250 % greater than that of its steamed conventional counterpart having a mesoporous surface area of 31.5 m^2/g. Nevertheless, there was a 25% decrease in the volume of the micropore upon treatment with CTAB-mediated hydrolysis as shown in Table 4.1. Likewise, treatment of conventional HZSM-5 with CTAB-mediated hydrolysis led to a 648.5% increase in the mesoporous surface area while the micropore volume decreased from 0.17 cm^3/g to 0.14 cm^3/g as shown in Table 4.1.

Scanning Electron Microscopy (SEM) and High Resolution Transmission Electron Microscopy (HRTEM) gave exciting results revealing the characteristics of our synthesized ordered mesoporous H-Galloaluminosilicate. The SEM images of conventional HZSM-5 and its treated counterpart are shown in Fig. 4.4A; this figure also includes that of H-galloaluminosilicate and its treated counterpart.

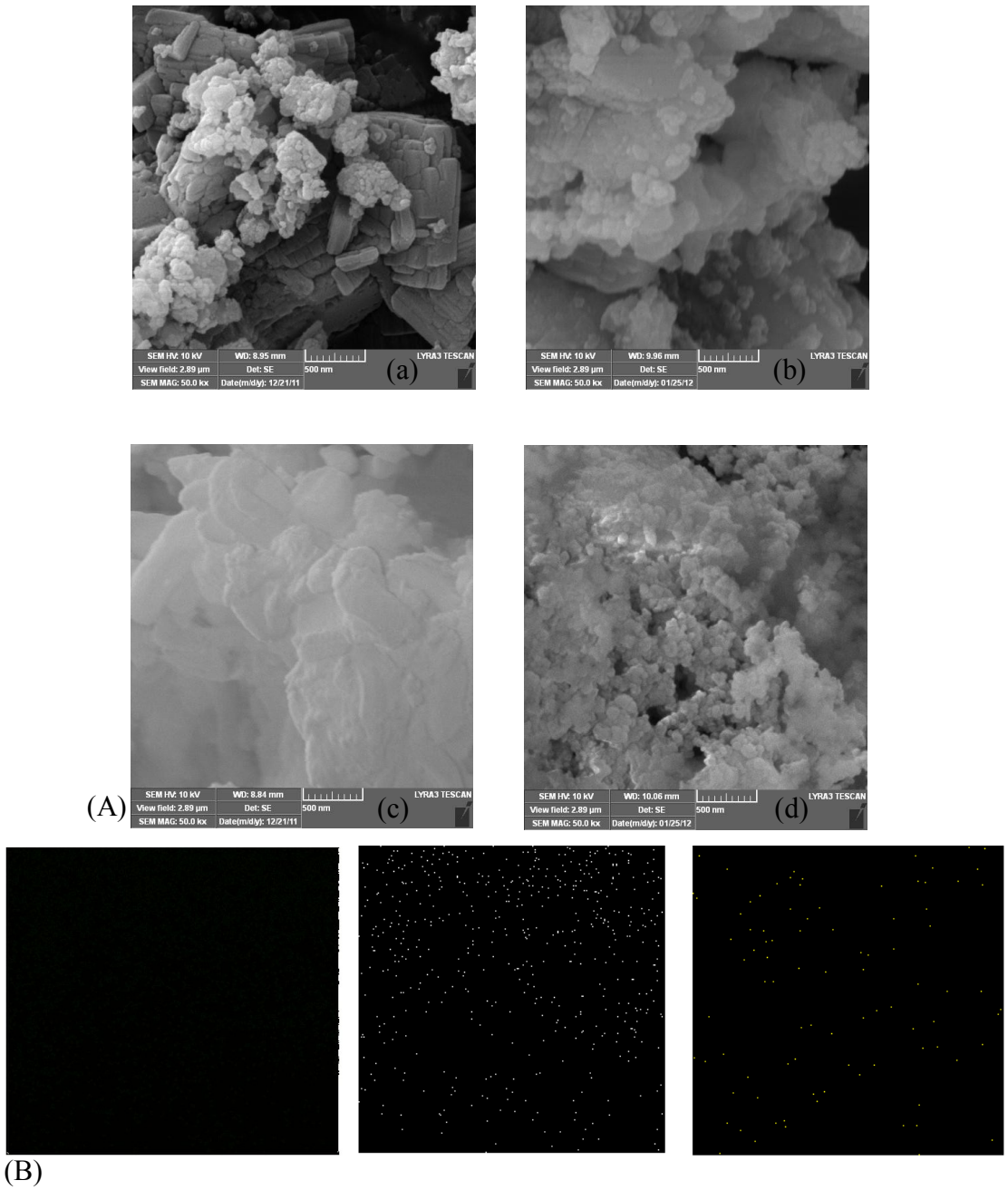

Figure 4.4. (A) SEM micrographs of conventional HZSM-5 (a) and steamed conventional H-Galloaluminosilicate (b), and ordered mesoporous HZSM-5 (c) and H-Galloaluminosilicate (d) (OH^-/T = 0.57). (B) depicts the corresponding elemental mappings by EDSEM of ordered mesoporous H-Galloaluminosilicate.

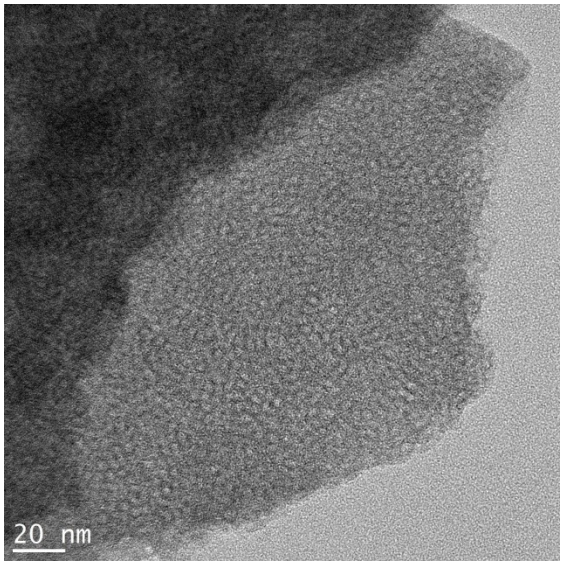

Figure 4.5. HRTEM micrographs of ordered mesoporous H-Galloaluminosilicate formed by CTAB-mediated hydrolysis in NaOH ($OH^-/T = 0.57$).

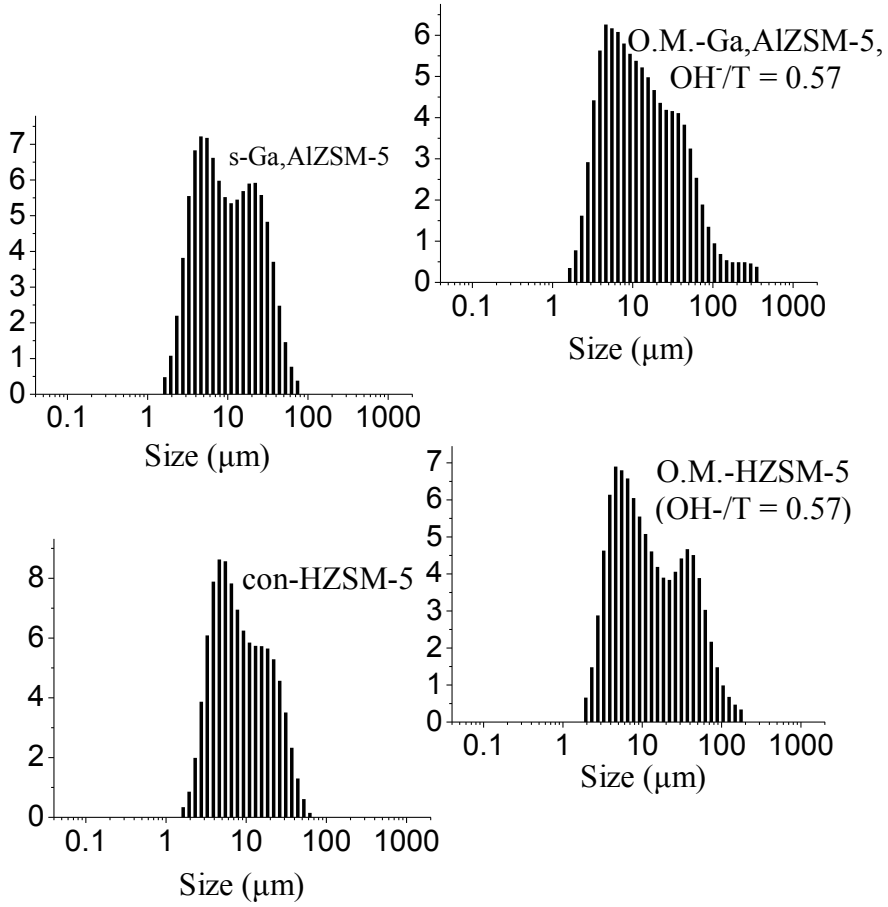

Figure 4.6. Particle size measurements of conventional and ordered mesoporous H-Galloaluminosilicate.

The HRTEM image of ordered mesoporous H-Galloaluminosilicate (OH^-/T = 0.57), showed in Figure 4.5, reveals the presence of ordered mesoporosity. In agreement with N_2 adsorption and XRD data, the pores appear to be of the order of ~ 3.0 nm.

4.2. Properties of active sites

4.2.1 Dispersion of Ga species

4.2.1.1 H_2-TPR

The H_2-TPR profiles of conventional and ordered mesoporous H-Galloaluminosilicate are depicted in Figure 4.7, the numerical results related to the TPR analysis are given in Table 4.2. The H_2-TPR profiles of conventional and ordered mesoporous HZSM-5 (not shown here) showed no distinct hydrogen consumption. The vertical lines in Figure 4.7 represent reduction temperatures corresponding to the reduction of Ga species; extracrystalline $Ga_2O_3 \rightarrow Ga_2O$ ($T < 600$ °C) and extra framework Ga species (*i.e.* $(GaO)^+ \rightarrow Ga^+$) (600 °C < T < 900 °C) [10,12,44-46]. Reduction to metallic Ga (zero-valent state) is not expected to take place, owing to the strong interactions with framework oxygen that stabilize Ga^+ species against further reduction [67]. The framework Ga^{3+} species (as the case with other framework metals) cannot be reduced at moderate temperature [67,68].

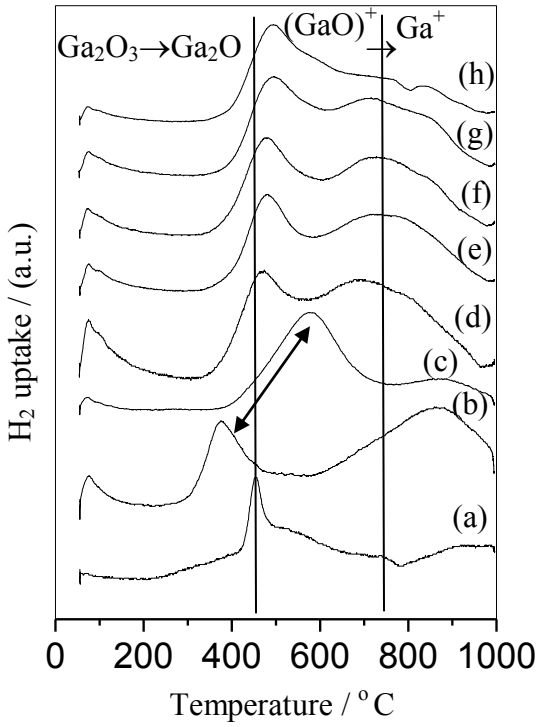

Figure 4.7. TPR curves for conventional and ordered mesoporous H-Galloaluminosilicate; a) bulk Ga_2O_3, b) con-Ga,AlZSM-5, c) s-Ga,AlZSM-5, d-h) O.M.-Ga,AlZSM-5 as a function of OH^-/T ratios: 0.41, 0.57, 0.65, 0.75 and 1.10, respectively.

Table 4.2. TPR data for conventional and ordered mesoporous H-Galloaluminosilicate

Catalysts	Peak maxima, °C		H_2/Ga[a]	A_{PII}/A_{tot}[b]
	Peak I	Peak II		
	$(Ga_2O_3 \rightarrow Ga_2O)$	$((GaO)^+ \rightarrow Ga^+)$		
	< 600 °C	600 < T < 900 °C		
Bulk Ga_2O_3	450	-	0.012	-
con-Ga,AlZSM-5	375	-	0.271	-
s-Ga,AlZSM-5	584	-	0.206	-
CTAB-mediated hydrolysis in NaOH ($x = OH^-/T$)				
x = 0.41	467	712	0.512	0.64
x = 0.57	478	753	0.574	0.73
x = 0.65	481	751	0.613	0.77
x = 0.75	492	752	0.614	0.71
x = 1.10	496	749	0.374	0.43

[a]: mole of H_2 consumed per mole of Ga (amount of Ga corresponds to the experimental value obtained by AAS), [b]: A_{PII}/A_{tot} is the ratio of area of the 2nd reduction peak (A_{PII})/total area ($A_{tot} = A_{PI} + A_{PII}$).

As can be seen from Figure 4.7a and Table 4.2, bulk β-Ga_2O_3 exhibited a marked reduction peak at ~ 450 ºC of partial reducibility. Zheng *et al.* [70] have also noted the low reducibility of β-Ga_2O_3, however, they reported a low reduction temperature (260 ºC). Such significant shift in the reduction temperature may arise from structural differences, as the reduction kinetics of metal oxide is greatly influenced by particle size, morphology, and defect density [70]. The TPR profile of conventional H-Galloaluminosilicate was dominated by one major reduction peak centered at ~ 375 ºC (Figure 4.7b), whereas steamed H-Galloaluminosilicate showed the presence of dominant peak at ~ 584 ºC (Figure 4.7c). These peaks can be assigned to the reduction of extracrystalline Ga_2O_3 (formed by partial degalliation of H-Galloaluminosilicate) having different particle sizes. The H_2-TPR profiles of samples after base treatment in the presence of CTAB were dominated by two major reduction peaks. The peak centered at ~ 467 – 496 °C is assigned to the reduction of dispersed extracrystalline Ga_2O_3, whereas the broad peak (centered at ~ 750 °C) can be assigned to the reduction of extra framework Ga species (*i.e.* $(GaO)^+$) (Figure 4.7d-h) [43]. It can be also seen from Figure 4.7 and Table 4.2 that when increasing the OH^-/T ratio (up to 0.75), there was a slight increase in the area of the high-temperature reduction peak (~ 750 °C), suggesting that extra framework species are more favorable at high OH^-/T ratio, which corresponds to higher extent of mesoporosity. Therefore, it can be summarized that all samples contain extracrystalline Ga_2O_3, extra framework species (only for ordered mesoporous H-Galloaluminosilicate), together with framework tetrahedral Ga^{3+} species. The presence of framework species was supported by ^{71}Ga MAS NMR, FTIR of -OH groups, and acidity measurements (described in the following sections). It is worth noting that H_2 uptake with

a maximum at ~ 74 °C was observed in the TPR profiles for all samples, which could be due to the reduction of quite low dispersed oxide on the outer surface [71].

The H_2/Ga (mol.), which was obtained by correlating the area under TPR curve to the (experimental) amount of Ga in the catalyst, was much lower than the stoichiometric value H_2/Ga of 1.5 (Table 4.2). This was observed for all samples, regardless of the treatment. It can be also seen that there is an increase in the reducibility of Ga (represented by H_2/Ga) upon CTAB-mediated hydrolysis. The reducibility of Ga for steamed sample increased from 0.206 to 0.614 upon increasing OH^-/T ratio up to 0.75.

4.2.1.2 ^{71}Ga MAS NMR

^{71}Ga MAS NMR has been also employed to characterize the nature of Ga species [72]. Tetrahedral framework Ga^{3+} gives rise to a signal at near 150 – 160 ppm, while Ga extra framework $(GaO)^+$ gives rise to a signal near 50 ppm [72-74]. Bulk Ga_2O_3 is composed of two resonance lines with maxima at ~ 5 – 11 and ~ 165 – 174 ppm, which are characteristics of Ga in sixfold (Ga^{VI}) and fourfold (Ga^{IV}) coordination to oxygen, respectively [69]. As can be seen from Figure 4.6, which displays ^{71}Ga MAS NMR of conventional and ordered mesoporous H-Galloaluminosilicate, conventional H-Galloaluminosilicate exhibited a single resonance line centered near 160 ppm, implying the presence of high concentration of framework Ga species. In case of steamed H-Galloaluminosilicate, it was observed there was an increase in the extent of degalliation as inferred from the following; i) the intensity of the 160 ppm resonance line decreased significantly with shift to ~ 140 ppm, and ii) the appearance of an additional resonance line near 5.0 ppm. On the contrary, the intensity of the line near 160 ppm increases and

that of the 5.0 ppm line decreases with increasing the OH^-/T ratio, upon CTAB-mediated hydrolysis treatment of steamed conventional H-Galloaluminosilicate. This implies that large part of extracrystalline Ga_2O_3 was re-dispersed into framework and/or extra framework species. It is also quite apparent that ^{71}Ga MAS NMR spectra of conventional, steamed and ordered mesoporous catalysts did not reveal the presence of extra framework Ga species, as suggested by the absence of the 50 ppm resonance line. This, however, does not mean that there is no extra framework species. These species are undetectable by ^{71}Ga NMR experiments since they are mainly localized in an environment of low symmetry of strong quadrupolar effect [73].

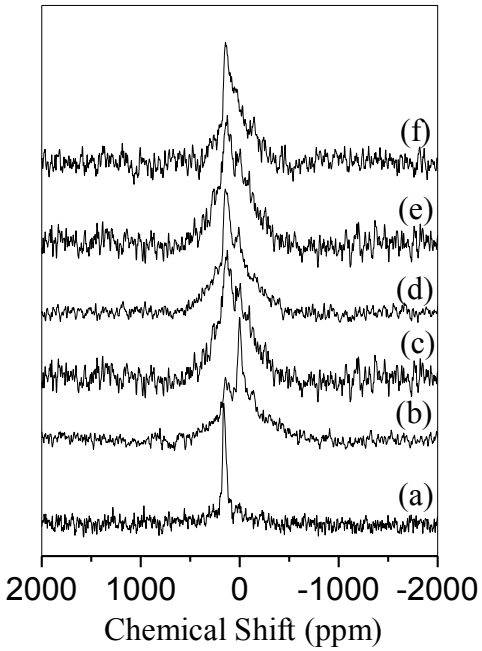

Figure 4.8. ^{71}Ga MAS NMR of ordered mesoporous H-Galloaluminosilicates; a) con-Ga,AlZSM-5, b) s-Ga,AlZSM-5, c-f) corresponds to OH^-/T ratio of 0.41, 0.57, 0.75, and 1.10.

4.2.2 Acidic properties

4.2.2.1 Surface -OH groups

The FTIR spectra in the OH stretching region of conventional and ordered mesoporous H-Galloaluminosilicate and HZSM-5 are depicted in Figure 4.9A-B. Regardless of zeolite precursor and CTAB-mediated hydrolysis treatment, three bands due to -OH vibrations can be identified for all samples. These bands are assigned as follows: 3603 – 3614 cm^{-1} for bridged silanol groups (*i.e.* Si-OH-Ga, which gives rise to Brɒnsted sites), 3661 - 3672 cm^{-1} for extra framework (Ga, or Al) species (Lewis acid sites), and 3742 cm^{-1} for external surface silanols (Si-OH) [75]. As can be also seen from, the intensity of FTIR band at ~ 3614 cm^{-1} for conventional H-Galloaluminosilicate was increased significantly upon steaming (Figure 4.9A), implying that there is a substantial increase in Brɒnsted acidity (this was further supported by NH_3 and pyridine sorption measurements (subsequent section)). Upon the CTAB-mediated hydrolysis treatment, the intensity of ~ 3614 cm^{-1} band decreased with a slight shift to lower wave number (viz. Si-OH-Ga at ~ 3611 - 3595 cm^{-1}) as the OH^-/T ratio increases. It was also shown by Figure 4.9A that the intensity of 3742 cm^{-1} increased upon hydrolysis treatment, suggesting that there is an increase in the external surface area (mesoporosity), which further supports XRD and N_2 sorption data (Table 4.1, Figure 4.1 and 4.3). The intensity of FTIR band characteristic of extra framework species (~ 3672 cm^{-1}) increased slightly upon steaming and treatment by CTAB-mediated hydrolysis. The FTIR spectra of HZSM-5 (Figure 4.9B) showed that the intensity of FTIR band at ~ 3603 cm^{-1} remains almost unchanged, whereas that of 3742 cm^{-1} increases with increasing the OH^-/T ratios, indicating an increase in the mesoporosity.

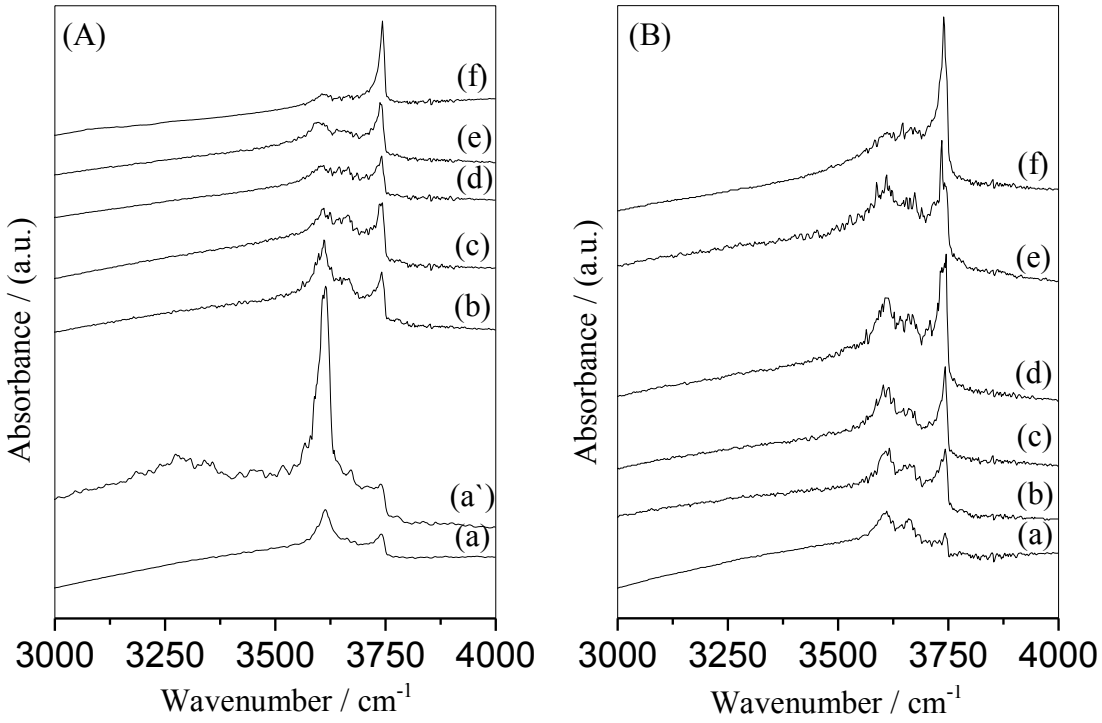

Figure 4.9. FTIR spectra in the OH stretching region of ordered mesoporous H-Galloaluminosilicate (A) and HZSM-5 (B); a) con-Ga,AlZSM-5 or con-HZSM-5; a`) s-Ga,AlZSM-5; and b-f) correspond to O.M.-Ga,AlZSM-5 as a function of OH^-/T ratio: 0.41, 0.57, 0.65, 0.75 and 1.10, respectively.

4.2.2.2 ^{27}Al MAS NMR

^{27}Al MAS NMR measurements (Figure 4.10) were carried out in order to determine the presence of tetrahedral and octahedral Al species, which are the precursors of Brρnsted and Lewis acid sites, respectively. Conventional HZSM-5 and H-Galloaluminosilicate showed the presence of resonance lines at ~ 57 and 0 ppm, which are characteristic of four-coordinate framework Al (T_d) and octahedral extra framework Al (O_h), respectively [76]. There was no noticeable well-defined peak in the 25 - 30 ppm region, which can be assigned either to distorted tetrahedral framework Al or fivecoordinate extra framework Al. Figure 4.10f also revealed that upon steaming of conventional H-Galloaluminosilicate, there was an increase in the extent of dealumination, as evidenced by the increase in the intensity of octahedral extra framework Al (near 0 ppm). However, it is apparent that upon CTAB-mediated hydrolysis treatment, most extra framework Al species associated with conventional samples were "re-aluminated" back on the zeolite outer surface. This was observed regardless of zeolite precursors and OH^-/T ratio (0.16 – 1.10). Groen *et al.* [54] observed that during mesopore formation by desilication, aluminum is re-aluminated back on zeolite external surface.

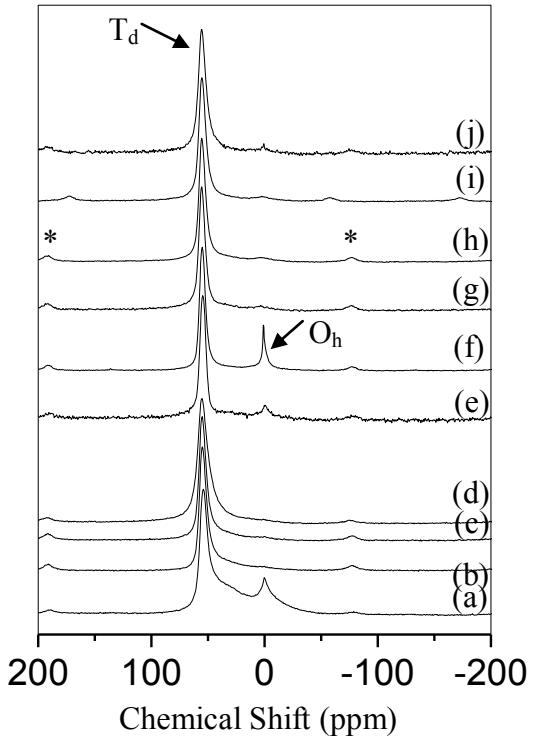

Figure 4.10. ^{27}Al MAS NMR spectra of ordered mesoporous HZSM-5 and H-Galloaluminosilicate formed by CTAB-mediated hydrolysis in NaOH of variable concentration (OH^-/T); a) 0.0 (con-HZSM-5), b) 0.41, c) 0.57, d) 1.10, e) con-Ga,AlZSM-5, f) s-Ga,AlZSM-5, g) 0.41, h) 0.57, i) 0.75 and j) 1.10. Spinning side bands are marked by asterisks (*), T_d: tetrahedral framework Al, and O_h: Octahedral extra framework Al.

4.2.2.3 Brönsted-Lewis acidity

The NH_3-TPD profiles for conventional and ordered mesoporous H-Galloaluminosilicate and HZSM-5 are shown in Figure 4.11A,B (respectively), whereas the FTIR spectra of adsorbed pyridine for H-Galloaluminosilicate based samples are depicted in Figure 4.12. The numerical results related to acidity measurements are given in Table 4.3. All NH_3 temperature programmed desorption (NH_3-TPD) profiles are characterized by two major desorption peaks with maxima in the following temperature regions; low-temperature (L.T.) region < 300 °C, and high-temperature (H.T.) region of 300 – 450 °C and > 450 °C (extended shoulder). The high-temperature region has been assigned to NH_3 desorption from Brρnsted and Lewis acid sites, respectively [77]. As can be seen, steamed conventional H-Galloaluminosilicate exhibited higher acidity than conventional H-Galloaluminosilicate. It can be also seen that the high-temperature desorption peak (H.T.) of conventional H-Galloaluminosilicate shifted to higher temperature upon steaming (*i.e.* 470 ºC compared to 434 °C observed for conventional H-Galloaluminosilicate) (Figure 4.11A, Table 4.3), suggesting that the acidity of steamed catalyst is of higher strength. Upon base hydrolysis of steamed H-Galloaluminosilicate in the presence of CTAB, there was a slight-gradual decrease in the total number of acid sites. Analysis of NH_3-TPD curves in the (H.T.) region revealed that the number of Brρnsted acid sites decreased, whereas that of Lewis acid sites increased with increasing the OH^-/T ratio (*i.e.* R = B/L ratio decreased from 6.94 to 1.63 upon CTAB-mediated hydrolysis of steamed H-Galloaluminosilicate up to $OH^-/T = 0.75$) (Table 3)). It can be also seen that ordered mesoporous samples exhibit weaker Brρnsted acid sites, whereas

the strength of Lewis acid sites appears to be similar, compared to steamed H-Galloaluminosilicate.

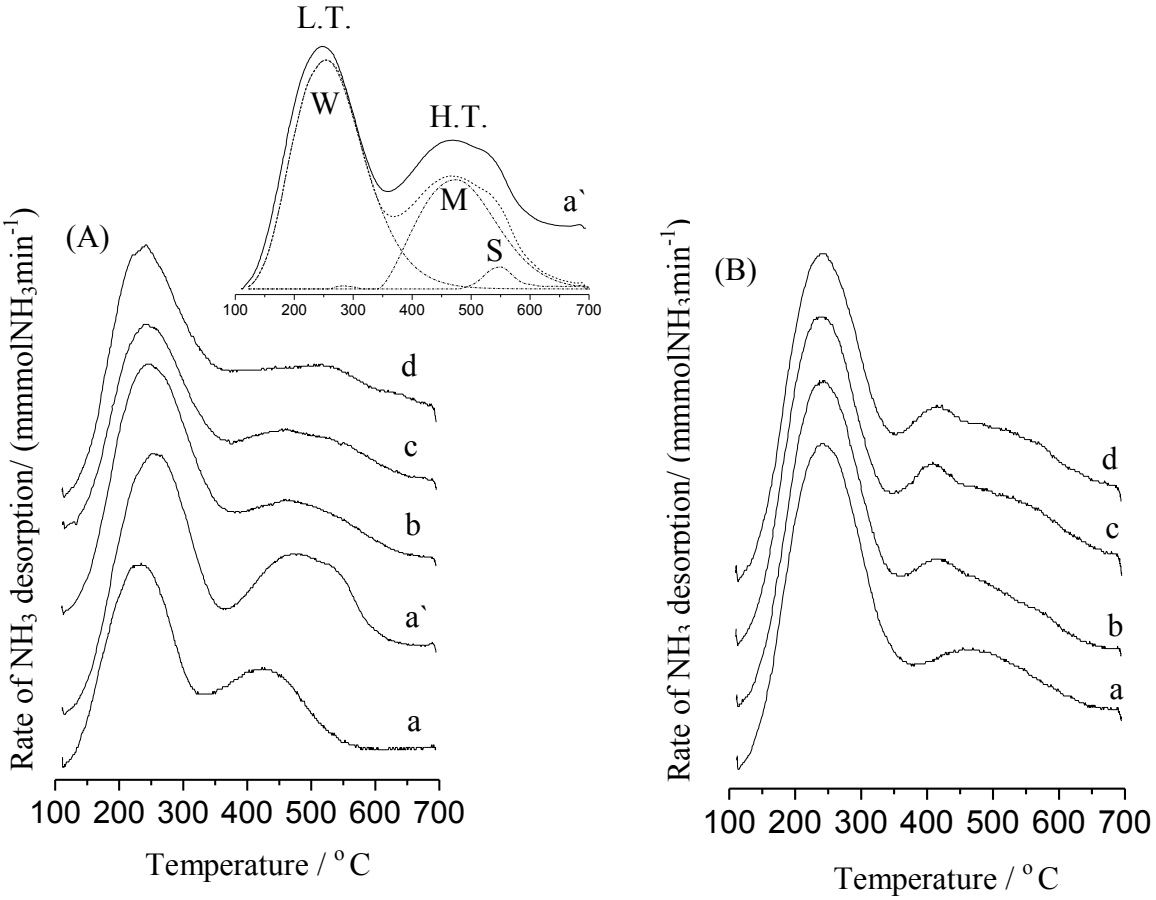

Figure 4.11. NH_3 TPD profiles of ordered mesoporous H-Galloaluminosilicate (A) and (B) HZSM-5 formed by surfactant mediated hydrolysis in NaOH of variable concentration (OH^-/T); a) 0.0 (con-Ga,AlZSM-5 or con-HZSM-5), a`) 0.0 (s-Ga,AlZSM-5), c) 0.41 C) 0.57, and d) 0.65. (L.T.: Low-temperature, H.T.: High-temperature, W: weak, M: medium, and S: strong).

Table 4.3. Acid sites characteristics of conventional and ordered mesoporous H-Galloaluminosilicate and HZSM-5 catalysts

Catalysts	T [b]	NH_3-TPD [a] L.T. (weak) < 300 °C	H.T. (medium & strong) 300 - 450 °C [c]	> 450 °C [d]	R[e]
con-HZSM-5	0.96	1.30(241)[f]	0.85(475)	0.11(551)	7.72(3.46)[g]
CTAB-mediated hydrolysis in NaOH (x = OH^-/T)					
x = 0.41	0.95	1.23(242)	0.84(415)	0.11(552)	7.63(3.57)
x = 0.57	0.97	1.18(239)	0.84(411)	0.13(550)	6.46(3.56)
x = 0.65	0.92	1.16(240)	0.80(413)	0.12(554)	6.66(3.31)
x = 0.75	0.94	1.21(239)	0.80(415)	0.14(554)	5.71(3.21)
x = 1.10	0.80	0.88(223)	0.52(372)	0.28(548)	1.86(1.31)
con-Ga,AlZSM-5	0.79	1.20(233)	0.67(434)	0.12(560)	5.58(11.0)
s-Ga,AlZSM-5	1.27	1.90(240)	1.11(470)	0.16(573)	6.94(10.5)
CTAB-mediated hydrolysis in NaOH (x = OH^-/T)					
x = 0.41	1.19	1.85(244)	0.94(464)	0.25(567)	3.76(5.34)
x = 0.57	1.16	1.60(241)	0.77(420)	0.39(564)	1.97(3.16)
x = 0.65	1.14	1.61(243)	0.73(423)	0.41(566)	1.78(2.23)
x = 0.75	1.13	1.67(244)	0.70(423)	0.43(559)	1.63(2.16)
x = 1.10	0.74	1.24(239)	0.63(446)	0.11(551)	5.72(2.65)

[a]: L.T. and H.T. correspond to low- and high-temperature NH_3 desorption peak, respectively; [b]: total number of acid sites is based on the amount of NH_3 desorbed above 300 °C (*i.e.* H.T. region), [c,d]: strong acid sites of Brönsted and Lewis nature, respectively [77]; [e]: R is the ratio of number of acid sites of the 300 - 450 °C region to those of the region higher than 450 °C (*i.e.* B/L); [f]: number in parenthesis corresponds to peak maximum; and [g]: number in parenthesis corresponds to B/L ratio obtained by pyridine sorption measurements (desorption of pyridine at 150 °C).

These observations were further supported by FTIR-pyridine sorption measurements depicted in Figure 4.12. As can be noted, the FTIR spectra of adsorbed pyridine for conventional, steamed and ordered mesoporous H-Galloaluminosilicate (Fig.4.12A) revealed the presence of Brönsted and Lewis acid sites, as inferred from the appearance of IR bands near 1545 (Brρnsted sites) and 1454 cm^{-1}(Lewis sites) corresponding to Zeolite-O-HPy^{+} (framework Al or Ga species), and Zeolite-$M^{-\delta}$ $Py^{+\delta}$ (M = extra framework Al or Ga species)), respectively [78]. The total, Brönsted and Lewis acid site concentration profiles as functions of the evacuation temperature (300 – 500 °C) are depicted in Figure 4.12B-D, respectively These figures show that amount of pyridine adsorbed on both Brρnsted and Lewis acid sites for conventional, steamed and ordered mesoporous H-Galloaluminosilicate decreased with increasing the evacuation temperature. It was also revealed that, for conventional H-Galloaluminosilicate, pyridine adsorbed on Lewis acid sites was almost removed at temperature as high as 500 °C (~ 68% loss). On the contrary, steamed H-Galloaluminosilicate showed ~ 57% loss in the amount of Lewis acid sites at evacuation temperature of 500 °C, whereas ordered mesoporous H-Galloaluminosilicate (OH^{-}/T range of 0.41 – 0.75) showed much lower reduction (15 – 32% loss). This implies that Lewis acid sites of ordered mesoporous H-Galloaluminosilicate are much stronger than those of conventional samples (the strength of Lewis acid sites increased in the following order; O.M.-Ga,AlZSM-5 >> s-Ga,AlZSM-5 > con.Ga,AlZSM-5).

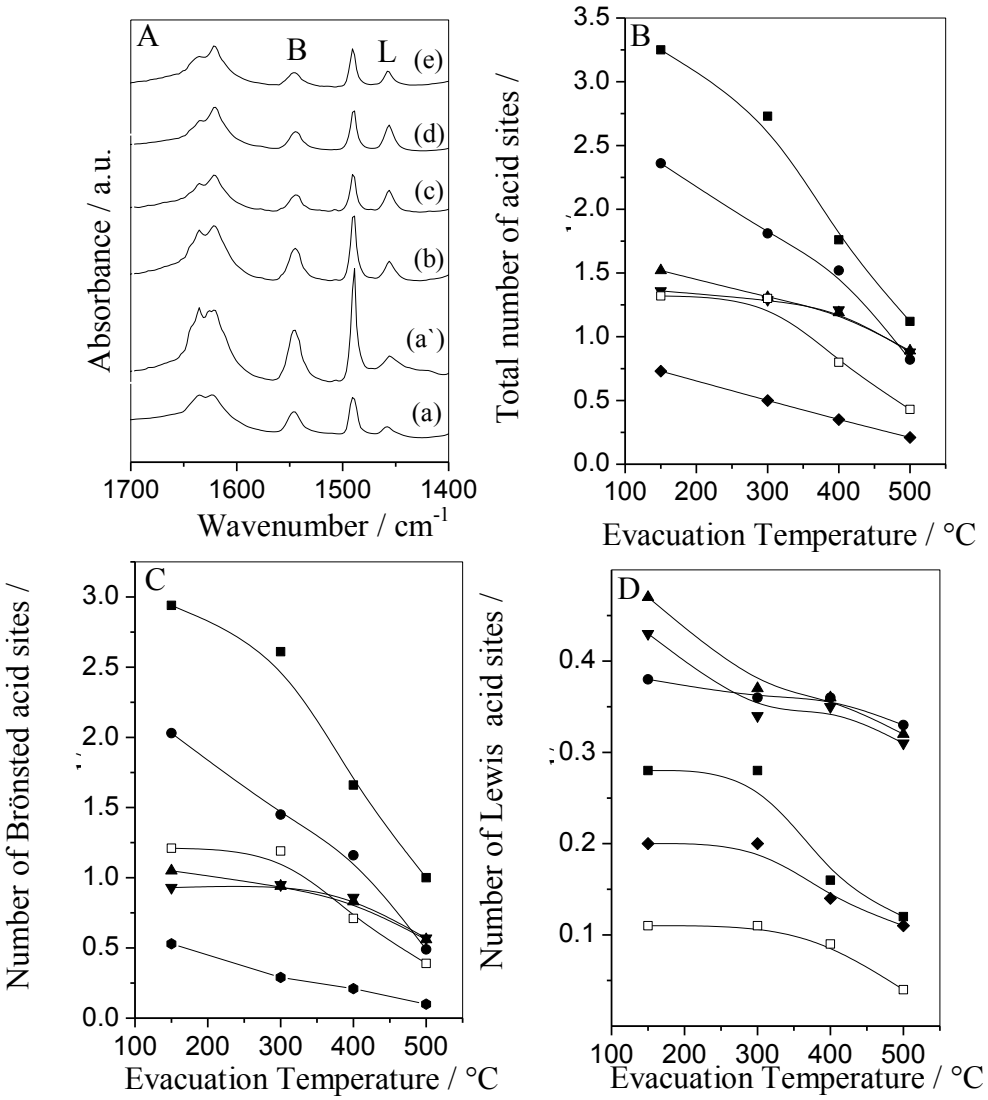

Figure 4.12. FTIR of adsorbed pyridine for ordered mesoporous H-Galloaluminosilicate. A) FTIR spectra of conventional and ordered mesoporous samples obtained by using OH^- /T ratio of; a) 0.0 (con.Ga,AlZSM-5), a`) 0.0 (s-Ga,AlZSM-5), b) 0.41, c) 0.57, d) 0.75, and e) 1.10; B-D) total number of acid sites, Brönsted sites, and Lewis sites as a function of pyridine evacuation temperature, respectively. For graphics (B-D): ■ con-GaAlZSM-5, □ s-Ga,AlZSM-5, (●,▲,▼,♦) corresponds to OH^-/T = 0.41, 0.57, 0.75, and 1.10, respectively.

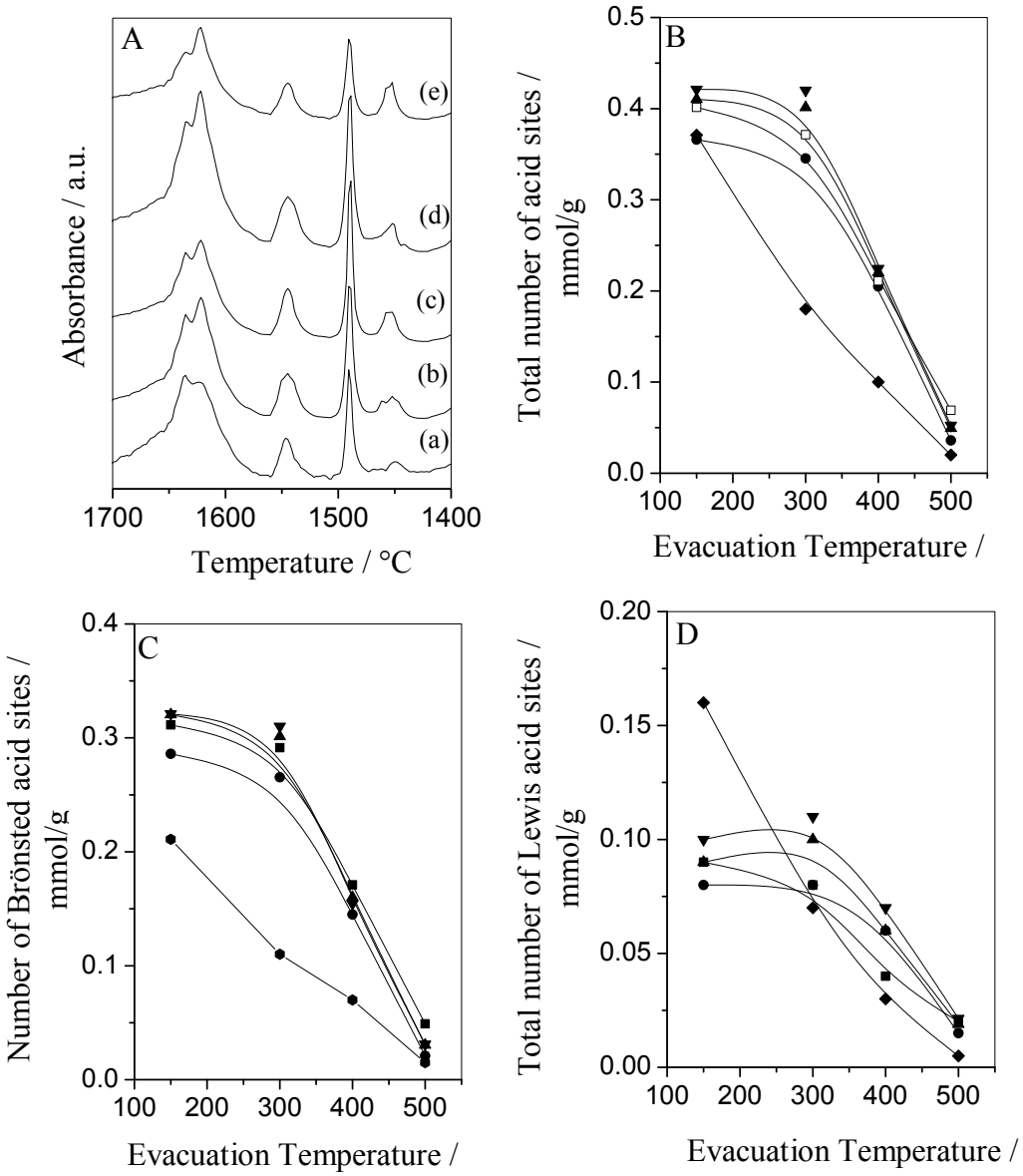

Figure 4.13. FTIR of adsorbed pyridine for conventional and ordered mesoporous H-ZSM-5. A) spectra of ordered mesoporous samples obtained by using OH^-/T ratio of; a) 0.0 (con.HZSM-5), b) 0.41, c) 0.57, d) 0.75, and e) 1.10; B-D) total number of acid sites, Brönsted sites, and Lewis sites as a function of pyridine evacuation temperature, respectively. For graphics (B-D): ■ con-HZSM-5, (●,▲,▼,♦) corresponds to OH^-/T = 0.41, 0.57, 0.75, and 1.10, respectively.

It can be also seen that the acidity of HZSM-5 was slightly affected by CTAB-mediated treatment, as deduced from NH_3-TPD (Figure 4.11B, Table 4.3) and pyridine sorption (Figure 4.13) measurements. Upon increasing the OH^-/T, there was a slight change in the number of Brρnsted and Lewis acid sites. It was also noted that Brρnsted and Lewis acid sites of ordered mesoporous HZSM-5 are weaker than those originally present in the conventional HZSM-5, as inferred from the shift to lower desorption temperature.

4.3. Propane aromatization

In propane aromatization over conventional and ordered mesoporous HZSM-5 and H-Galloaluminosilicate catalysts, the products obtained are saturated and olefinic hydrocarbons in the range between C_1-C_6 and aromatic hydrocarbons in the range between C_6-C_8 (benzene-toluene-xylene (BTX)). Table 4.4 and 4.5 show the data of propane aromatization over conventional H-Galloaluminosilicate and HZSM-5 catalysts, respectively. As can be seen, the selectivity to BTX over conventional H-Galloaluminosilicate was unequivocally much higher than that of HZSM-5. This has been observed many times before [7-25] and was attributed to the low dehydrogenation selectivity of Brρnsted sites [79] as compared to that of Ga species.

Table 4.4. Propane aromatization activity over conventional and ordered mesoporous H-Galloaluminosilicate formed by CTAB-mediated hydrolysis in variable [NaOH]

Catalysts	Ga,AlZSM-5		CTAB-Mediated Hydrolysis of s-Ga,AlZSM-5,x=OH^-/T						
	a	b	x = 0.16	0.41	0.50	0.57	0.65	0.75	1.10
C_3 conversion (wt%)	42.0	30.8	36.6	43.5	53.5	56.3	48.0	38.4	25.0
BTX yield (wt%)[c]	21.9	11.9	16.1	19.4	27.6	28.1	21.2	16.9	10.8
Product selectivity (wt%)									
Methane	14.2	19.9	24.7	22.9	19.2	19.6	17.9	21.7	15.0
Ethene	5.21	5.52	2.95	3.38	2.43	2.93	3.40	4.53	6.51
Ethane	9.70	20.1	16.1	16.0	16.4	17.4	14.6	15.1	17.0
Propene	4.53	2.59	1.72	2.42	2.37	3.15	4.58	3.81	6.67
Butane[d]	5.25	4.93	4.86	4.76	3.47	2.85	3.82	5.27	5.08
Pentane	0.42	0.26	0.48	0.48	0.27	0.18	0.24	0.49	0.26
Benzene	18.9	15.2	18.6	18.8	22.7	22.2	21.1	18.3	18.3
Toluene	23.5	17.8	19.6	20.1	22.5	21.8	22.7	19.1	18.3
Ethylbenzene	0.90	0.54	1.77	0.92	0.69	0.86	0.67	0.70	0.50
Xylene	9.57	5.72	6.00	5.74	6.40	5.90	7.69	6.04	5.92
Heavier Aromatics (C_8^+)	7.79	7.38	6.37	4.43	3.57	3.11	3.32	4.80	5.94
BTX[c]	52.0	38.7	43.9	44.6	51.5	49.9	51.5	44.2	43.2

[a]: no steam treatment, [b]: steam treatment, [c] Including ethylbenzene, [d] n-butane, butenes, and isobutane

Table 4.5. Propane aromatization activity over conventional and ordered mesoporous HZSM-5 formed by CTAB-mediated hydrolysis in variable [NaOH]

Catalysts	con. HZSM-5	CTAB-Mediated Hydrolysis of con.HZSM-5						
		x = OH^-/T						
		x = 0.16	0.41	0.50	0.57	0.65	0.75	1.10
C_3 conversion (wt%)	31.7	30.2	29.0	27.0	27.1	24.5	25.5	13.3
BTX yield (wt%)[a]	8.55	8.21	8.07	7.40	7.72	7.25	7.29	3.78
Product selectivity (wt%)								
Methane	35.1	33.6	35.2	34.3	35.1	34.2	34.6	31.4
Ethene	7.39	8.15	9.37	9.70	8.50	8.86	7.63	10.6
Ethane	17.9	16.6	15.3	14.9	14.1	14.6	14.4	12.9
Propene	2.76	3.27	1.72	2.82	2.97	2.91	2.74	2.46
Butane[b]	5.10	5.08	6.48	5.76	5.13	5.33	6.42	5.29
Pentane	0.29	0.32	0.37	0.37	0.30	0.37	0.77	0.56
Benzene	11.5	11.4	11.8	11.1	12.5	12.4	12.4	10.3
Toluene	11.9	11.5	12.3	12.4	12.5	12.5	12.5	12.3
Ethylbenzene	1.52	0.52	0.55	0.74	0.61	2.34	2.34	0.73
Xylene	3.55	3.62	3.71	3.94	3.48	3.85	3.85	5.11
Heavier Aromatics (C_8^+)	3.96	3.81	3.57	3.92	4.34	2.90	2.90	8.46
BTX[a]	26.9	27.2	27.8	27.4	28.5	29.6	29.6	28.5

[a] Including ethylbenzene, [b] n-butane, butenes, and isobutane

We can see, from Table 4.4, a decrease in both the propane conversion and BTX selectivity of steamed conventional H-Galloaluminosilicate. Whereas, there was enhanced catalytic performance upon introducing ordered mesopores, via surfactant-mediated hydrolysis, in the catalyst structure. This is shown in Table 4.5. There is clearly an improvement in the conversion of propane over both hierarchical H-Galloaluminosilicate and steamed conventional H-Galloaluminosilicate. The former gave conversion in the range of 25.0 and 56.3% while the latter gave conversion at 30.8%. Figure 4.14A depicts the reliance of propane conversion on OH^-/T. We clearly see a maxima in the relationship suggesting that there is likely to be destruction of the zeolitic structure as we increased the concentration of NaOH. In contrary to this, the surfactant-mediated hydrolysis treatment of typical HZSM-5 did not yield any positive improvement compared to its form without treatment. This is depicted in Table 4.5 and Figure 4.14B.

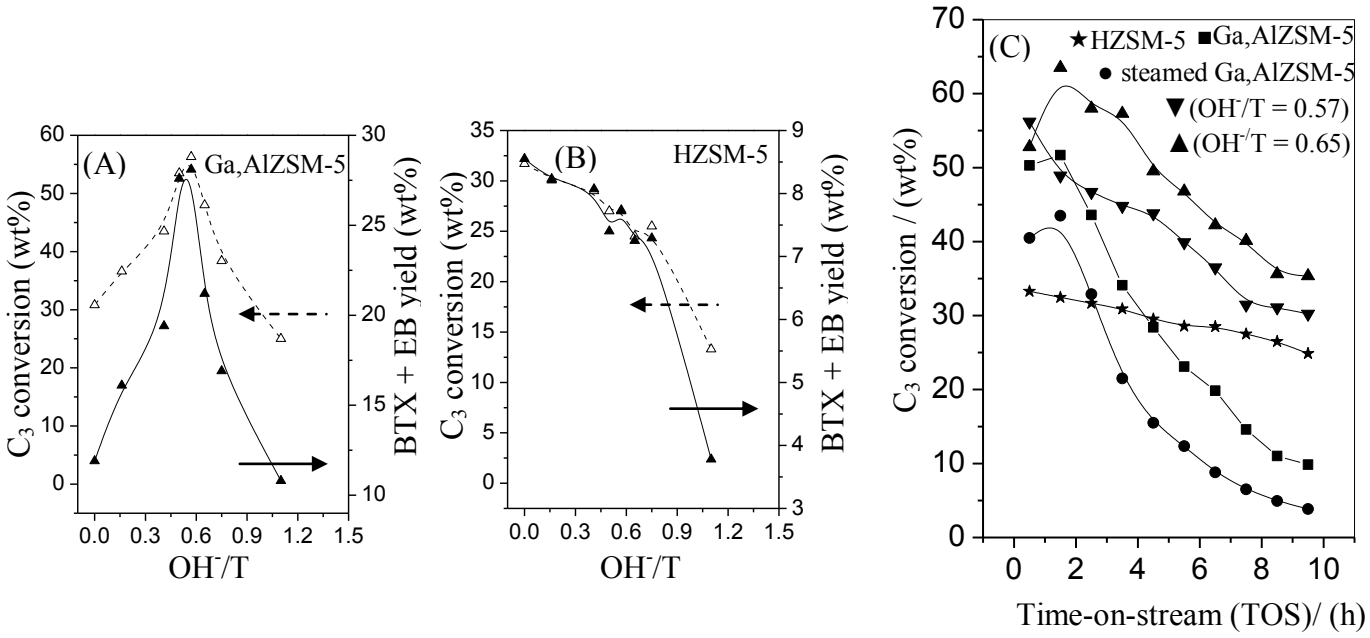

Figure 4.14. Propane conversion and BTX aromatics yield of conventional and ordered mesoporous and H-Galloaluminosilicate (A) and HZSM-5 (B) as a function of OH^-/T. (C) presents the deactivation behavior (TOS = 10 hours) of selected catalysts.

From Figure 4.14C, we see a drop in deactivation rate of the H-galloaluminosilicate with hierarchical structure when used on propane transformation for 10 hours. In contrast, its conventional counterpart exhibited fast deactivation rate. For the mesoporous catalyst, we observed a 33% drop in activity while for its steamed conventional counterpart we observed an 80% decrease in activity for 10 hours time-on-steam.

A comparison of the selectivity at the same conversion level of 25%, to BTX, as regards to conventional and hierarchical mesoporous catalysts can be seen in Figure 4.15. The figure clearly shows the superiority of ordered mesoporous H-galloaluminosilicate over its conventional steamed counterpart in terms of selectivity. Numerically, its selectivity rose from 42% to 58.3%. It's also obvious that there is a modest change in BTX selectivity with respect to hydroxide concentration. In addition, no considerable difference was observed in the BTX selectivity of conventional HZSM-5 upon treatment with surfactant-mediated hydrolysis. Numerically, as shown in Figure 4.15, the difference was 3% for concentration ratios of 0.75 and 0.41.

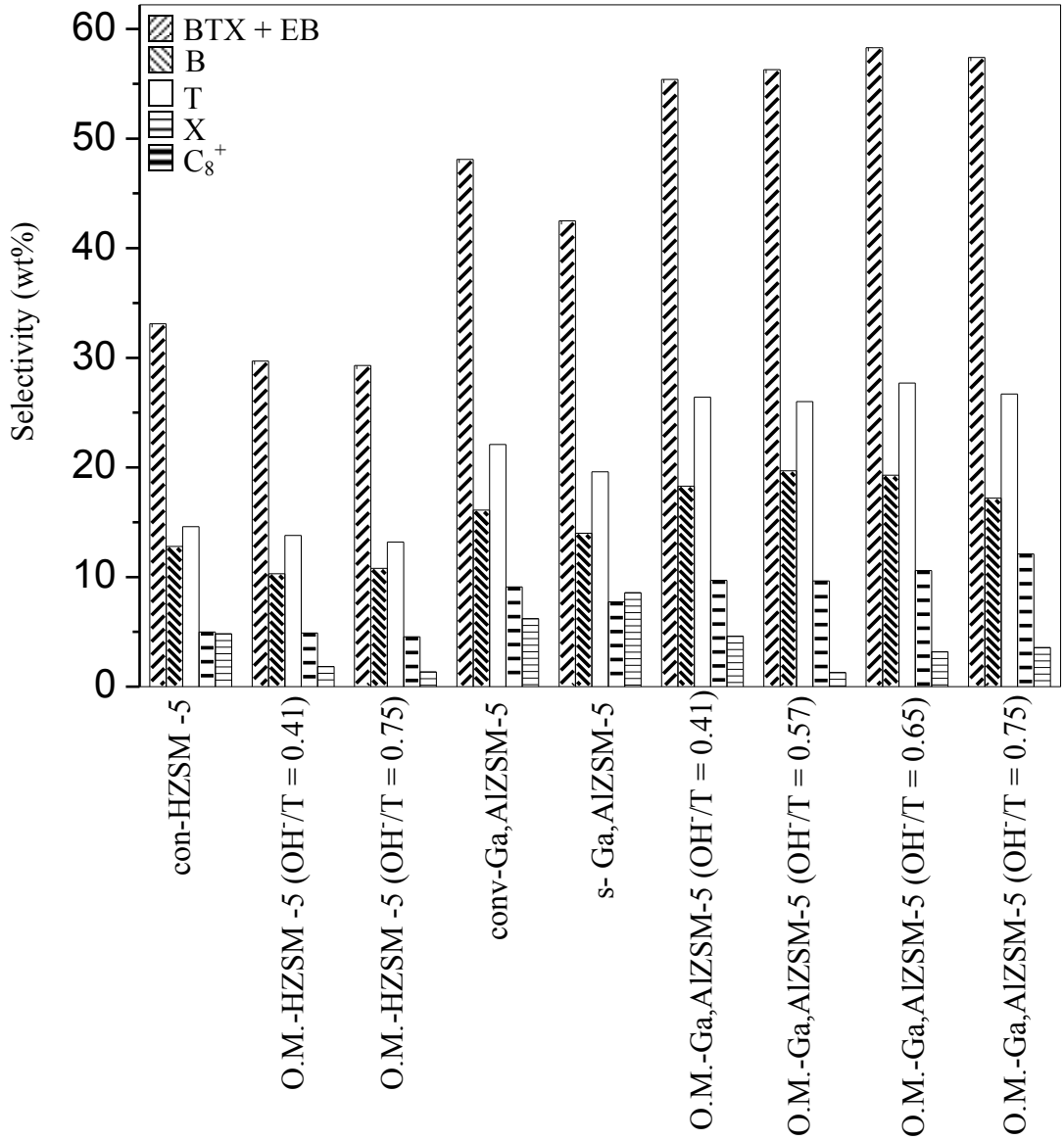

Figure 4.15. Aromatics selectivity of propane aromatization over conventional and ordered mesoporous H-Galloaluminosilicates and HZSM-5 at ~ 25 % propane conversion

4.4. Effect of ordered mesoporosity on the aromatization performance of H-Galloaluminosilicate

Usually, the activity of a zeolitic catalyst can be enhanced by introducing microporous/mesoporous system in the structure due to improvement in diffusion of reactant and product species. Nevertheless, this will be advantageous if the reaction is limited by diffusion and the inherent characteristics of the hierarchical zeolites are preserved. Herein, it was observed that there was no much difference in the activity of the reaction of propane aromatization over ordered mesoporous HZSM-5 and conventional HZSM-5 (Table 4.4), irrespective of the undisputable evidence of mesoporous/microporous structure as further proven by textural and structural data. Based on this, we can deduce that introduction of ordered mesoporosity in conventional HZSM-5 catalysts has no effect on propane aromatization, which means the reaction is not really hindered by diffusion. To buttress this, NH_3-TPD and FTIR of chemisorbed pyridine measurements (Table 4.3, Figure 4.11, and Figure 4.13) revealed that there was no considerable difference in the acidity of the conventional catalyst upon undergoing surfactant mediated base hydrolysis.

However, treatment of H-galloaluminosilicate showed significant enhancement in the transformation of propane in contrast to the treatment of HZSM-5. The results suggest that the introduction of mesoporosity, which aids the movement of reaction species, in the catalyst structure of H-galloaluminosilicate, was not the main impetus behind the improved catalytic performance in terms of stability and aromatization activity.

In the light of this, we can conclude that the actual effect of introduction of ordered mesoporosity in H-galloaluminosilicate was the enhanced dispersion of active gallium species which are present as extra framework [7-25]. A careful study of our characterization results reveals the presence of ordered mesopores and comparatively higher Brönsted acidity in the hierarchical mesoporous H-galloaluminosilicate catalyst. The study also reveals properly-conserved zeolitic properties and extra framework gallium species which are adequately-dispersed. Therefore, the characterization results corroborate our conclusion that the enhanced performance of ordered mesoporous H-galloaluminosilicate is simply due to the enhanced distribution of active gallium species. But what could have led to these improvements?

Due to the cumbersome size of the active gallium species formed during wet impregnation of gallium into HZSM-5, it becomes an uphill task to incorporate the same into the support/parent catalyst (HZSM-5) [58]. As a result of this, these active species tend to remain on the outside surface of the zeolite. Usually, they remain as extracrystalline gallium oxide. Since it was the objective of our research to see the effect of introduction of mesoporosity into gallium-containing zeolite, we noticed an enhancement in the aromatization performance of the hierarchical catalyst (via surfactant-mediated hydrolysis of steamed H-galloaluminosilicate) as a result of proper and improved dispersion of gallium species. Based on this, we have proposed a scheme to describe this whole process. The first is gallination, second is degalliation and the third step is re-galliation of the active outer gallium species:

1) Gallination – Different authors have come to a conclusion that incorporation of gallium into the zeolitic structure via uninterrupted preparation of H-galloaluminosilicate

usually culminates into the creation of both framework gallium ion and evenly-dispersed gallium oxide; both of which have high reducibility properties. This method of incorporation leads to high amount of gallium ions in the framework, in tetrahedral form, of the catalyst structure. Nevertheless, we still have gallium species resident outside the framework due to partial substitution or even removal of gallium during calcination. Table 4.2 and Figure 4.7, showing the hydrogen-TPR data of our characterization, throw in a vital information that the coexistence of gallium species on the outside of the framework and within is unparalled and non-challengeable. Moreover, detection was not made of extra framework gallium species which are usually the most active for this reaction. Notwithstanding, these extra framework gallium ions will be created if there is hydrogen in the feed. They will be formed from the reduction of extracrystalline gallium oxide to gallium (I) ions. These are shown in the two equations below [40, 80]:

$$Ga_2O_3+2H_2 \rightarrow Ga_2O+2H_2O \quad \text{(i)}$$

$$Ga_2O+2H^+Z^- \rightarrow 2Ga^+Z^-+H_2O \quad (Z^- \text{is the anionic zeolite framework}) \quad \text{(ii)}$$

We have reached a consensus that the superficial change in oxidation state of the extracrystalline Ga_2O_3, with hydrogen to gallium ratio of 0.271 and reduction temperature of 375^oC shown in Table 4.2, will enhance the formation of the effective catalyst species thereby enhancing the performance of the catalyst in the aromatization of propane. Likewise, incorporation of gallium into the zeolitic structure only leads to the formation of extracrystalline Ga_2O_3.

2) Degalliation - All of FTIR spectra of chemisorbed pyridine, of hydroxyl groups at 3614cm^{-1} band (Figure 4.9) and of NH_3-TPD revealed that Brönsted acid sites increased in number upon steaming Conventional H-galloaluminosilicate as shown in

Table 4.3 and Figures 4.11 to 4.12. Clearly, we see from our data of ^{71}Ga MAS NMR and H_2-TPD, the stimulation of degalliation which was made obvious by the peak indicating extracrystalline Ga_2O_3 being reduced at 584^{o}C. From this we can infer that removal of gallium goes along with its incorporation in the framework. Moreover, part of the cumbersome gallium oxide of the gallium-containing HZSM-5 could be re-distributed when the catalyst is steamed thereby forming the gallium species shown in the equation below [19]:

$$Ga_2O_3+H_2O\rightarrow 2GaO(OH) \qquad \text{(iii)}$$

This species could be embedded into the framework due to the interface of the defected zeolitic framework equation (iv),

$$n(\equiv Si\text{-}OH)+GaO(OH)\rightarrow[\equiv Ga\text{-}OH\text{-}Si\equiv]+H_2O \qquad \text{(iv)}$$

It might also interact with Brönsted sites in order to form gallium species on the outside of the catalyst structure as shown in equation (v):

$$GaO(OH)+H_z^{+}(Br\rho nstedsites)\rightarrow GaO^{+}+H_2O \qquad \text{(v)}$$

or there might be removal of water thereby forming agglomerations of gallium oxide as shown in equation (vi):

$$2GaO(OH)\rightarrow Ga_2O_3+H_2O \qquad \text{(vi)}$$

As mentioned earlier, steaming led to the re-distribution of the extracrystalline gallium oxide (created by removal of gallium from typical H-galloaluminosilicate) concurrently with the removal of gallium from the framework. Irrespective of the occurrence of this phenomenon, we still have a high amount of Brönsted acid sites. Results from catalyst

testing also revealed the superior aromatization performance of conventional H-galloaluminosilicate over its steamed counterpart. This observation suggests that there is low amount of the active extra framework species as a result of the formation of extracrystalline gallium oxide species created by steaming, as shown in Table 4.2. It should be noted that gallium species in the framework are not reclusively active; rather it is their combination with gallium species in the outer framework that is vital for optimum performance in the aromatization of propane [45, 82-83].

3) Re-gallination- We might also infer the facilitation of transport of the extracrystalline gallium oxide (Ga_2O_3) as a result of the creation of mesopores in the zeolitic passage. This would also lead to the creation of extra framework gallium species which are relatively active. A careful study of our temperature-programmed reduction characterization revealed the presence of extra framework gallium species as reflected by a peak whose intensity increases with the surface area of the mesopores. Data gotten from 71Ga MAS NMR also suggested a decrease in the quantity of extracrystalline gallium oxide as mesopores are being created. All these results have been corroborated by the Ammonia-TPD and pyridine absorption measurements. They revealed an increase in Lewis sites and a decrease in Brönsted sites as mesopores are being formed. Some authors also reported this phenomenon of a metal being added back into a zeolitic structure [81]. They specifically observed this during desilication where aluminium is added back into the zeolitic structure. Consequently, this supports our discovery of the enhanced dispersion of the active gallium species during the creation of hierarchical topology in a steamed H-Galloaluminosilicate.

Ordered mesoporous H-Galloaluminosilicate prepared via surfactant mediated hydrolysis, using NaOH with concentration of 0.40M, of steamed H-Galloaluminosilicate displayed optimum aromatics yield and propane conversion. We can infer from this that there exists an intense relationship between the concentration of NaOH and activity of this aromatization reaction. Consequently, this affects the dispersion of gallium, total number of acid sites and the degree of ordered mesoporosity. Moreover, we note an intense reliance of the aromatization of propane on different catalytic attributes as shown in Figure 4.16. As a result, we can relate the optimum propane transformation performance to mesopore surface area, Lewis and Brönsted sites, gallium reducibility; all of which have values of 107 m^2/g, 0.39 $mmolg^{-1}$, 0.77 $mmolg^{-1}$ and 0.574 respectively.

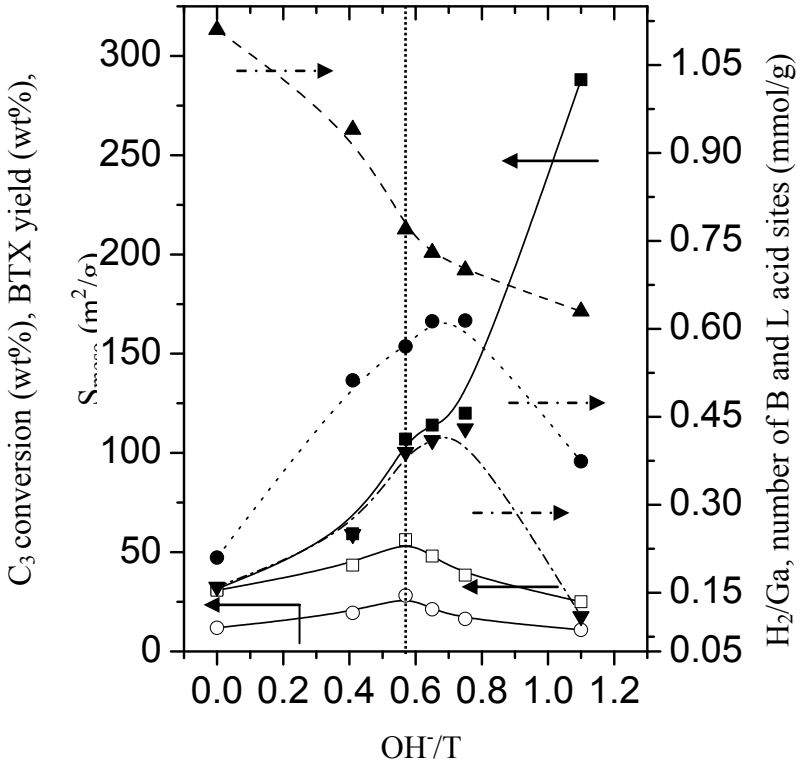

Figure 4.16. Effects of concentration of hydrolysis solution (in terms of OH^-/T ratio) for ordered mesoporous H-Galloaluminosilicate on propane conversion □, BTX yield ○, mesopore surface area ■, reducibility of Ga species H_2/Ga ●, and total number of B sites▲ and L sites.

4B. Results and discussion

4.5. Elemental Compositions

Table 4.6 shows the molar Si/Al and Ga/(Al+Ga) ratios in the solids, and the Si, Al, and Ga concentration in the filtrates of parent and Ga-containing HZSM-5 (Si/Al = 11), upon post-synthesis treatments. The amounts of Si, Al, and Ga extracted from pure and Ga-containing HZSM-5 of Si/Al ratio of 40 are given in Table 4.7. Figure 4.17 A,B depicts the relationship between the concentration of NaOH and the amounts of Si and Ga per gram zeolite dissolved in the NaOH solution.

It can be seen from Table 4.6 that there is only a negligible change in the Si/Al ratio upon post-synthesis treatments of parent HZSM-5 by either CTAB-mediated assembly of zeolite seed into MCM-41 mesostructure, or CTAB-mediated coating with MCM-41 mesostructure (e.g. the amount of Si extracted from zeolite was very small, 0.8-1.30 % of total Si content as evidenced by the filtrate analysis (Tables 4.6,4.7). This was observed regardless of zeolite Si/Al and concentration of NaOH. On the contrast, the amount of Si extracted from the zeolite framework was more susceptible to the concentration of NaOH and zeolite Si/Al, upon alkaline post-treatment (desilication approach). Table 4.6 shows that the Si/Al decreased from 11 in the parent HZSM-5 to 11.1 and 10.8 in those treated with 0.05 and 0.10 M of NaOH, respectively. The Si/Al ratio decreased further to 10 upon treatment with more concentrated NaOH solution (0.20 M). Similar trend was observed for parent HZSM-5 of Si/Al ratio of 40; however, it is apparent that the level of Si dissolution was much higher. The Si/Al ratio of HZSM-5 (Si/Al = 40) decreased from 40 to 37.5 and 35 in those treated with 0.05 and 0.10 M of

NaOH (corresponding to ~ 40 - 50 % decrease, as compared to NaOH-treated samples of Si/Al = 11). This was further evidenced by the filtrates analysis, which showed that the amounts of Si in the filtrate of NaOH-treated HZSM-5 (Si/Al = 40) are 3-fold higher than the amounts of Si in the filtrates of treated HZSM-5 of Si/Al = 11 (Table 4.6,4.7, Fig.4.17A,B). It was also revealed by these analyses that not only Si, but also some amounts of Al were removed from the zeolite. For HZSM-5 (Si/Al = 11), the Si concentration in the filtrates was approximately one order of magnitude higher than the Al concentration, suggesting the preferential extraction of Si species from the zeolite framework. Only traces of Al could be detected in the filtrates of NaOH-treated samples of Si/Al = 40. These findings further confirm the essential role of framework aluminum in controlling the process of silicon extraction and subsequently the formation of intracrystalline mesopores [1-4]. Extraction of Si species from HZSM-5 of Si/Al of 11 is very difficult, owing to the high concentration of framework aluminum species that stabilizes the surrounding silicon atoms to high degree against hydrolysis by OH^-. On the contrary, the cleavage of Si-O-Si bond is much easier for HZSM-5 (Si/Al = 40), owing to the low concentration of neighboring Al tetrahedral.

The solid and filtrate analysis for mesoporous Ga-containing HZSM-5 samples further confirms that only alkaline post-synthesis treatments causes changes in the elemental composition. The Si/Al of Ga-containing HZSM-5 (Si/Al = 11) decreased slightly upon treatment with NaOH, regardless of Ga loadings. However, more pronounced reduction was noted for those of Si/Al of 40 (e.g. the Si/Al of Ga-containing HZSM-5 with Ga loading of 0.35 decreased from 40 to 35 and 28 upon treatment with NaOH solution of 0.05 and 0.10 M, respectively. More notably, it is apparent that Ga is

leaching as well during treatment with NaOH, but to a different degree depending on Si/Al and NaOH concentration (Table 4.6, 4.7, Fig.4.17A,B). The Ga extraction was so sever for samples of Si/Al = 11 and Ga/(Al+Ga) = 0.6, reaching 91 % upon treatment with NaOH solution of 0.20M. This was further confirmed by the analysis of solid samples, which showed that Ga loading decreased significantly from 0.1 0.01 upon treatment with NaOH (0.20 M). Whereas, treatment of Ga-containing HZSM-5 (Si/Al = 40, Ga/(Al+Ga) = 0.6) with NaOH concentration of 0.20 M, resulted only in ~ 20 % Ga removal. These findings imply that there is no preferential extraction of Si species in the presence of Ga.

The elemental compositions of Ga-containing mesoporous HZSM-5 are given in Table 4.8. As expected, the addition of Ga via aqueous impregnation onto mesoporous HZSM-5 (regardless of post-treatment approaches or Si/Al) did not cause any change in the elemental compositions.

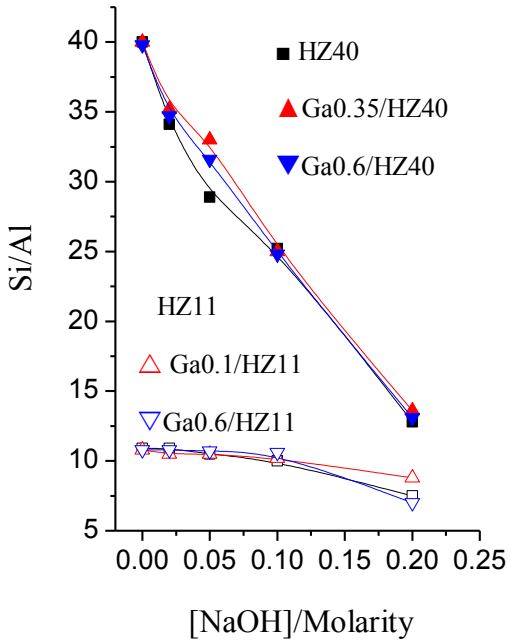

Figure 4.17: Si/Al (A) and % of Si (B) extracted from HZSM-5 zeolite framework as a function of concentration of NaOH. (A`) Ga/(Al+Ga) and (B`) % of Si and Ga extracted from Ga-containing zeolite framework upon alkaline treatment using increasing concentration of NaOH solutions (filtrates analysis).

Table 4.6. Treatments conditions and elemental compositions of mesoporous parent and Ga-containing HZSM-5 of Si/Al = 11.

Sample	Treatment conditions	ICP [a]					% Yield
		Solid		Filtrate			
		Si/Al [b]	Ga/(Al+Ga) [c]	Si_{ext} (mg gz^{-1}) (% Si_{ext})	Al_{ext} (mg gz^{-1}) (% Al_{ext})	Ga_{ext} (mg gz^{-1}) (% Ga_{ext})	
HZ11	Parent	10.9	-	-	-	-	-
HZ11-DSZ0.05	Desilication, 0.05 M	10.5	-	10.1(2.6)	1.50(1.1)	-	99
HZ11-DSZ0.10	Desilication, 0.10 M	10.0	-	30.6(7.8)	1.73(1.2)	-	95
HZ11-DSZ0.20	Desilication, 0.20 M	7.50	-	83.3(21.)	3.37(2.5)	-	80
HZ11-SMH0.20	SMH, 0.20 M	10.8	-	4.80(1.2)	< 0.01	-	96
HZ11-SMH0.30	SMH, 0.30 M	10.9	-	3.67(0.9)	< 0.01	-	96
HZ11-SMH0.40	SMH, 0.40 M	10.8	-	3.11(0.8)	< 0.01	-	96
HZ11-SMH0.50	SMH, 0.50 M	11.0	-	3.95(1.0)	< 0.01	-	93
MCM-41//HZ11	Overgrow.-MCM-41	16.8	-	3.11(0.8)	< 0.01	-	100
Ga0.1/HZ11	Impregnation	10.8	0.10	-	-	-	100
Ga0.1/HZ11-DSZ0.05	Desilication, 0.05 M	10.5	0.03	9.40(2.3)	0.69(2.1)	2.56(36.3)	98
Ga0.1/HZ11-DSZ0.10	Desilication, 0.10 M	10.2	0.02	29.0(7.3)	0.61(1.9)	5.23(74.0)	97
Ga0.1/HZ11-DSZ0.20	Desilication, 0.20 M	8.50	0.01	89.1(22.)	0.51(1.6)	7.20(91.1)	95
Ga0.1/HZ11-SMH0.20	SMH, 0.20 M	11.1	0.10	0.81(0.2)	< 0.02	0.01(0.20)	93
Ga0.1/HZ11-SMH0.30	SMH, 0.30 M	11.0	0.10	0.61(0.1)	< 0.02	0.01(0.20)	93
Ga0.1/HZ11-SMH0.40	SMH, 0.40 M	11.0	0.09	0.52(0.1)	< 0.02	0.01(0.20)	100
Ga0.1/HZ11-SMH0.50	SMH, 0.50 M	11.0	0.10	4.71(1.1)	< 0.02	0.01(0.20)	100
MCM-41//Ga0.1/HZ11	Overgrow.-MCM-41	19.0	0.10	3.20(0.7)	< 0.02	0.01(0.20)	100
Ga0.6/HZ11	Impregnation	10.8	0.55	-	-	-	100
Ga0.6/HZ11-DSZ0.05	Desilication, 0.05 M	10.7	0.06	7.51(2.0)	2.81(9.6)	28.1(44.4)	87
Ga0.6/HZ11-DSZ0.10	Desilication, 0.10 M	10.6	0.05	20.7(5.6)	1.01(3.4)	48.4(76.4)	88
Ga0.6/HZ11-DSZ0.20	Desilication, 0.20 M	7.00	0.01	90.6(24.)	0.39(1.3)	58.1(91.7)	88
Ga0.6/HZ11-SMH0.20	SMH, 0.20 M	10.8	0.54	3.31(0.9)	< 0.01	0.01(0.02)	95
Ga0.6/HZ11-SMH0.30	SMH, 0.30 M	10.7	0.54	3.11(0.8)	< 0.01	0.01(0.02)	95
Ga0.6/HZ11-SMH0.40	SMH, 0.40 M	10.8	0.54	3.84(1.0)	< 0.01	0.01(0.02)	100
Ga0.6/HZ11-SMH0.50	SMH, 0.50 M	10.6	0.54	4.81(1.3)	< 0.01	0.01(0.02)	100
MCM-41//Ga0.6/HZ11	Overgrow.-MCM-41	16.8	0.54	3.11(0.8)	< 0.01	0.01(0.02)	100

[a]: by ICP-OES, [b] : nominal Si/Al = 11.0; [c] : nominal Ga loading (Ga/(Al+Ga)) = 0.10 and 0.60

Table 4.7. Treatments conditions and elemental compositions of mesoporous parent and Ga-containing HZSM-5 of Si/Al = 40.

Sample	Treatment conditions	ICP [a]					% Yield
		Solid		Filtrate			
		Si/Al[b]	Ga/(Al+Ga)[c]	Si_{ext} (mg gz^{-1} (% $Si_{ext}t$)	Al_{ext} (mg gz^{-1} (% $Al_{ext}t$)	Ga_{ext} (mg gz^{-1} (% $Ga_{ext}t$)	
HZ40	Parent	40.0	-	-	-	-	-
HZ40-DSZ0.05	Desilication, 0.05 M	28.9	-	73.1(17.4)	< 0.01	-	96
HZ40-DSZ0.10	Desilication, 0.10 M	25.2	-	146(34.8)	< 0.01	-	79
HZ40-DSZ0.20	Desilication, 0.20 M	12.8	-	268(63.0)	< 0.01	-	45
HZ40-SMH0.20	SMH, 0.20 M	40.0	-	4.23(1.01)	< 0.01	-	87
HZ40-SMH0.30	SMH, 0.30 M	40.0	-	4.12(0.98)	< 0.01	-	96
HZ40-SMH0.40	SMH, 0.40 M	39.8	-	3.89(0.92)	< 0.01	-	96
HZ40-SMH0.50	SMH, 0.50 M	39.8	-	5.53(1.32)	< 0.01	-	96
MCM-41//HZ40	Overgrow.-MCM-41	51.5	-	5.10(1.21)	< 0.01	-	100
Ga0.35/HZ40	Impregnation	40.0	0.35	-	-	-	100
Ga0.35/HZ40-DSZ0.05	Desilication, 0.05 M	33.0	0.34	65.6(15.2)	< 0.01	1.45(10.5)	93
Ga0.35/HZ40-DSZ0.10	Desilication, 0.10 M	25.2	0.33	121(28.0)	< 0.01	2.05(14.2)	68
Ga0.35/HZ40-DSZ0.20	Desilication, 0.20 M	13.6	0.33	224(52.3)	< 0.01	2.31(16.7)	43
Ga0.35/HZ40-SMH0.20	SMH, 0.20 M	40.0	0.35	1.13(0.27)	< 0.01	0.01(0.10)	99
Ga0.35/HZ40-SMH0.30	SMH, 0.30 M	40.5	0.35	1.16(0.27)	< 0.01	0.01(0.10)	100
Ga0.35HZ40-SMH0.40	SMH, 0.40 M	40.3	0.35	1.24(0.29)	< 0.01	0.01(0.10)	100
Ga0.35/HZ40-SMH0.50	SMH, 0.50 M	40.3	0.35	1.13(0.26)	< 0.01	0.01(0.10)	99
MCM-41//Ga0.35/HZ40	Overgrow.-MCM-41	66	0.35	1.13(0.26)	< 0.01	0.01(0.10)	100
Ga0.6/HZ40	Impregnation	39.8	0.60	-	-	-	100
Ga0.6/HZ40-DSZ0.05	Desilication, 0.05 M	31.6	0.41	62.6(15.0)	< 0.01	10.1(21.8)	93
Ga0.6/HZ40-DSZ0.10	Desilication, 0.10 M	24.8	0.42	127(31.0)	< 0.01	8.80(19.0)	81
Ga0.6/HZ40-DSZ0.20	Desilication, 0.20 M	13.1	0.42	244(60.0)	< 0.01	9.18(19.8)	50
Ga0.6/HZ40-SMH0.20	SMH, 0.20 M	39.8	0.57	1.27(0.31)	< 0.01	0.01(0.03)	96
Ga0.6/HZ40-SMH0.30	SMH, 0.30 M	38.6	0.56	1.67(0.41)	< 0.01	0.01(0.03)	100
Ga0.6/HZ40-SMH0.40	SMH, 0.40 M	38.6	0.57	1.38(0.34)	< 0.01	0.01(0.03)	100
Ga0.6/HZ40-SMH0.50	SMH, 0.50 M	38.1	0.60	4.52(1.11)	< 0.01	0.01(0.03)	100
MCM-41//Ga0.6/HZ40	Overgrow.-MCM-41	57.1	0.60	3.11(0.76)	< 0.01	0.01(0.03)	100

[a]: by ICP-OES, [b]: nominal Si/Al = 40.0; [c]: nominal Ga loading (Ga/(Al+Ga)) = 0.35 and 0.60

4.6. Structural, textural and morphological properties

4.6.1. X-ray diffraction measurements

The XRD patterns of parent microporous and mesoporous zeolites of Si/Al ratios of 11 and 40 are shown in Figure 4.18 A,B (Supplementary Information). While, the XRD patterns of mesoporous Ga-containing HZSM-5 of Si/Al = 11 and Ga loading (Ga/(Al+Ga)) of 0.10 and 0.60 are depicted on Figure 4.19A,B. Figure 4.20A,B presents the XRD patterns of mesoporous Ga-containing HZSM-5 of higher Si/Al ratio (40.0). The structural parameters of all samples are summarized in Tables 4.9 and 4.10.

The XRD patterns of mesoporous HZSM-5 obtained by different post-treatment methods (Figure S-1A,B) exhibit XRD reflections that are characteristic of MFI structure with a certain decrease of the characteristic reflections. Further it is seen from Figure S-1, that long-range ordering, type of mesoporosity, and degree of hexagonal MCM-41 mesostructural ordering were influenced by post-synthesis methods, which in turn were affected by zeolite Si/Al ratio. For example, upon alkaline treatment, there was no change in the position of the XRD peaks, suggesting the preservation of long-range ordering and microporous structure. The degree of crystallinity of HZSM-5 (Si/Al = 11) evaluated by the ratio between the areas of the diffraction peaks ($2\theta = 20 – 25°$) of the NaOH-treated samples (up to 0.10 M NaOH) and parent sample, was higher than 90 % (Figure 18A, Table 4.9). Whereas, the relative crystallinity of samples treated by more concentrated NaOH solution (0.20 M) dropped to the level of ca. 70 %. Upon hydrothermal CTAB-mediated assembly of zeolite seed into MCM-41 structure using NaOH, the crystallinity was ca. 90 % up to [NaOH] = 0.20 M. At higher [NaOH], the crystallinity decreased

significantly reaching a level of ca. 50 % for samples treated in the presence of 0.50 M NaOH. The crystallinity of composite MCM-41//HZ11 (obtained by CTAB-mediated coating of HZSM-5 with mesoporous MCM-41 layer (overgrowth of MCM-41 structure)) was ca. 70 %. Thus, post-treatment methods result in crystallinity loss, according to CTAB-mediated assembly < desilication ≅ overgrowth of MCM-41 mesostructure.

Figure 4.18A also revealed the presence of reflection lines in the low- 2θ regions, that is 1.2 - 4°. These lines, which can be indexed as (100), (110), and (200) (the last two higher order peaks appear to merge into a low-intensity ill-defined peak), are characteristic of 1D-hexagonal mesostructure MCM-41 [5]. They only appeared in samples obtained by CTAB-mediated assembly and overgrowth of MCM-41 mesostructure. Thus, suggesting that such methods form "ordered mesoporosity of MCM-41 structure", whereas alkaline treatment leads to "random mesoporosity" (mesoporosity by alkaline treatment was confirmed by N_2 sorption measurements, which will be discussed in subsequent section). It was also noted that the extent of hexagonal MCM-41 mesostructural ordering upon CTAB-mediated hydrolysis treatment depends on the concentration of NaOH solution. The ordered MCM-41 mesostructures were only seen in samples obtained with NaOH solutions higher than 0.20 M, where such ordering increases with increasing the concentration of NaOH solutions.

The XRD patterns of mesoporous HZSM-5 of higher Si/Al ratio (Figure 4.18B, Table 4.10)) revealed similar pattern of changes upon post-treatments. However, it is apparent that the level of structural preservation is lower than that of HZSM-5 of Si/Al ratio of 11. The relative crystallinity of HZSM-5 (Si/Al = 40) was around 60 % upon treatment with 0.10 M NaOH solution, whereas samples obtained by CTAB-mediated

assembly approach using 0.20 M NaOH exhibit relative crystallinity of ca. 70 % (Table 4.10). Furthermore, the hexagonal MCM-41 mesostructures are better ordered than those of zeolite of Si/Al ratio of 11, as evidenced by the low-angle XRD patterns (Figure 4.18B).

As expected, the XRD patterns of mesoporous Ga-containing HZSM-5 (Figure 4.19,4.20) exhibit the typical reflections of HZSM-5. No XRD reflections belonging to bulk β-Ga_2O_3 particles can be resolved from the XRD patterns, implying that Ga species exist as highly dispersed extracrystalline (nanosized) oxides at the external zeolite surface and/or dispersed extra framework species. However, the presence of extra framework species is very doubtful since gallium was incorporated by impregnation. Upon alkaline treatment, the structural integrity of Ga-containing HZSM-5 was affected in a similar way as those of corresponding parent HZSM-5. This may suggest that Ga presence or loadings has little or no effect on the degree of crystallinity, which can be attributed to the leaching of Ga species as evidenced by the elemental analysis (Table 4.6,4.7). It was also seen that the relative crystallinity of samples obtained by post-synthesis methods other than desilication was not affected either by gallium. This despite the fact that elemental analysis showed that gallium species were not lost during these post-treatments. Therefore, the inert role of gallium species can be related to the fact that most gallium species exist as extracrystalline gallium oxide on the external surface and not as framework or extra framework species. Interestingly, low-angle XRD patterns revealed that gallium species played a promoting role on the degree of MCM-41 mesostructures ordering. Mesoporous gallium-containing HZSM-5 of high Ga loading (Ga/(Al+Ga) = 0.60) and regardless of Si/Al ratios exhibit higher intensity of (100) diffraction peak as

compared to lower loading, implying a higher degree of hexagonal structural ordering. Thus, it can be said that Ga species have an important role with respect to the structural ordering of MCM-41. It is worth noting that the crystallinity and MCM-41 ordering of mesoporous HZSM-5 were slightly reduced upon the addition of gallium by impregnation, as shown in Figure 4.20, Table 4.11).

4.6.2. Fourier Transform Infrared measurements

The FTIR spectra of mesoporous parent and Ga-containing HZSM-5 in the lattice vibration region (400 - 1400 cm^{-1}) are shown in Figure 4.21. Details of peaks assignment [6,7] are shown in the figure. As shown in this figure, all samples exhibit an intense band near 550 cm^{-1}, indicative of the five-membered ring subunits analogous to those found in HZSM-5. It can be also seen that the 550 cm^{-1} band is progressively reduced by increasing the concentration of NaOH solutions for alkaline and CTAB-mediated assembly post-treatments of samples containing Si/Al of 40. These findings further supports the XRD data (Table 4.9,4.10), since it is has been reported that the reduction in the 550 cm^{-1} band is a reflection of zeolite crystallinity loss [8].

The IR spectra also showed that the band near 1100 cm^{-1}, which is assigned to the internal (intra-tetrahedral) vibrations in the asymmetric region, shifted to lower wavenumber upon increasing the concentration of NaOH solutions, i.e. the asymmetric stretching band of HZSM-5 (Si/Al = 40) and corrosponding Ga-containing HZSM-5 (Ga/(Al+Ga = 0.60) shifted from 1100 to ~ 1093 cm^{-1}, upon alkaline treatment with NaOH solution of 0.10 M. Le van Mao et al [9 and reference therein] reported that symmetric and asymmetric stretching vibrations of the T-O bond (T stands for Si, or Al)

are very sensitive to variations in the density of the framework Al sites (Al tetrahedral). In particular, it was mentioned that the asymmetric stretching band of the T-O bond shifts to lower frequency when the content of tetrahedral Al sites increased. The FTIR results given in Table 4.9 and 4.10 show that there is a clear relationship between the frequency of this stretching band and the Si/Al ratio of alkaline post-treated samples. Decreasing the Si/Al ratio was always associated with the shift to lower wavenumber (i.e. increasing the variation of frequency with respect to that of parent HZSM-5 (ΔF_{asym})). However, the asymmetric band of samples obtained by CTAB-mediated assembly approach using high concentration of NaOH (> 0.30 M), also exhibited a shift to lower wavenumber. This is despite the fact that there was no significant change in the Si/Al ratio.

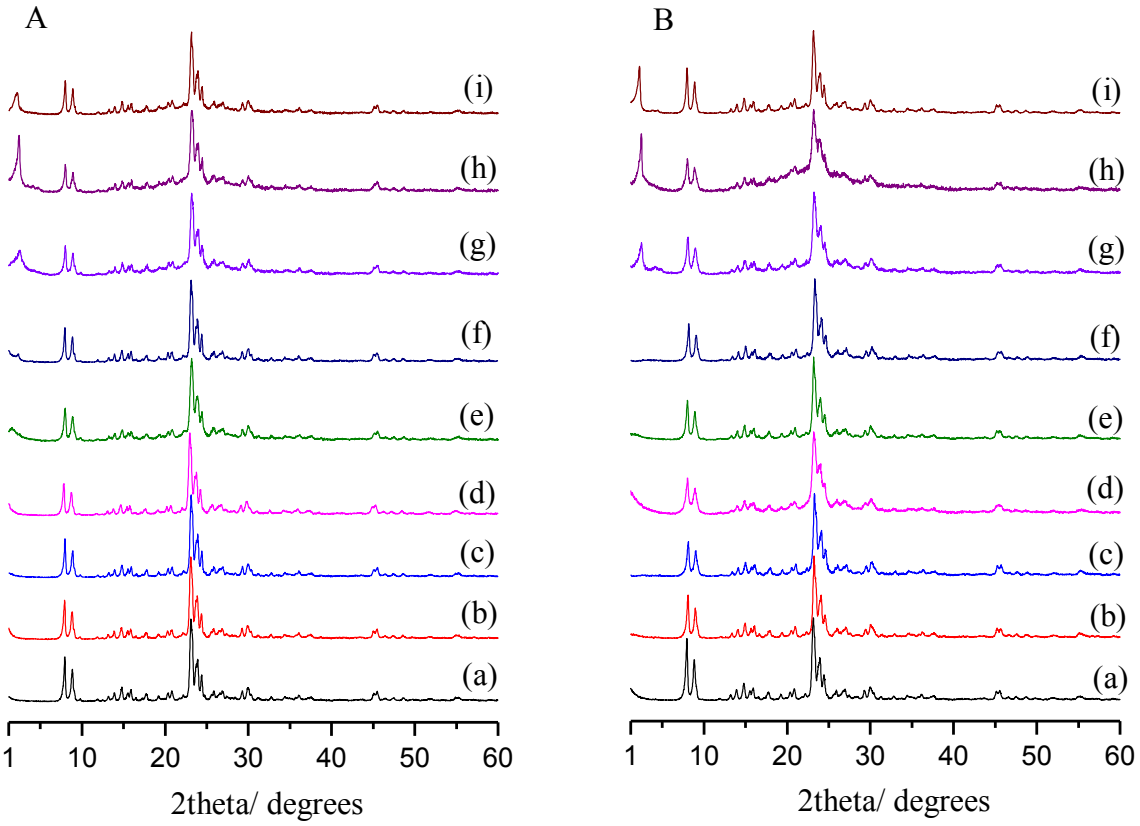

Figure 4.18: XRD patterns of mesoporous HZSM-5 of Si/Al = 11 (A) and 40 (B)

obtained by different post-synthesis methods; a) HZ11 or HZ40; b-d) desilication using 0.05, 0.10 and 0.20 M NaOH; e-h) CTAB-mediated assembly of zeolite seed using 0.30, 0.40 and 0.50 M NaOH; and i) composite MCM-41//HZ.

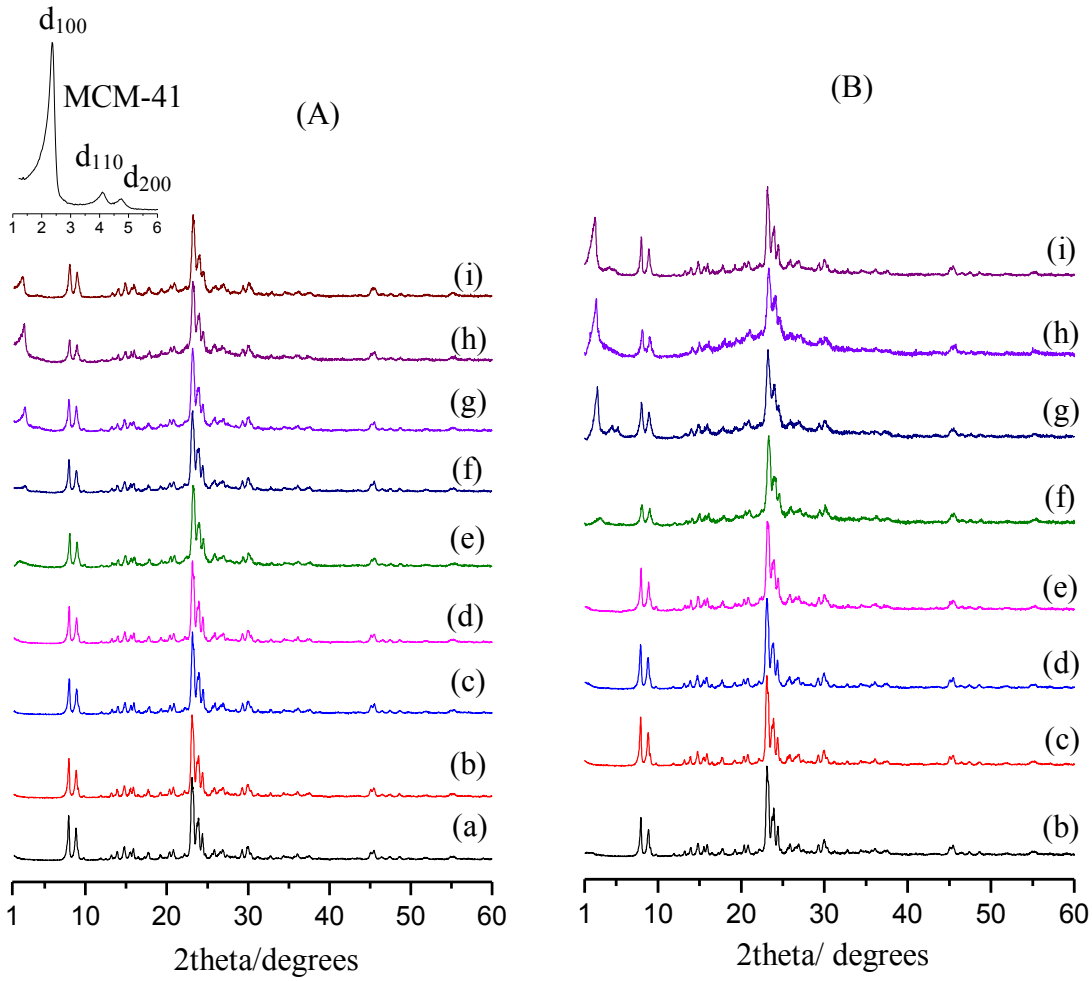

Figure 4.19: XRD patterns of mesoporous Ga-containing HZSM-5 (Si/Al = 11) of different Ga loadings (A and B corrosponds to Ga/(Al+Ga) of 0.10 and 0.60, respectively) obtained by different post-synthesis methods; a) HZ11; b) Ga0.1 or 0.60/HZ11; c-e) desilication using 0.05, 0.10 and 0.20 M NaOH; f-h) CTAB-mediated assembly of zeolite seed using 0.30, 0.40 and 0.50 M NaOH; and i) composite MCM-41//Ga/HZ11.

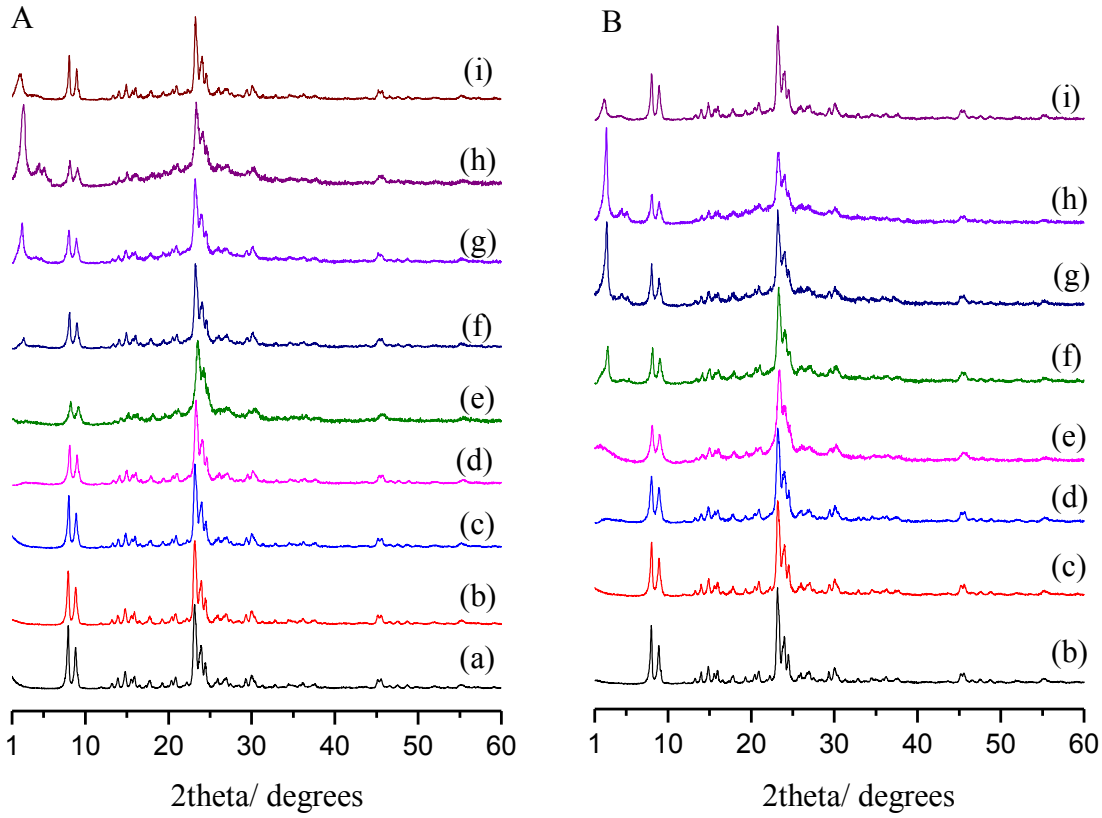

Figure 4.20: XRD patterns of mesoporous Ga-containing HZSM-5 (Si/Al = 40) of different Ga contents (A and B corrosponds to Ga/(Al+Ga) of 0.35 and 0.65, respectively) obtained by different post-synthesis methods; a) HZ40; b) Ga/HZ40 (Ga/(Al+Ga) = 0.35 or 0.60); c-e) desilication using 0.05, 0.10 and 0.20 M NaOH; f-h) CTAB-mediated assembly of zeolite seed using 0.30, 0.40 and 0.50 M NaOH; and i) composite MCM-41//Ga/HZ40.

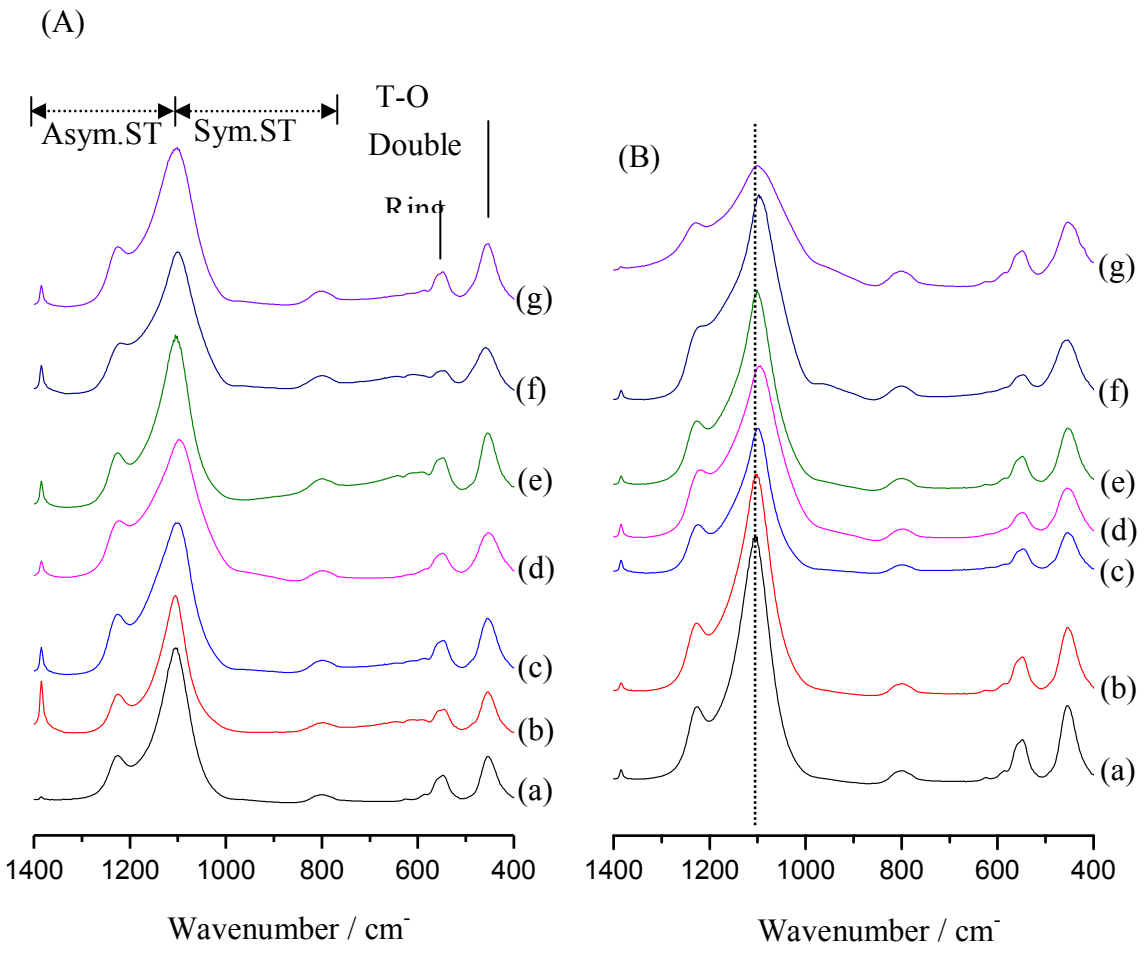

Figure 4.21: FTIR spectra of mesoporous parent (A) and Ga-containing HZSM-5 (Ga/(Al+Ga) = 0.60, Si/Al = 80) (B) obtained by different post-synthesis treatments; a) HZ40 or Ga0.6/HZ40; b-d) desilication using 0.05, 0.10 and 0.20 M NaOH; e,f) CTAB-mediated assembly of zeolite seed using 0.20, and 0.50 M NaOH; and g) composite MCM-41//HZ40 or MCM-41//Ga0.6/HZ40. (T stands for framework cations Si or Al; Asym.ST and Sym.ST correspond to asymmetric and symmetric stretch vibration, respectively).

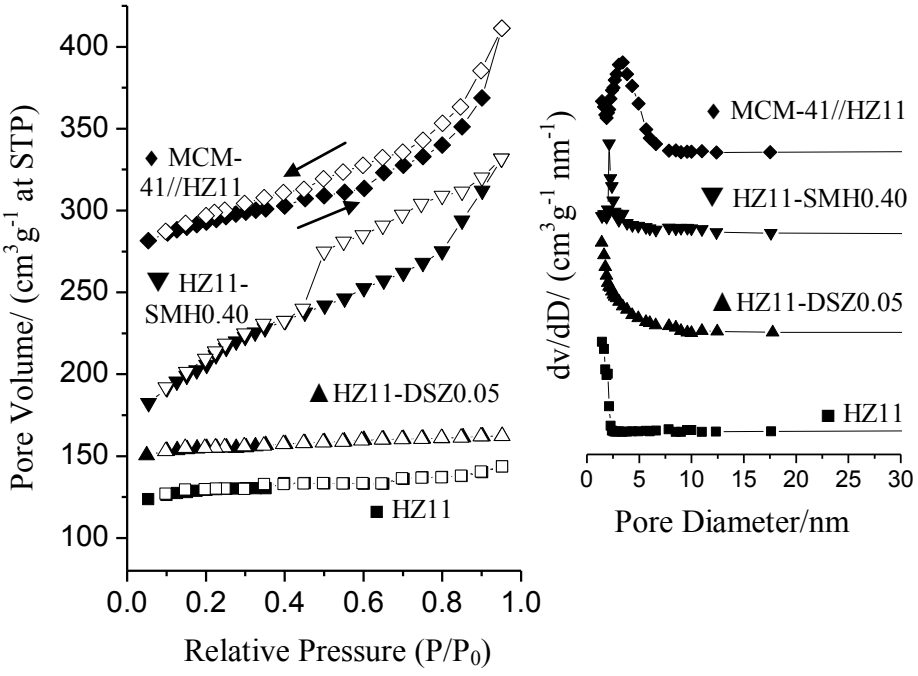

Figure 4.22: N_2-adsorption-desorption isotherms and derived BJH mesopore size distribution of mesoporous HZSM-5 (Si/Al = 11), obtained by alkaline treatment, CTAB-mediated assembly of HZSM-5 seed, and coating with MCM-41 mesostructure. Inset: Pore size distribution

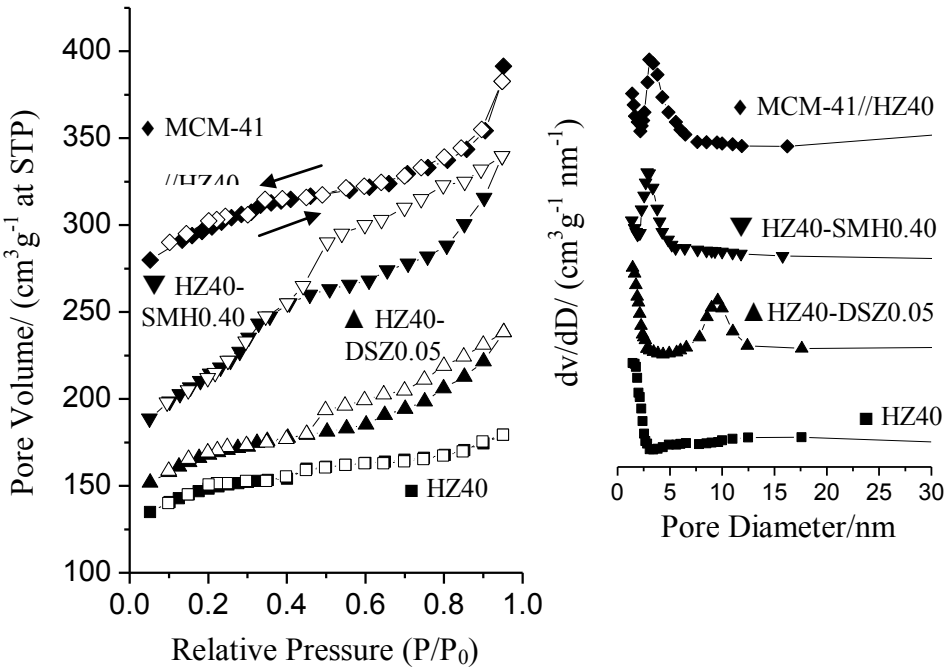

Figure 4.23: N_2-adsorption-desorption isotherms and derived BJH mesopore size distribution of mesoporous HZSM-5 (Si/Al = 40), obtained by alkaline treatment, CTAB-mediated assembly of HZSM-5 seed, and coating with MCM-41 mesostructure. Inset: Pore size distribution.

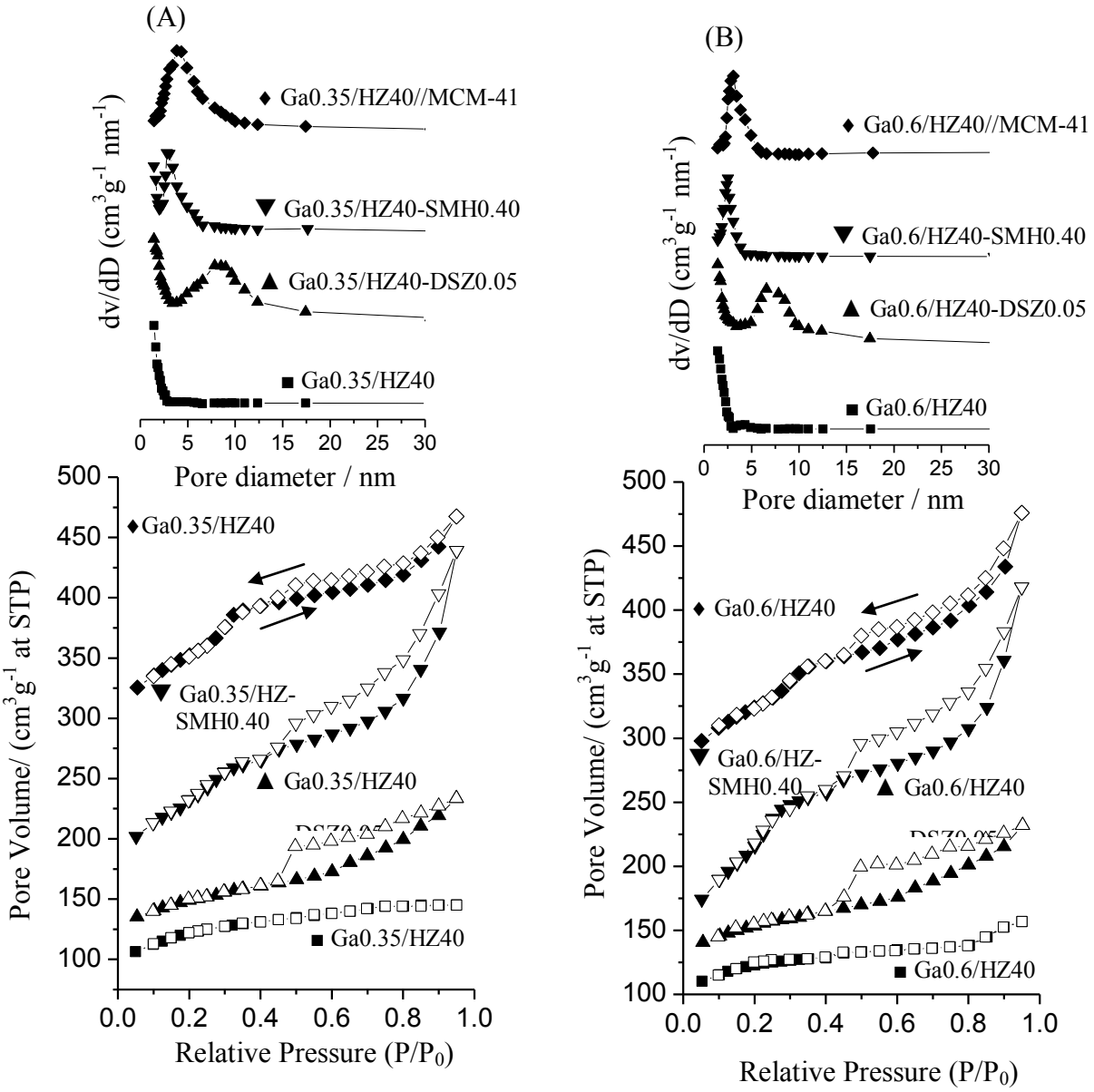

Figure 4.24: N_2-adsorption-desorption isotherms and derived BJH mesopore size distribution of mesoporous Ga-containing HZSM-5 (Si/Al = 40, Ga/(Al+Ga) = 0.35 (A) or 0.60 (B)) obtained by alkaline treatment, CTAB-mediated assembly of HZSM-5 seed, and coating with MCM-41 mesostructure. Inset: Pore size distribution.

Table 4.8 Textural and structural properties of mesoporous HZSM-5 and Ga-containing HZSM-5 of Si/Al = 11

Catalysts	N_2-adsrption					XRD		FTIR
	S_{BET} (m^2g^{-1})	V_{micro} (cm^3/g)[a]	V_{meso} (cm^3/g)[a]	S_{meso} (m^2g^{-1})[b]	d_{meso}[c] (nm)	d_{100} (nm)	Cryst[d] (%)	ΔF_{asym} [e]
HZ11	390	0.18	0.22	35.0	-	-	100	0.0
HZ11-DSZ0.05	387	0.19	0.23	28.8	-	-	97	0.0
HZ11-DSZ0.10	370	0.17	0.24	32.3	-	-	93	2.0
HZ11-DSZ0.20					-	-	70	4.0
HZ11-SMH020	410	0.16	0.29	220	-	-	90	0.0
HZ11-SMH040	484	0.14	0.41	298	2.74	3.47	55	4.0
HZ11-SMH0.50						3.62	50	0.0
MCM-41//HZ11	401	0.12	0.41	138	3.41	4.00	70	0.0
Ga0.1/HZ11	360	0.18	0.19	40.0	-	-	96	0.0
Ga0.1/HZ11-DSZ0.05	360	0.19	0.22	51.0	-	-	95	0.0
Ga0.1/HZ11-DSZ0.10	365	0.20	0.25	56.0	-	-	90	3.0
Ga0.1/HZ11-DSZ0.20					-	-	62	4.0
Ga0.1/HZ11-SMH0.20	388	0.15	0.28	115		-	85	0.0
Ga0.1/HZ11-SMH0.40	517	0.10	0.51	346	2.64	3.42	61	4.0
Ga0.1/HZ11-SMH0.50						3.53	50	5.0
MCM-41//Ga0.1/HZ11	473	0.11	0.46	250	3.11	3.50	51	0.0
Ga0.6/HZ11	328	0.15	0.20	45.0	-	-	95	0.0
Ga0.6/HZ11-DSZ0.05	315	0.14	0.19	41.0	-	-	95	0.0
Ga0.6/HZ11-DSZ0.10	317	0.15	0.20	39.0	-	-	92	3.0
Ga0.6/HZ11-DSZ0.20					-	-	60	3.0
Ga0.6/HZ11-SMH0.20	352	0.14	0.26	154	-	-	80	0.0
Ga0.6/HZ11-SMH0.40	403	0.13	0.37	246	2.51	3.25	55	2.0
Ga0.6/HZ11-SMH0.50						3.40	50	3.0
MCM-41//Ga0.6/HZ11	466	0.11	0.42	191	3.35	3.65	55	0.0

[a]: micropore volume calculated using the t-plot [55]; [b]: S_{meso} includes the mesoporous and external surface area; [c]: mesopore average pore diameter was calculated using from the adsorption branch using the Kruk, Jaroniec, Sayari (KJS) method [60]; and [d]: Relative crystallinity (RC) from XRD measurements; and [e]: ΔF_{asym} variation of frequency of asymmetric stretching vibration (ν_{asym}) with respect to that of the parent zeolite, ± 2.0 cm^{-1} [89].

Table 4.9. Textural and structural properties of mesoporous HZSM-5 and Ga-containing HZSM-5 of Si/Al = 40.

Catalysts	N_2-adsrption					XRD		FTIR
	S_{BET} (m^2g^{-1})	V_{micro} (cm^3/g)[a]	V_{meso} (cm^3/g)[a]	S_{meso} (m^2g^{-1})[b]	d_{meso}[c] (nm)	d_{100} (nm)	Cryst[e] (%)	ΔF_{asym}[f]
HZ40	425	0.19	0.23	68	-	-	100	-
HZ40-DSZ0.05	450	0.19	0.31	125	9.12	-	74	0.0
HZ40-DSZ0.10	485	0.17	0.44	171	10.0	-	60	7.0
HZ40-DSZ0.20						-	56	8.0
HZ40-SMH020	463	0.18	0.34	150	-	-	70	0.0
HZ40-SMH040	540	0.11	0.49	300	2.84	3.56	55	7.0
HZ40-SMH0.50						3.94	45	8.0
MCM-41//HZ40	445	0.14	0.39	250	3.35	3.94	64	0.0
Ga0.35/HZ40	386	0.18	0.25	91	-	-	94	0.0
Ga0.35/HZ40-DSZ0.05	436	0.17	0.35	139	7.83	-	80	0.0
Ga0.35/HZ40-DSZ0.10	463	0.15	0.49	193	8.95	-	75	7.0
Ga0.35/HZ40-DSZ0.20						-	50	8.0
Ga0.35/HZ40-SMH0.20	468	0.17	0.37	160	2.64	3.16	74	2.0
Ga0.35HZ40-SMH0.40	550	0.10	0.56	410	2.81	3.40	59	7.0
Ga0.35/HZ40-SMH0.50						3.62	43	8.0
MCM-41//Ga0.35/HZ40	555	0.10	0.43	350	3.84	4.10	57	2.0
Ga0.6/HZ40	360	0.18	0.27	85	-	-	92	0.0
Ga0.6/HZ40-DSZ0.05	404	0.18	0.32	130	6.65	-	75	3.0
Ga0.6/HZ40-DSZ0.10	421	0.14	0.41	220	8.85	-	70	6.0
Ga0.6/HZ40-DSZ0.20						-	45	9.0
Ga0.6/HZ40-SMH0.20	417	0.16	0.31	135	-	3.20	70	2.0
Ga0.6/HZ40-SMH0.40	550	0.08	0.48	370	2.52	3.32	46	7.0
Ga0.6/HZ40-SMH0.50						3.39	44	7.0
MCM-41//Ga0.6/HZ40	510	0.10	0.47	380	3.42	3.77	50	1.0

For notes, refer to Table 4.9.

4.7 Propane Aromatization

Results of propane conversion at 540^{o}C on parent HZSM-5, mesoporous gallium-containing HZSM-5 of Si/Al ratio 80 are shown in the tables and figures below. Tables 4.11 and 4.12 show the data of propane aromatization over conventional and mesoporous Ga-containing HZSM-5, of Si/Al ratio of 80, with Ga loading of 0.35 and 0.65 respectively. It can be seen that catalysts, irrespective of the Ga loading, with random mesoporosity generated at low NaOH concentration showed improved conversion and BTX yield over conventional microporous Ga-containing HZSM-5 for both Ga loading. Also, the ordered mesoporous catalyst with lower Ga loading (0.35) exhibited higher conversion and BTX yield over the microporous Ga-containing HZSM-5 upon CTAB-mediated base hydrolysis treatment up to 0.40M. This has been attributed to loss of zeolitic intrinsic properties as NaOH concentration increases. However, the ordered mesoporous catalyst with higher Ga loading (0.65) showed lower conversion and BTX yield with respect to its microporous counterpart.

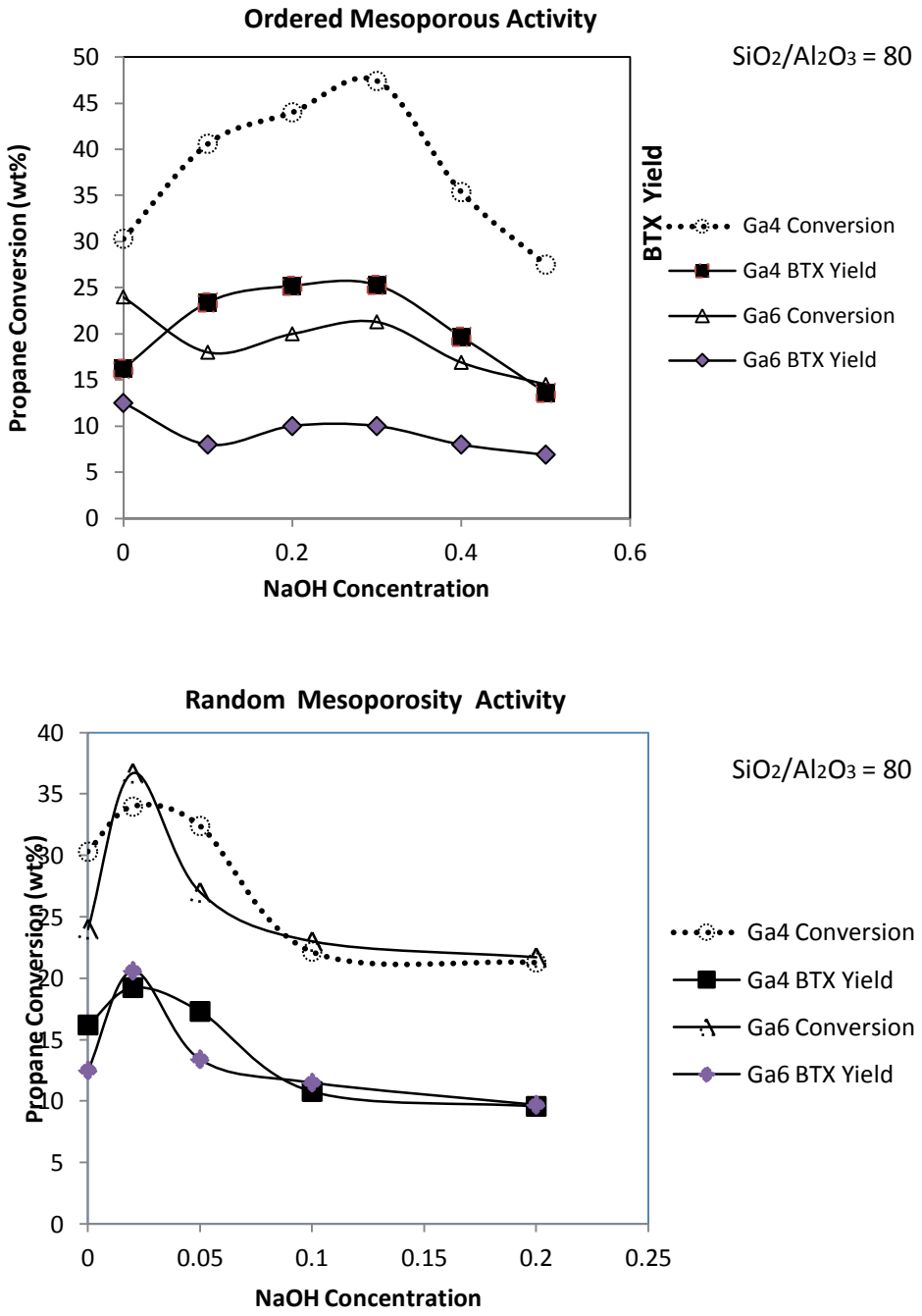

Fig.4.25: The variation of the propane conversion and BTX yield with NaOH concentration over the treated catalysts with SiO_2/Al_2O_3 of 80. ($Ga4 \triangleq \frac{Ga}{Ga+Al} = 0.35$; $Ga6 \triangleq \frac{Ga}{Ga+Al} = 0.65$)

Table 4.10: Aromatization of propane over conventional and mesoporous Ga-containing HZSM-5 (SiO_2/Al_2O_3 = 80, Ga/(Al+Ga) = 0.35)

Catalyst	Microporous Ga/HZSM-5	Mesoporous Ga/HZSM-5					
		Random Mesoporosity			Ordered Mesoporosity		
		x = 0.02	0.05	0.1	0.1	0.2	0.3
C_3 conversion (%)	30.26	33.97	32.36	22.17	40.61	44.2	47.43
BTX yield (%)	16.61	19.24	17.31	10.78	23.41	25.21	25.32
Selectivity (%)							
Methane	13.2	19.08	13.64	8.41	13.49	14.79	14.86
Ethene	5.57	4.45	4.62	4.71	3.87	4.22	3.15
Ethane	13.04	8.55	14.09	22.15	10.02	9.32	9.35
Propene	0.79	0.8	1.29	1.24	0.8	1.17	0.73
Butane [a]	1.81	1.89	2.22	2.02	2.03	1.84	1.86
Pentane	0.3	0.42	0.33	0.43	0.41	0.34	0.5
Benzene	22.28	23.77	21.59	17.29	22.94	21.66	21.09
Toluene	23.89	24.82	22.87	21.44	24.6	24.77	22.55
Ethylbenzene	0.96	1.19	0.85	0.94	0.85	0.77	1.03
Xylene	8.71	8.04	9.04	9.9	10.11	10.59	9.75
Heav. Aromatics [b]	6.39	3.94	6.2	6.37	8.1	8.26	12.44
BTX	54.87	56.63	53.5	48.62	57.65	57.02	53.39

Table 4.11: Aromatization of propane over conventional and mesoporous Ga-containing HZSM-5 (SiO_2/Al_2O_3 = 80, Ga/(Al+Ga) = 0.65)

Catalyst	Microporous Ga/HZSM-5	Mesoporous Ga/HZSM-5					
		Random Mesoporosity			Ordered Mesoporosity		
		x = 0.02	0.05	0.1	0.1	0.2	0.3
C_3 conversion (%)	24.31	36.74	27.3	20.65	18.14	20.13	21.3
BTX yield (%)	12.5	20.59	13.39	9.52	8.01	10.02	9.97
Selectivity (%)							
Methane	11.07	19.01	10.94	10.4	12.64	10.33	9.02
Ethene	5.04	5.32	3.52	3.49	4.4	4.88	3.23
Ethane	20.47	10.62	25.1	25.43	28.04	23.12	28.51
Propene	1.64	1.53	1.21	1.14	1.43	1.23	1.22
Butane [a]	1.57	1.65	1.65	1.46	1.33	1.56	1.58
Pentane	0.28	0.3	0.37	0.29	0.21	0.33	0.24
Benzene	20.61	24.27	19.58	18.07	16.71	19.03	17.68
Toluene	21.92	24.49	21.52	19.83	19.04	21.48	20.32
Ethylbenzene	0.84	0.82	0.88	0.72	0.57	0.73	0.63
Xylene	8.88	7.28	7.93	8.17	8.41	9.28	8.79
Heav. Aromatics [b]	3.81	2.22	3.13	6.66	3.43	3.91	4.33
BTX	51.42	56.04	49.03	46.07	44.16	49.79	46.79

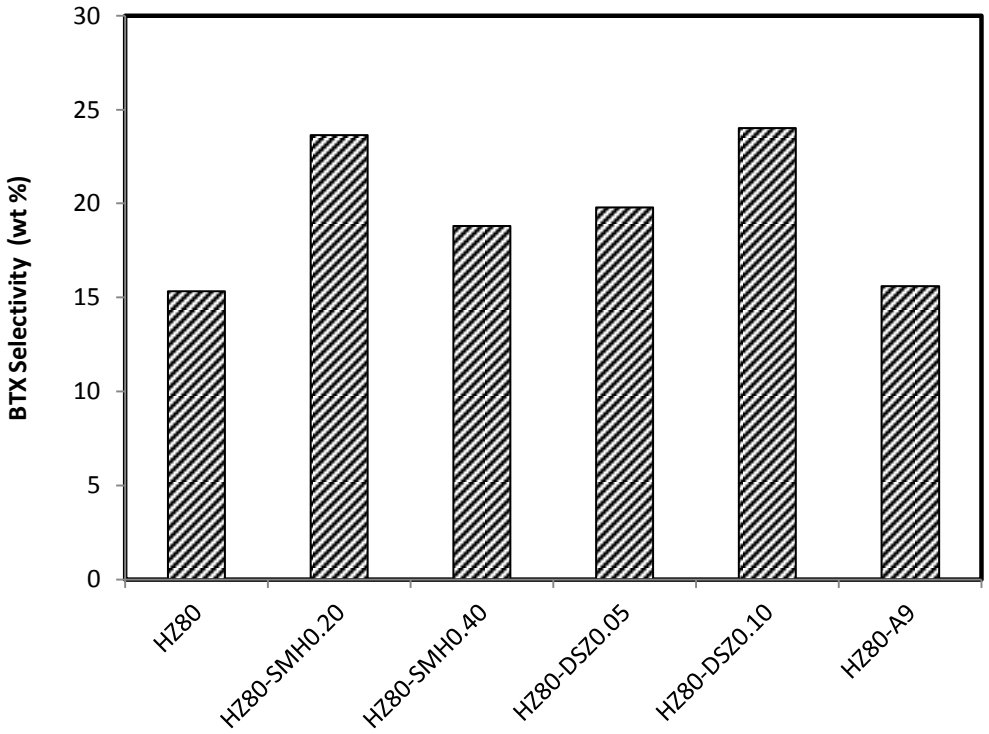

Fig. 4.26: BTX selectivity of propane aromatization over HZSM-5, ordered mesoporous and random mesoporous HZSM-5 at ~13.5% propane conversion.

Figure 4.26 depicts that the CTAB-mediated hydrolysis treatment and desilication of HZSM-5 led to an improvement in the BTX selectivity. Figures 4.27A and B depict the effect of treatment on BTX selectivities. Fig. 4.27A shows that upon treatment via any of the three methods there is a significant improvement in the selective ability of the gallium-containing catalyst with low gallium content. However, the same was not seen for catalyst with high gallium content as shown in Fig.4.27B. This figure shows slight improvement only for catalysts in which MCM-41 grew and also for desilicated catalysts at low concentration (i.e.0.05M).

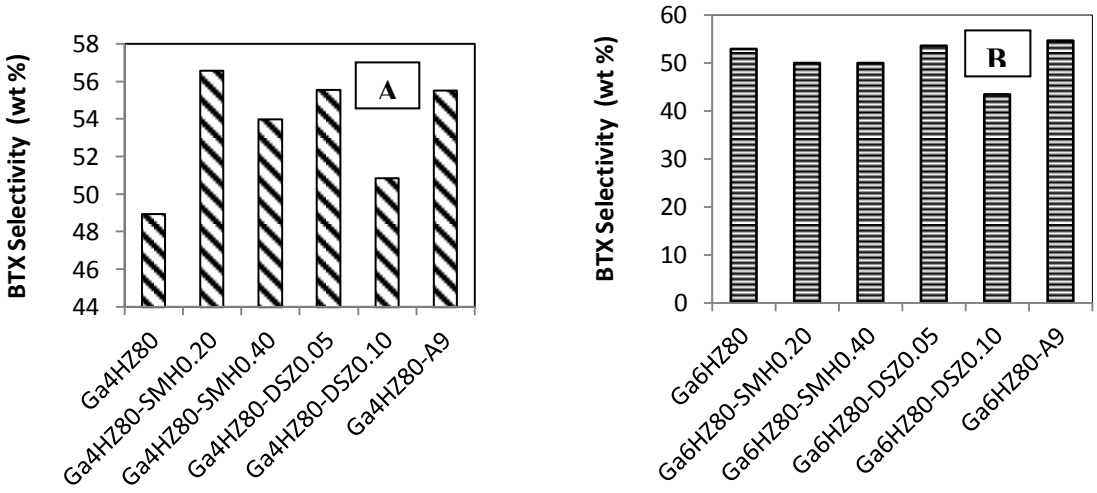

Fig.4.27: BTX selectivities of microporous and mesoporous low and high Ga-containing HZSM-5.

CHAPTER FIVE

KINETIC MODELING OF PROPANE AROMATIZATION OVER MICROPOROUS AND MESOPOROUS Ga/HZSM-5

5.1 Kinetic Study

Microporous Ga-containing H-ZSM-5 (Si/Al = 80) and Mesoporous Ga-containing H-ZSM-5, obtained via surfactant mediated hydrolysis, of the same Si/Al ratio were used as catalysts in this work. The microporous catalyst was prepared by impregnation of H-ZSM-5 zeolite with gallium nitrate solution via the incipient impregnation technique. Kinetic studies were performed at temperatures 480, 510 and 540^{o}C. Along with varying temperatures, the experiment was performed at different weight hour space velocities (WHSV) in order to obtain different degrees of conversions. Analysis of reaction products was done on line using Varian GC with FID (Varian 450-GC), equipped with an HP-INNOWax capillary column (polyethylene glycol) (60m length × 0.32mm I.D. × 0.50μm film thickness). The total pressure in all experiments was 1atm.

This work sought to investigate, kinetically, the promotional effect of the introduction of mesoporosity in the gallium-modified HZSM-5. Due to the complexity of this reaction, the model was based solely on a mechanism derived from the product distribution where several species were lumped together.

5.2. Experimental

5.2.1. Materials

$Ga(NO_3)_3.8H_2O$, NaOH, NH_4NO_3 were gotten from Sigma-Aldrich Company Ltd while NH_4ZSM-5, of Si/Al = 40) was purchased from Catal. International Ltd.

5.2.2. Catalyst Preparation

Gallium was incorporated into HZSM-5 by aqueous impregnation using 1.60g of $Ga(NO_3)_3.8H_20$. The solution was placed inside an oven at 50^{o}C for 12 h to slowly remove the water, which was further dried in a 100^{o}C oven. This was later calcined at 550^{o}C at 1^{o}C/min ramping. Mesoporosity was introduced via treating the microporous catalyst with NaOH in the presence of cationic surfactant. Usually, as reported earlier [51], 2.45g of CTAB was dissolved in 55ml of 0.30M NaOH. This was stirred for 1 hour at room temperature after which 2.0g of the microporous catalyst was added to the solution at the same room temperature. The mixture was then placed in an oven at a temperature of 100^{o}C for 24 hours. pH was adjusted to 9.0 and placed back into the oven and aged for another 24 hours. The resulting solid was then filtered, dried and calcined to transform into the H-form.

5.2.3. Catalytic testing

The reactions of propane over microporous and mesoporous gallium-containing HZSM-5 were carried out in a fixed bed continuous flow micro-reactor with dimension$0.312\ I.D.\times 0.562\ O.D.\times 15.0\ cm\ length$. Reaction temperature was varied between 480^{o}C and 540^{o}C with flow rate of feed high enough to overcome any diffusional limitation. Catalysts were sieved to a particle size of 500-1000μm. Constant

weight of the samples was used and fed into the reactor with varying volumetric flow rate of feed diluted with varying flow rate of N_2. That is, the experiment was done at different weight hour space velocities (WHSV) in order to have different degrees of conversion. Analysis of reaction products was done on line using Varian GC with FID (Varian 450-GC), equipped with an HP-INNOWax capillary column (polyethylene glycol) (60m length × 0.32mm I.D. × 0.50μm film thickness). The total pressure in all experiments was 1atm.

The conversion of propane,$X_{propane}$, was calculated using

$$X_{propane} = \frac{\sum A_i - A_{propane}}{\sum A_i} \times 100$$

where $A_i \; and \; A_{propane}$ are the corrected chromatographic areas for species i and propane respectively. The selectivity S_i and yield,Y_i, to particular product was calculated using the following

$$S_i = \frac{A_i}{\sum A_i - A_{propane}} \times 100$$

$$Y_i = \frac{X_{propane} \times S_i}{100}$$

5.3 Results and Discussions

5.3.1 Catalytic activity

The effect of temperature on a reaction cannot be over emphasized as can be seen in the tabulated result below that conversion of propane increases with increase in temperature. Also, at low temperatures, the dominant reactions are those of cracking and slight dehydrogenation. As temperature increases, aromatics start to form. Moreover, we see an incremental trend in the yield of BTX (Benzene, Toluene and Xylene). This effect is presented in Fig. As expected, propane conversion increased with temperature for all catalysts used. No conversion was observed for propane at temperatures below 673K and gas hourly space velocities which were greater than 30,000. As a result of this the temperature range used was 753-813K. The main products for the aromatization of propane over gallium-modified HZSM-5, both microporous and mesoporous, were ethane, methane, benzene, toluene, xylene and Ethylbenzene. However, small quantities of ethylene, butane, and heavier hydrocarbons (C8+) were observed. Moreover, we also observed trace amounts of n-butylenes and its isomeric counterparts.

5.3.2. Benzene, Toluene, Xylene (BTX) selectivity

The BTX selectivity during the aromatization of propane over microporous and mesoporous Ga/HZSM-5 were compared in Fig. 3. at iso-conversion level of ~13%. Results display the superior selectivity to BTX observed over the mesoporous Ga/HZSM-5 as compared to the microporous counterpart. BTX selectivities over both catalysts show dependence on temperature as shown in Fig. 4.

Table 5.1
Product Distribution at various reaction conditions for propane aromatization over Ga4HZ80

Temperature	Contact Time (s)	*Propane Conv.(%)*	Yield (%)		
			Propylene	*Cracking Products*	*BTX*
	0.276	3.11	0.37	0.84	1.17
	0.320	3.38	0.33	0.96	1.40
480°C	0.380	3.57	0.31	0.85	1.37
	0.484	4.92	0.21	1.34	2.31
	0.639	6.04	0.31	1.77	2.80
	0.940	7.18	0.24	1.76	3.88
	1.330	7.22	0.29	2.48	3.43
	0.276	4.72	0.28	1.48	2.05
	0.320	5.00	0.22	1.51	2.30
510°C	0.380	5.45	0.18	1.63	2.59
	0.484	7.22	0.26	2.10	3.58
	0.639	10.74	0.30	3.26	5.57
	0.940	14.46	0.24	4.71	7.76
	1.330	16.70	0.35	5.73	9.11
	0.276	7.66	0.31	2.27	3.78
	0.320	9.54	0.30	3.35	4.09
540°C	0.380	11.15	0.34	3.19	4.84
	0.484	13.22	0.44	3.35	7.09
	0.639	19.30	0.49	6.20	10.33
	0.940	20.28	0.43	6.46	11.52
	1.330	29.32	0.46	10.92	15.60

Table 5.2
Product Distribution of propane aromatization over Ga4HZ80-SMH0.30

Temperature	Contact Time (s)	*Propane Conv.(%)*	Yield (%)		
			Propylene	*Cracking Products*	*BTX*
	0.276	3.74	0.23	0.91	1.64
	0.320	5.59	0.27	1.11	2.43
480°C	0.380	5.46	0.31	1.17	2.59
	0.484	9.15	0.28	1.76	4.45
	0.639	10.07	0.31	2.47	5.86
	0.940	11.06	0.23	3.19	5.87
	1.330	11.95	0.41	3.97	6.27
	0.276	7.72	0.54	1.69	3.91
	0.320	8.76	0.40	1.85	4.62
510°C	0.380	10.47	0.48	2.15	5.61
	0.484	13.86	0.37	3.03	7.85
	0.639	14.20	0.58	3.10	7.86
	0.940	18.46	0.61	6.57	9.27
	1.330	19.04	0.34	10.99	11.14
	0.276	15.54	0.48	4.06	8.87
	0.320	16.54	0.42	4.07	9.77
540°C	0.380	20.56	0.47	5.15	12.47
	0.484	27.08	0.58	7.34	16.30
	0.639	28.28	0.63	7.63	17.45
	0.940	38.88	0.67	12.51	23.27
	1.330	39.78	0.62	12.14	24.16

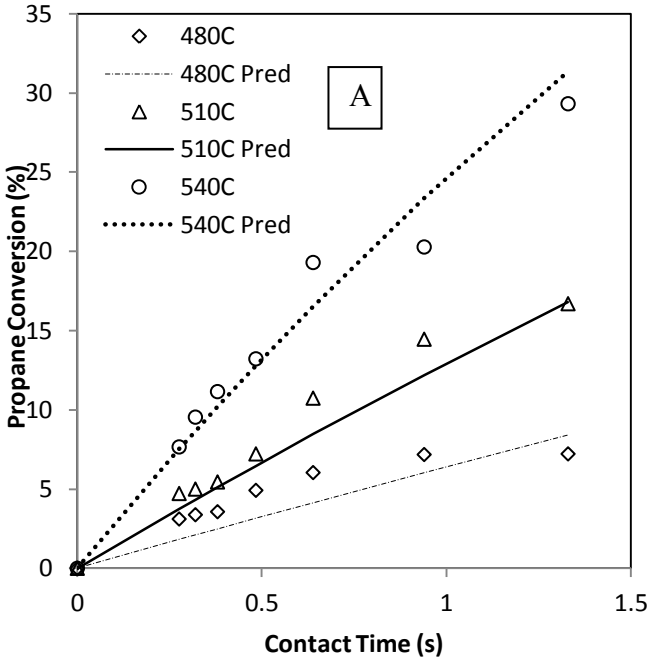

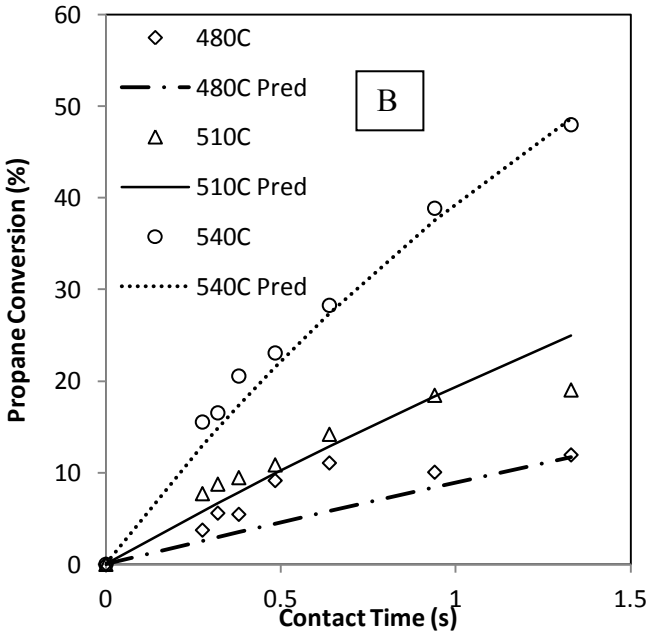

Fig.5.1 Propane Conversion with respect to contact time at different temperatures over: (A). Microporous Ga4HZ80 and (B). Mesoporous Ga4HZ80-SMH0.30.

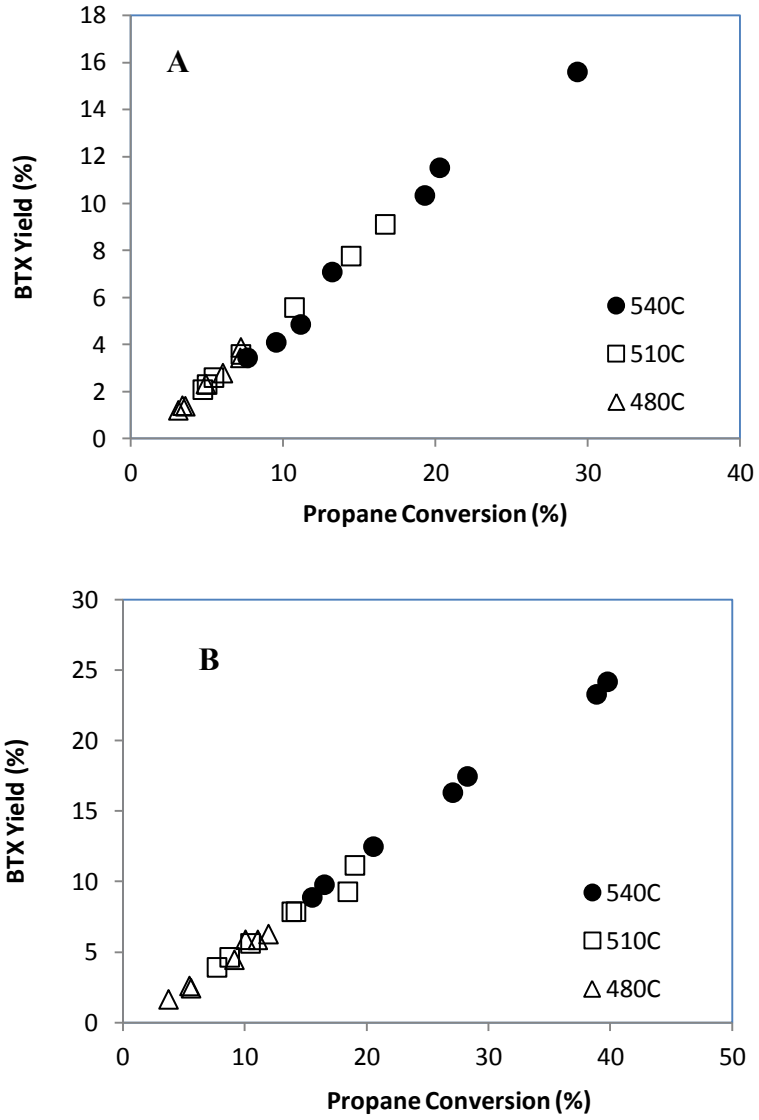

Fig.5.2 Dependence of BTX yield on propane conversion for: (A) GaHZ80, (B) Ga4HZ80-SMH0.30 at reaction temperatures (•) 540°C, (□) 510°C, (Δ) 480°C.

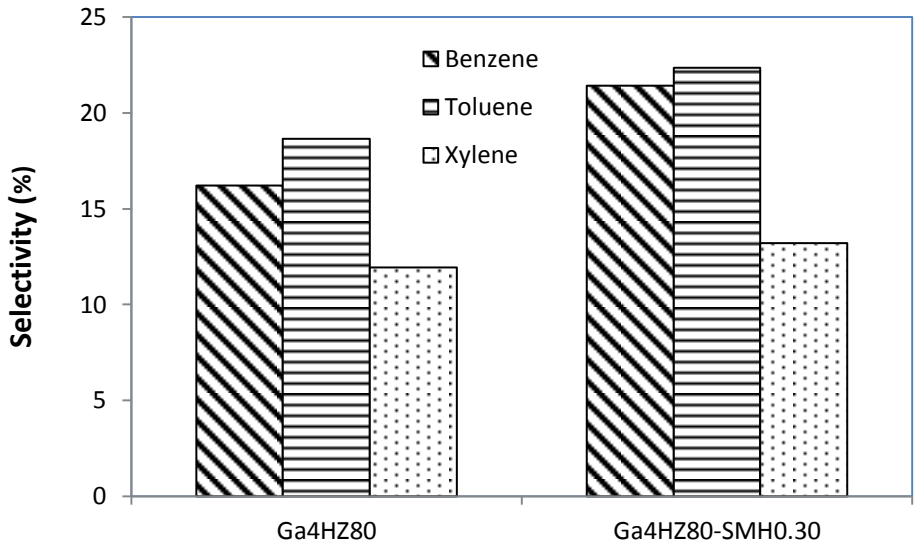

Fig.5.3 BTX selectivity of propane aromatization over the different catalysts at ~13% propane conversion.

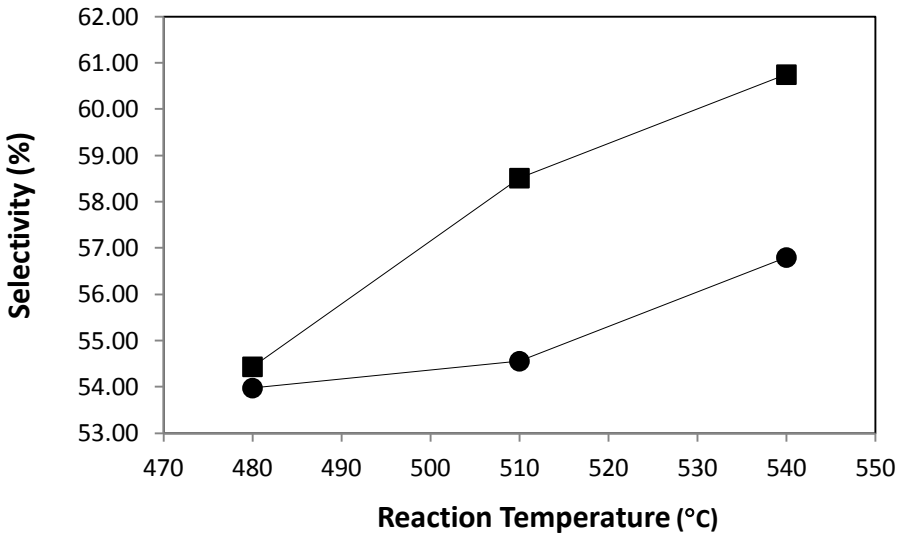

Fig.5.4 BTX Selectivity as a function of reaction temperature at 1.33s over :(•) Ga4HZ80 and (■) Ga4HZ80-SMH0.30.

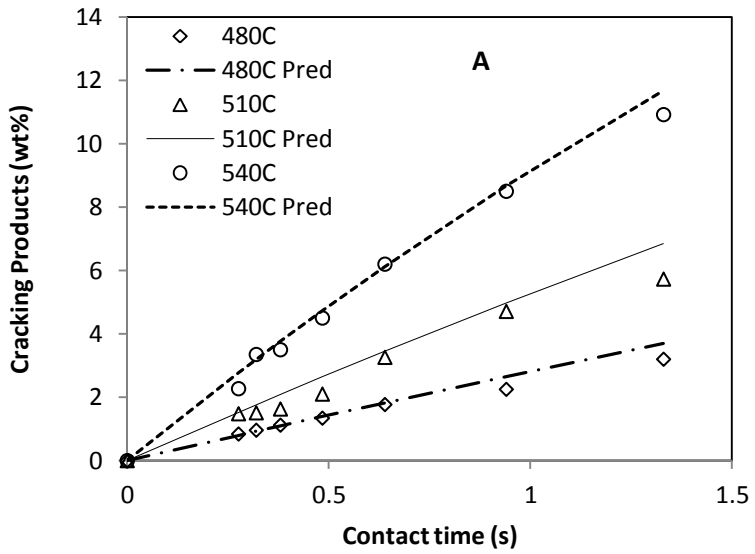

Fig.5.5 Comparison between experimental results and model predictions for the yield of cracking products at the reaction temperatures of 480°C (◊), 510°C (Δ) and 540°C (o).

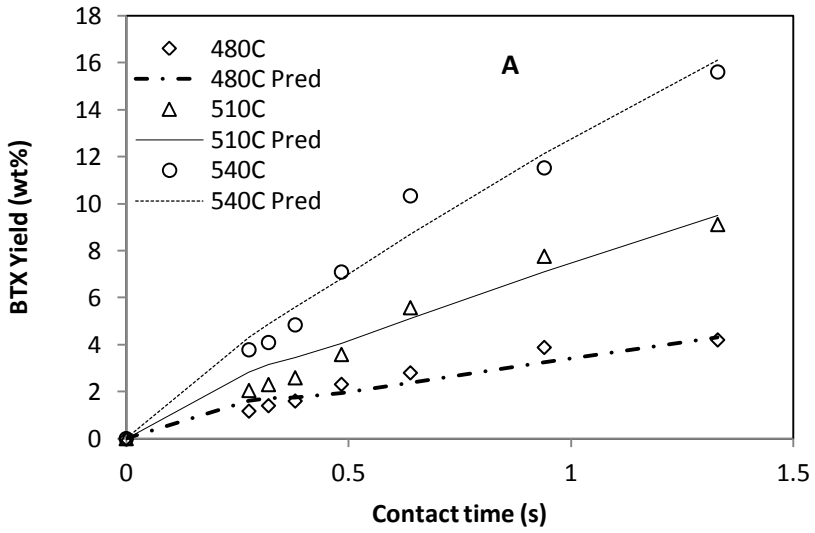

Fig.5.6. Comparison between experimental results and model predictions for BTX yield at the reaction temperatures of 480°C (◊), 510°C (Δ) and 540°C (o).

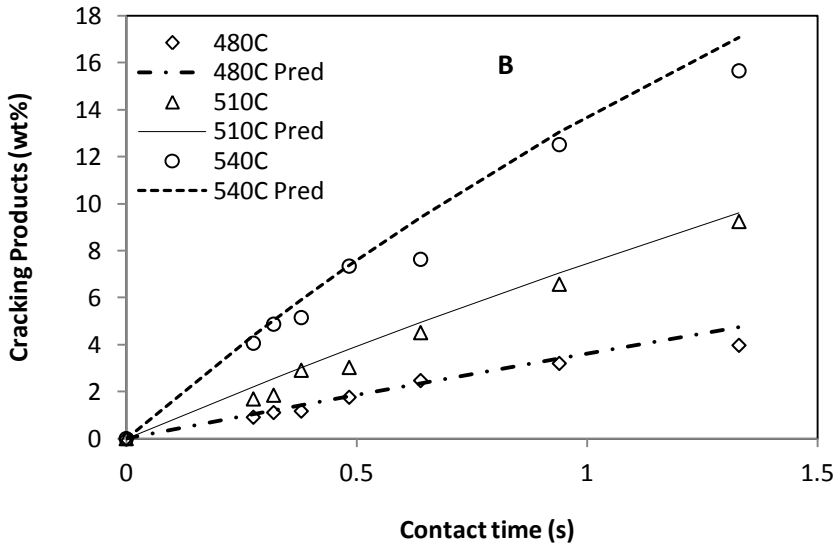

Fig.5.7 Comparison between experimental results and model predictions for the yield of cracking products at the reaction temperatures of 480^{o}C (◊), 510^{o}C (Δ) and 540^{o}C (o).

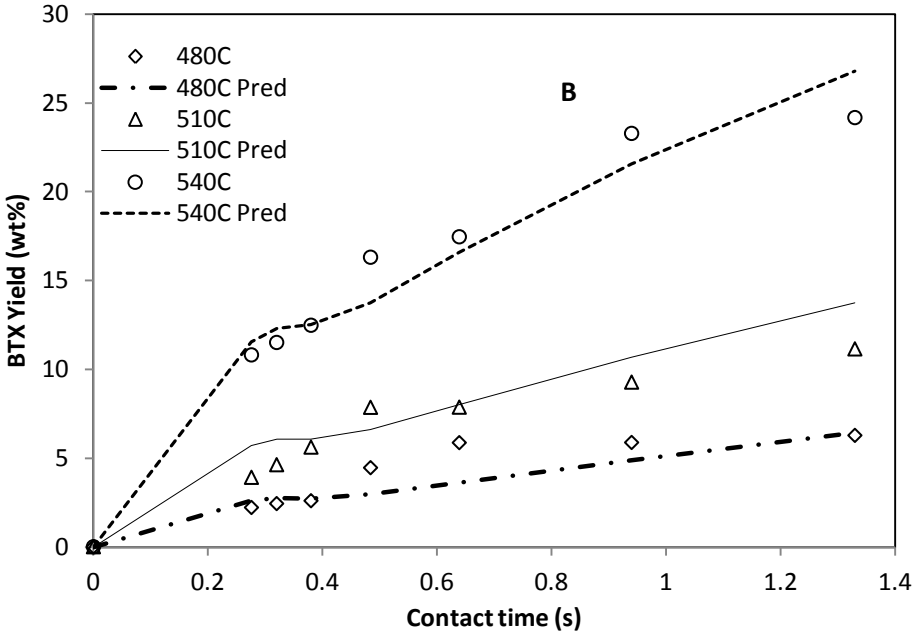

Fig.5.8 Comparison between experimental results and model predictions for BTX yield at the reaction temperatures of 480°C (◊), 510°C (Δ) and 540°C (o).

5.3.2. Benzene, Toluene, Xylene (BTX) yield

The yields of benzene, toluene and xylene (BTX) were found to increase with both temperature and time, in a related manner with propane conversion. From the result, we observed maximum BTX yield, of approximately 15.60 and 24.20% for Ga4HZ80 and Ga4HZ80SMH0.30 catalysts respectively, attained at reaction temperature of 540^{o}C and 1.33s contact time. This suggests that for longer contact time, there are definitely dehydrocyclization reactions leading to more aromatic formation.

5.4. Kinetic modeling

Knowledge of the kinetics of a reaction can provide valuable insights into the mechanism of the catalytic reaction and the challenge being posed by the complexity of the aromatization reaction has led us to make some assumptions in the development of the kinetic model in order to minimize its large dimensionality. That is, the kinetic modeling would be carried out using a simplified reaction network. Before proposing a model, the reaction mechanism of this catalytic process must be known. This mechanism, or pathway, can easily be gotten from the behaviour of each hydrocarbon species in the product stream. The behaviour is reflected in the change in yields of the hydrocarbon species as a function of percentage conversion of propane.

5.4.1. Model formulation

This modeling was executed on the basis of a scheme that lumped several species (e.g. cracking products were lumped together, benzene, toluene and xylene were also lumped together, heavier aromatics were ignored) and presented a macroscopic view of the

reaction mechanism. The high temperature transformation of propane over metal-containing HZSM-5 proceeds through two competitive monomolecular reactions i.e. cracking and dehydrogenation [84]. In addition, based on the results obtained, the model was developed under non-deactivating conditions of the metal-containing HZSM-5 catalysts.

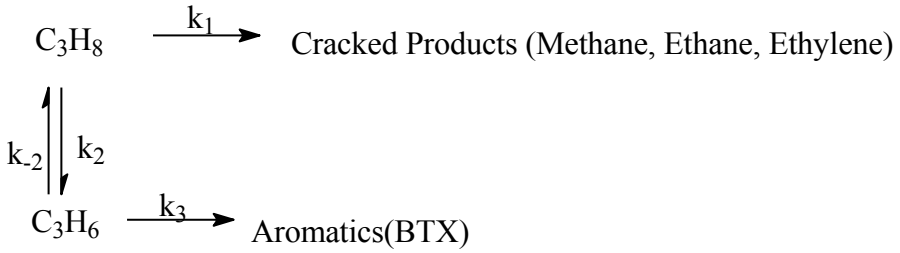

Scheme 1. Simplified reaction scheme for propane aromatization

A micro-reactor, which is a continuous flow fixed bed reactor, was used for the reaction. Generally, for each independent reacting species, the material balance equation can be written as:

$$\frac{dC_i}{d\tau} = r_i \qquad (1)$$

Where r_i and C_i represent the reaction rate and molar concentration of each species in the system respectively, τ is the contact time which is described as the ratio between the catalyst weight (W) and the mass flow rate of the feed (m). In this study, its unit is in seconds. The contact time is also known as the inverse of the weight hour space velocity ($WHSV^{-1}$).

Moreover, C_i was expressed in terms of the mass fraction of each species, y_i, according to the following equation:

$$C_i = \frac{y_i F_{TM}}{MW_i \nu_o} \tag{2}$$

Where F_{TM} is the total mass flow rate, MW_i is the molecular weight of species i and ν_o is the total volumetric flow rate.

The equilibrium constant between propane and propylene is dependent on temperature but independent on pressure and concentration. This dependency was determined by using the thermodynamic relation given below:

$$\ln K = -\frac{\Delta G_r^o}{RT}$$

where ΔG_r^o is the standard Gibbs free energy of the reaction, T is the reaction temperature in Kelvin, and R is the universal gas constant. Usually the Gibbs free energy is expressed in terms of correlation constants in a quadratic expression:

$$\Delta G_{f,i}^o = a_i + b_i T + c_i T^2$$

Where $\Delta G_{f,i}^o$ is the Gibbs free energy of formation of species i in a reaction system; $a_i, b_i, and\ c_i$ are correlation constants unique for different species. These constants

specific to the species being considered in this reaction, i.e. propane and propylene, are given in Table 5.3 below.

Table 5.3

Correlation Coefficients of Gibbs free energy of Formation of Ideal Gas at a Temperature T[19]

Compound	a	b	c	$T_{min}(K)$	$T_{max}(K)$
C_3H_8	-105.603	0.26475	3.25×10^{-5}	298.15	1000
C_3H_6	19.412	0.13685	2.57×10^{-5}	298.15	1000

So the temperature dependent equilibrium constant was calculated to be:

$$K = exp\left\{-\frac{15036.69}{T} + 15.38 + 8.12 \times 10^{-4}T\right\}$$

According to the mechanism above, the rate of disappearance and formation of species can be written as follows:

Rate of disappearance of propane is:

$$r_p = \frac{dC_p}{d\tau} = -\left(k_1 C_p - k_2\left(\frac{C_{3-}C_H}{K} - C_p\right)\right) G_1 \quad (3)$$

Rate of appearance of propylene:

$$r_{3-} = \frac{dC_{3-}}{d\tau} = \left(k_2(C_p - C_{3-}C_H/K) - k_3 C_p\right) G_2 \quad (4)$$

Rate of appearance of cracking products:

$$r_{cr} = \frac{dC_{cr}}{d\tau} = \left(k_1 C_p\right) G_3 \quad (5)$$

Rate of appearance of aromatics:

$$r_A = \frac{dC_A}{d\tau} = (k_3 C_{3-}) G_4 \quad (6)$$

Where $G_1 to\ G_5$ are the lumped constants given by:

$$G_1 = \frac{MW_p V_0}{F};\ G_2 = \frac{MW_{3-} V_0}{F};\ G_3 = \frac{MW_{cr} V_0}{F};\ G_4 = \frac{MW_A V_0}{F} \quad (7)$$

MW_A is the average molecular weight of benzene, toluene and xylene. MW_p, MW_{3-}, and MW_{cr} are the molecular weights of propane, propylene and cracking products respectively. F is the total mass flow rate and V_0 is the total volumetric flow rate.

k_i is the temperature dependent rate constant given by the Arrhenius relation below:

$$k_i = A_i e^{-E_i/RT} \quad (8)$$

In order to reduce parameter interaction between the preexponential factor (A_i) and activation energy(E_i), Agarwal and Brisk [85] postulated a reparametrization of $k_i$by centering the temperature at an average reaction temperature ofT_0, i.e.

$$k_i = k_0 exp\left[\frac{-E_i}{R}\left(\frac{1}{T} - \frac{1}{T_0}\right)\right] \quad (9)$$

Where k_0 is the rate constant at T_0.

5.4.2. Model Assumptions

In formulating this model, we took into consideration the following assumptions:

1. The model assumes negligible catalyst deactivation since contact time was small.

2. Dehydrogenation of propane to propylene follows a reversible path while cracking reaction follows an irreversible pathway.
3. This model has ignored the formation of C_8+ hydrocarbons because, overall, their presence is negligible at the contact times considered.
4. The reactor operates under isothermal condition which is justified by the negligible temperature change observed during the reaction.
5. Formation of butanes and its isomers has also been ignored because of the very low concentrations observed.

5.4.3. Estimation of model parameters

The system of coupled differential equations was solved using fourth order Runge-Kutta coupled with non-linear regression analysis in order to determine the values of the 6 parameters (k_{01}, E_1, k_{02}, E_2 and k_{03}, E_3). This was done for the two catalysts (Ga4HZ80 and Ga4HZ80-SMH0.30). The results are tabulated, in table 5.4, along with their equivalent 95% confidence limits. Table 5.5 shows the correlation 6×6 matrices that expose the degree of correlation between any pair of parameter in our kinetic model. The values in the matrices are low and moderate, except for few, indicating good and acceptable parameter sets. Moreover, the correlation coefficient value is close to unity (0.99) which indicates a good fit between the model and experimental data. Figures 5.5 – 5.8 show the comparison between the experimental and predicted values for the yield of the cracking products and BTX. The parity plots, shown in figures 5.9 and 5.10, for

propane aromatization of the two catalysts also indicate the appropriateness of the proposed model.

Table 5.4

Estimated kinetic parameters for microporous and mesoporous gallium-containing catalysts.

Parameters	Values		
	k_1	k_2	k_3
Ga4HZ80			
E_i (kJ/mol)	110	70	220
95% CL	0.50	2.50	5.50
k_{0i} ($\times 10^3$ s^{-1})	60	40	62175
95% CL	0.50	1.50	25974.5
Ga4HZ80-SMH030			
E_i (kJ/mol)	130	12.65	140
95% CL	1.00	6.15	6.0
k_{0i} ($\times 10^3$ s^{-1})	70	60	868830
95% CL	2.00	4.00	6.0

Table 5.5

Correlation matrix for propane aromatization over microporous and mesoporous catalysts.

	k_1	E_1	k_2	E_2	k_3	E_3
Ga4HZ80						
k_1	1.0000	-0.9356	-0.0614	0.0712	-0.1115	0.0803
E_1	-0.9356	1.0000	0.0498	-0.0725	0.1087	-0.0748
k_2	-0.0614	0.0498	1.0000	-0.9359	-0.8241	-0.0449
E_2	0.0712	-0.0725	-0.9359	1.0000	0.8335	-0.2583
k_3	-0.1115	0.1087	-0.8241	0.8335	1.0000	-0.3367
E_3	0.0803	-0.0748	-0.0449	-0.2583	-0.3367	1.0000
Ga4HZ80-SMH030						
k_1	1.0000	-0.9425	-0.0234	0.0238	-0.1044	0.0939
E_1	-0.9425	1.0000	0.0226	-0.0296	0.0941	-0.0850
k_2	-0.0234	0.0226	1.0000	-0.9561	-0.9082	0.8478
E_2	0.0238	-0.0296	-0.9561	1.0000	0.8761	-0.9089
k_3	-0.1044	0.0941	-0.9082	0.8761	1.0000	-0.9419
E_3	0.0939	-0.0850	0.8478	-0.9089	-0.9419	1.0000

For propane aromatization over Ga4HZ80, our value for dehydrogenation apparent activation energy, E_d, of 70 $kJmol^{-1}$ compares favorably with that of Gabrienko A.A. et al [86] who reported an apparent activation energy of 80 $kJmol^{-1}$ using Zn-modified zeolite BEA as catalyst for propane aromatization. Narbeshuber et al [84] reported an apparent activation energy of 95 $kJmol^{-1}$ for dehydrogenation of propane over HZSM-5. Wang et al [87] obtained dehydrogenation apparent activation energy of 70 $kJmol^{-1}$ over a HZSM-5 acid catalyst. Harris et al [88] estimated a value of 81.4 $kJmol^{-1}$ for propane transformation over a Ga-loaded ZSM-5 catalyst.

The decrease in dehydrogenation activation energy can be related to the improved dispersion of gallium metal species in the catalyst structure. Also, the increase in cracking activation energy relates to the decrease in acidity of the catalyst upon introduction of mesopores.

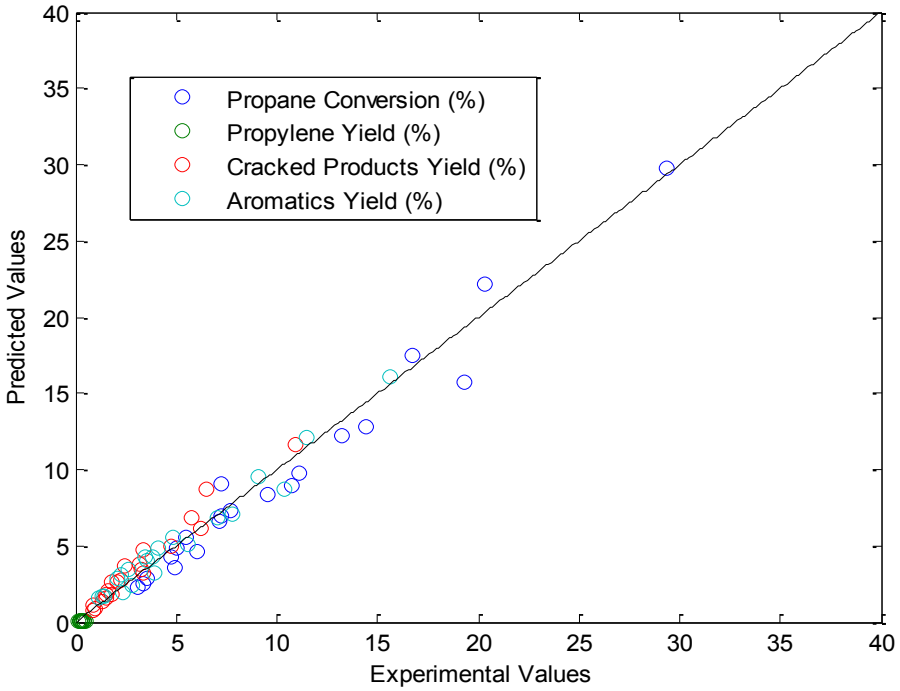

Fig.5.9 Overall comparison between the experimental results and model predictions of microporous catalyst using the proposed reaction scheme.

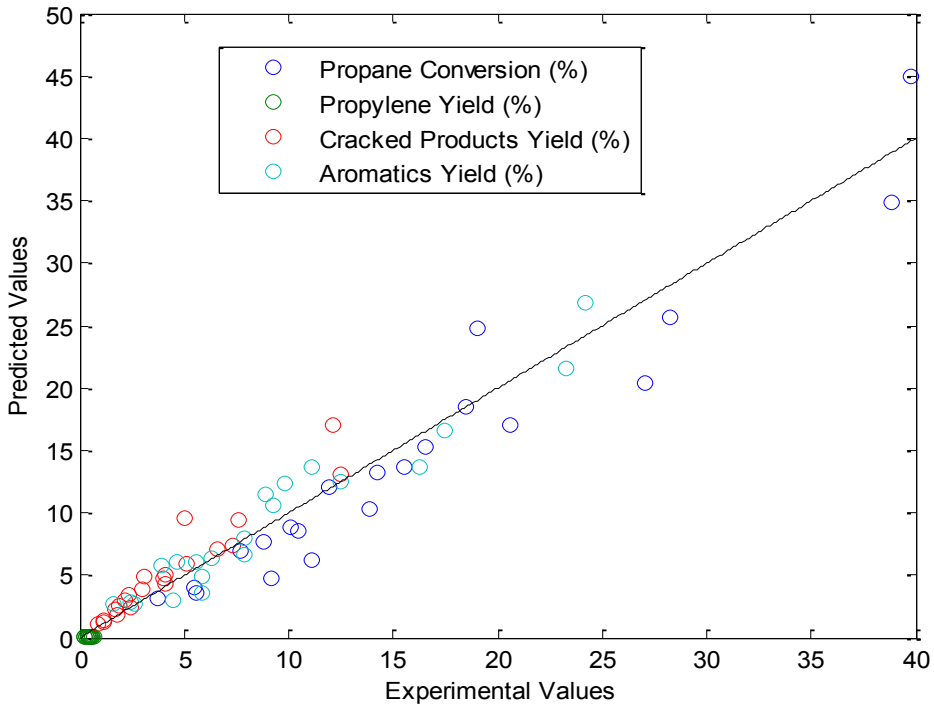

Fig. 5.10 Overall comparison between the experimental results and model predictions of mesoporous catalyst using the proposed reaction scheme.

CHAPTER SIX

CONCLUSIONS AND RECOMMENDATIONS

6.1 Conclusions

The kinetics of propane aromatization was successfully carried out over microporous gallium-containing HZSM-5 and mesoporous gallium-containing HZSM-5 obtained via CTAB-mediated hydrolysis of the microporous catalyst. Our study substantiates the following conclusions:

(1). Propane conversion and BTX yield increase significantly with increase in reaction temperature and contact time.

(2). Cracking products increase with temperature regardless of the presence of mesopores In the catalyst structure.

(3). Incorporation of mesopores improved the dispersion of gallium and this is reflected in the increase in BTX yield, selectivity at comparable conversion and propane conversion.

These improvements were observed at reaction temperature of 540^{o}C. Conversion increased by 35.7% while BTX yield increased by 55% at the highest contact time.

(4). Kinetic parameters for the propane aromatization showed that apparent activation energies for cracking increased as follows: $E_{Ga4HZ80} < E_{Ga4HZ80\text{-}SMH0.30}$ while the

apparent activation energies for dehydrogenation decreased as follows: $E_{Ga4HZ80} > E_{Ga4HZ80\text{-}SMH0.30}$.

(5). Our results agree with the literature in that the activation energy for the competitive reaction, cracking, was higher than that of dehydrogenation to propylene for both microporous and mesoporous catalysts.

In addition, the investigation into the synthesis of stable H-Galloaluminosilicate with hierarchical pore architecture by CTAB-mediated base hydrolysis, and their application in propane aromatization led to the following conclusions:

- CTAB-mediated hydrolysis of steamed H-Galloaluminosilicate, which was obtained via hydrothermal (*in situ*) method, can be considered as an effective method for improving the dispersion of the catalytically active aromatization species, and thus the aromatization performance.
- The ordered mesoporous H-Galloaluminosilicate with mesoporous/microporous hierarchical structure exhibited superior aromatization performance and stability, as compared with steamed conventional H-Galloaluminosilicate.
- An optimum aromatization performance over ordered mesoporous H-Galloaluminosilicate was achieved for samples obtained using a concentration of hydrolysis solution that corresponded to OH^-/T ratio of 0.57. This optimum performance indicates an optimum balance between ordered mesoporosity, gallium dispersion, Lewis sites (dehydrogenation sites), and Brρnsted sites (cracking-oligomerization sites).

- The enhancement in aromatization ability over steamed conventional H-Galloaluminosilicate was tentatively linked to the hydrothermal *(in situ)* synthesis and presence of ordered mesoporosity, which facilitated the penetration of Ga_2O_3 into the micropores and thus the formation of extra framework Ga species that is the actual active sites in alkane aromatization (viz. (gallination-degalliation-"re-gallination" of extracrystalline Ga_2O_3)).

Lastly, the investigation into the incorporation of mesoporosity into Gallium-containing HZSM-5 catalyst (commercial) led to the following conclusion:

The CTAB- mediated assembly of Ga-containing HZSM-5 zeolite seed into mesoporous MCM-41 structure proved more active than the desilicated counterpart at low gallium content.

6.2 Recommendations

- Investigation of adsorption kinetics encompassing the micro-kinetic study of propane aromatization over mesoporous Ga-containing HZSM-5 should be ventured into.
- Comprehensive study of catalyst deactivation of mesoporous Ga-containing HZSM-5 should be undertaken.

NOMENCLATURE

A	aromatics
A_i	pre-exponential factor for the *i*th reaction (s^{-1})
Cr	cracking products
E_i	apparent activation energy of the *i*th reaction step
F	total mass flow rate
ΔG_r^o	standard Gibbs free energy of reaction
K	equilibrium constant for propane dehydrogenation
k_i	rate constant for reaction *i*
MW_{cr}	average molecular weight of cracking products (g/mol)
MW_i	molecular weight of species *i* (g/mol)
P	propane
r_i	rate of reaction for species *i*
r^2	correlation coefficient
R	universal gas constant (J/mol K)
SMH	surfactant mediated hydrolysis
T_o	average temperature
v_o	total volumetric flow rate ($m^3/\min$)
3-	propylene

REFERENCES

1. N.Y. Chen, W.E. Garwood and F.G. Dwyer, Shape Selective Catalysis in Industrial Applications, Chem. Ind. Ser., Vol.36, Marcel Dekker, New York and Basel, 1989, p.205.
2. Schleyer, Paul von Ragué (2001). "Introduction: Aromaticity". *Chemical Reviews* **101** (5): 1115–8.
3. Fabri, Jörg, Graeser, Ulrich, and Simo, Thomas A., Xylenes, Ullmann's Encyclopedia of Industrial Chemistry, 2002, Wiley-VCH, Weinheim.
4. B. S. Furniss et al., *Vogel's Textbook of Practical Organic Chemistry*, 5th edition, Longman/Wiley, New York, 1989.
5. Vincent A.Welch, Kevin J. Fallon, Heinz-Peter Gelbke "Ethylbenzene" *Ullmann's Encyclopedia of Industrial Chemistry*, Wiley-VCH, Weinheim, 2005.
6. Nal Y. Chen and Tsoung Y.Yan, Ind. Eng. Chem. Process Des. Dev. 1986, 25, 151-155.
7. M. Guisnet, N.S. Gnep, Applied Catalysis A: General, 89 (1992), 1-30.
8. www.uop.com/cyclar
9. N.Y. Chen, Australian Patent 465697 (Published: 12-10-72; Priority: 13-04-70, US27563; to Mobil Oil Corporation)
10. J. Cattanach, Australian Patent 484975 (Published: 14-11-74; Priority: 17-05-72, US253942; to Mobil Oil Corporation)
11. Nai Y. Chen, Tsoung Y. Yan, Ind. Eng. Chem. Process Des. Dev.,1986, 25 (1), pp 151-155.

12. T. Mole and J.R. Anderson, Applied Catalysis 17 (1985) 141-154.
13. M.Guisnet, N.S. Gnep, D. Aittaleb and Y.J. Doyemet, Applied Catalysis A: General, 87 (1992) 255-270.
14. G.M. Kramer, G.C. McWicker and J.J. Ziemiak, J. Catal., 92 (1985) 355.
15. G.B. McWicker, G.M. Kramer and J.J. Ziemiak, J. Catal., 110 (1988) 171.
16. J. Abbot and B.W. Wojciechowski, J. Catal., 115 (1989) 1.
17. Y. Ono and K. Kanae, J. Chem. Society. Faraday Trans., 87 (1991) 663.
18. E.A. Lombardo and W. Keith Hall, J. Catal., 112 (1988) 565.
19. Olah, G.A., Halpern, Y., Shen, J., Mo, Y.K , J. Am. Chem. Soc., 1971, 93 (5) 1251.
20. Kitagawa H., Sendoda Y., Ono Y., Journal of Catalysis 101, 12-18 (1986).
21. M. Guisnet and D. Lukyanov, Studies in Surface Science and Catalysis 90, 367-378 (1994).
22. J. Bandiera and Y. Ben Taarit, Appl. Catal., 62 (1990) 309.
23. M. Guisnet, N.S. Gnep, F. Alario, Appl.Catal., 89 (1992) 1-30.
24. G. Caeiro, R.H. Carvalho, X. Wang, M.A.N.D.A. Lemos, F. LEmos, M. Guisnet, F. RAmoa Ribeiro, Journal of Molecular Catalysis A 255 (2006) 131-158.
25. T. Inui, F. Okazumi, Journal of Catalysis 90 (1984) 366-367.
26. C.W.R. Engelen, J.P. Wolthuizen, J.H.C. Van Hooff, Applied Catalysis 19 (1985) 153-163.
27. N.S. Gnep, J.Y. Doyemet, A.M. Seco, F. Ramao Ribeiro, M. Guisnet, Applied Catalysis 35 (1987) 93-108.
28. B.H. Davis, G.A. Westfall, J. Watkins, J. Pezzanite, J. Catalysis, 42 (1976), 247.

29. R. Burch, L.C. Garla, Journal of Catalysis, 71 (1981), 360.

30. H. Lieske, J. Volter, Journal of Catalysis, 90 (1984) 96.

31. A. Palazov, C. Bonev, G. Kadinov, D. Shopov, G. Lietz, J. Volter, Journal of Catalysis, 71 (1981), 1.

32. M.S. Kharson, G. Gadinov, A. Palazov, Reaction Kinetics Cataysis Letter, 10 (1979), 267.

33. K. Aristirova, Chr. Dimitrov, K. Dyrek, K.H. Hallmeier, Z. Popova, S. Witkowski, Applied Catalysis A 81 (1992) 15-26.

34. J. Guo, H. Lou, H. Zhao, L. Zheng, X. Zheng, Journal of Molecular Catalysis A 239 (2005) 222-227.

35. Claudio C.S., Yiu L.L., Martin S., Catalysis Letters 47 (1997) 143-154.

36. M.Shibata, H.Kitagawa, Y.Sendoda and Y.Ono, Proc.7 th Int. Congress on Zeolites, 1986, Kodansha Elsevier, Tokyo, 1986,p.717.

37. T. Inui, Y.Makino, F.Okazumi, S.Nagano and A. Miyamoto,Ing.Eng.Chem.Res.,26 (1987)p.647.

38. H.Kitagawa, Y.Sendoda and Y.Ono, J.Catal.,101 (1986) 12.

39. B.S.Kwak, W.M.H.Sachtler, W.O.Haag, Journal of Catalysis, 149 (1994) 465.

40. G.L. Price, V. Kanazirev, Journal of Catalysis, 126 (1990) 267.

41. P. Chu, US Patent 4, 120, 910 (1978).

42. P.Meriaudeau, S.B. Abdul Hamid, C.Naccache, Journal of Catalysis, 139 (1993) 683.

43. B.S.Kwak, W.M.H.Sachtler, Journal of Catalysis, 145 (1994) 456.

44. Izabela Nowak et al, Applied Catalysis A: General, 251 (2003) 107-120.

45. V.R.Choudhary, A.K.Kinage, C.Sivadinarayana, P.Devadas, S.D. Sansare, M.Guisnet, J. Catal., 158 (1996), 34-50.

46. N. Al-Yassir, M.N. Akhtar, S. Al-khattaf, J. Porous Mater., 19 (2012), 943-960.

47. Yousheng Tao, Hirofumi Kanoh, Lloyd Abrams, and Katsumi Kaneko, Chem.Rev.,106 (2006), 896-910.

48. Janssen, A.H., Koster, A.J. and de Jong, K.P, Chem. Int. Ed.,40 (2001) 1102-1104.

49. Masaru Ogura, Shin-ya Shinomiya, Junko Tateno, Yasuto Nara, Eiichi Kikuchi, Masahiko Matsukata, Chemistry Letters, 29 (2000) 882-883.

50. M.N. Akhtar, N.Al-Yassir, S.Al-Khattaf, Jiri Cejka, Catalysis Today, 179 (2012) 61-72.

51. N. Al-Yassir, M.N. Akhtar, K.Ogunronbi, S. Al-Khattaf, Journal of Molecular Catalysis A: Chemical 360 (2012) 1-15.

52. Narbeshuber T.F, Brait A., Seshan K., Lercher J.A., Journal of Catalysis 172, (1997) 127-136.

53. Aditya B., Shuo-Huan Hsu, Gary Blau, James M. Caruthers, Venkat Venkatasubramanian, W. Nicholas D., Journal of Catalysis 235 (2005) 35-51.

54. K. R. Kloetstra, H. W. Zandbergen, J. C. Jansen, H. van Bekkum, *Microporous Mater.* **6** (1996) 287-293.

55. B. C. Lippens, J. H. de Boer, *J. Catal.* **4** (1968) 319-323.

56. E. P. Barret, L. G. Joyner, P. H. Halenda, *J. Am. Chem. Soc.* **73** (1973) 373-380.

57. J. C. Groen, W. Zhu, S. Brouwer, S. J. Huynink, F. Kapteijn, J. A. Moulijn, J. Perez-

Ramirez, *J. Am. Chem. Soc.* **129** (2007) 355-360.

58. H.Wang, Y. Liu, T.J. Pinnavaia, J. Phys. Chem. B 110 (2006) 4524 - 4526.

59. R. Szostak, Molecular Sieves: Principles of Synthesis and Identification, Van Norstrand Reinhold Catalysis Series, **36** (1989) 290.

60. M. Kruk, M. Jaroniec, A. Sayari, *Langmuir* **13** (1997) 6267-6273

61. B. Gil, S. I. Zones, S. J. Hwang, M. Bejblová, J. Čejka, *J. Phys. Chem. C.*, **112** (2008) 2997-3007.

62. N. Žilková, M. Bejblová, B. Gil, S. I. Zones, A. W. Burton, C. Y. Chen, Z. Musilova, J. Čejka, *J. Catal.,* **266** (2009) 79-91.

63. C. T. Kresge, M. E. Leonowicz, W. J. Roth, J. C. Vartuli, J. S. Beck, *Nature* **359** (1992) 710-712.

64. P.A. Jacobs, H.K. Beyer, J. Valyon, *Zeolites* **1** (1981) 161-168.

65. C. E. A. Kirschhock, R. Ravishankar, F. Verspeurt, P. J. Grob, P. A. Jacobs, J. A. Martens, *J. Phys. Chem., B* **103** (1999) 4965-4971.

66. S. J. Gregg, K. S. W. Sing, Adsorption, Surface Area and Porosity; Academic Press, London, 1982.

67. G.D. Meitzner, E. Iglesia, J.E. Baumgartner, E.S. Huang, *J. Catal.,* **140** (1993) 209-225.

68. S. V. Sirotin, I. F. Moskovskaya, B. V. Romanovsky, *Catal. Sci. Technol.,* **1** (2011) 971-980.

69. B. Zheng, W. Hua, Y. Yue, Z. Gao, *J. Catal.,* **232** (2005) 143-151.

70. O.J. Wimmers, P. Arnoldy, J.A. Moulijn, *J. Phys. Chem.,* **90** (1986) 1331-1337.

71. S. V. Sirotin, I. F. Moskovskaya, B. V. Romanovsky, *Catal. Sci. Technol.,* **1** (2011) 971-980.

72. B. Sulikowski, Z. Olejniczak, V.C. Corberan, *J. Phy. Chem.,* **100** (1996) 10323-10330.

73. C. Bigey, B.-L. Su, *J. Mol. Catal. A.,* **209** (2004) 179-187.

74. K-J. Chao, P-Hung. Liu, *Catalysis Surveys from Asia*, **9** (2005) 11-15.

75. R. Fricke, H. Kosslick, G. Lischke, M. Richter, *Chem. Rev.,* **100** (2000) 2303-2405.

76. P.P. Man, J. Klinowski, *J. Chem. Phys. Lett.***, 147** (1988) 581-584.

77. F. Lonyi, J. Valyon, *Microporous. Mesoporous Mater.,* **47** (2001) 293-301.

78. S. Rajagopal, J.A. Marzari, R. Miranda, *J. Catal.,* **151** (1995) 192-203.

79. Y.V. Joshi, K.T. Thomson, *J. Catal.,* **246** (2007) 249-265.

80. K.M. Dooley, C. Chang, G.L. Price, *Appl. Catal. A.* **84** (1992) 17-30.

81. J. C. Groen, L. A. A. Peffer, J. A. Moulijn, J. Pérez-Ramírez, *Chem. Eur. J,* **11** (2005) 4983-4994.

82. V. R. Choudhary, P. Devadas, *Appl. Catal. A.,* **168** (1998) 187-200.

83. T. V. Choudhary, A. Kinage, S. Banerjee, V. R. Choudhary, *Energy & Fuels* **20** (2006) 919-922.

84. T.F. Narbeshuber, H. Vinek, J.A. Lercher, Journal of Catalysis 157, 388-395 (1995).

85. A.K. Agarwal, M.L. Brisk, Sequential experimental design for precise parameter estimation – 1. Use of reparametrization, Ind. Eng. Chem. Process Des. Dev. 24 (1985) 203-207.

86. A.A. Gabrienko, S.S. Arzumanov, D. Freude, A.G. Stepanov, J. Phys. Chem. C 2010, 114, 12681-12688.

87. X. Wang, H. Carabineiro, F. Lemos, M.A.N.D.A. Lemos, F. Ramoa Ribeiro, J. Mol. Catal. A: Chem. 2004, 216, 131-137.

88. J.L. Harris, N. Krisko, X.M. Wang, Appl. Catal. A 1992, 83, 59-74.

89. G. Coudurier, C. Naccache, J.C. Vedrine, J. Chem. Soc. Chem. Comm, 1413-1415 (1982).

Vitae

Name	: KEHINDE EMEKA OGUNRONBI
Nationality	: NIGERIAN
Date of Birth	: 7/8/1985
Email	: kennyronbi@gmail.com
Address	: No 4, Camaria Hospital Road, Basorun, Ibadan, Nigeria.
Academic Background	: BSc. Chemical Engineering (2nd Class Upper Division) Obafemi Awolowo University (O.A.U), Ile-Ife, Osun State, Nigeria, 2008. MS. Chemical Engineering (Distinction) King Fahd University of Petroleum and Minerals, Dhahran, Saudi Arabia, 2013.
Phone Number:	+966531215839.